BEHAVIOR OF CONCRETE UNDER BIAXIAL CYCLIC COMPRESSION

by

Joseph Gary Zisman
Ingeniero Civil, Anahuac University
(1979)

Submitted in partial fulfillment
of the requirements for the degree of

Master of Science

at the

Massachusetts Institute of Technology

February 1982

Signature of Author _____
Department of Civil Engineering, September 15, 1981

Certified by _____
Oral Buyukozturk
Thesis Supervisor

Accepted by _____
Chairman, Department Committee

ABSTRACT

BEHAVIOR OF CONCRETE UNDER BIAXIAL CYCLIC COMPRESSION

by

JOSEPH GARY ZISMAN

Submitted to the Department of Civil Engineering on September 15, 1981 in partial fulfillment of the requirements for the degree of Master of Science

An experimental program was conducted to study the behavior of plain concrete under biaxial compressive cyclic stresses, i.e., compressive normal stresses which alternatingly increase and decrease along two orthogonal directions. Biaxial loading was achieved by subjecting square concrete plates to in-plane loading, where vertical stress was applied to specimens uniaxially confined in the horizontal direction at given constant strain levels. Four main types of tests were performed: monotonic loading to failure, cycles to the envelope curve, cycles to prescribed values of vertical stress and cycles between fixed maximum and minimum vertical stress levels. Each type of test was performed on both unconfined specimens and specimens under different confinement levels (values of constant horizontal strain). Complete stress-strain histories were recorded, analyzed and compared in order to assess the effects of uniaxial strain confinement on concrete behavior under different loading conditions. The observation and comparison of the behavior exhibited by confined and unconfined specimens helped to explain the mechanisms of the deformational behavior of concrete. Results of the uniaxial cyclic and biaxial monotonic tests were compared to those previously obtained by other investigators.

Up to date no research on the behavior of concrete under biaxial cyclic stress has been performed. Hence, this investigation provides new information which can be ultimately applied to the analysis and design of concrete structures subjected to biaxial cyclically varying stresses, such as slabs, thin shells and shear walls.

Thesis Supervisor: Oral Buyukozturk
Title: Associate Professor

ACKNOWLEDGEMENTS

The author would like to thankfully acknowledge the technical advice, supervision and support from his thesis supervisor, Professor Oral Buyukozturk. The author also wishes to acknowledge the cooperation in this project of the Department of Civil Engineering at Cornell University, for providing the brush bearing platens which constituted an essential component of the equipment utilized in this investigation.

The author wishes to acknowledge Mr. Arthur Rudolph's exceptional skill and enthusiasm in constructing the specimen molds and lateral loading frame, without which this project would not have been possible. Special thanks are extended to Mr. Tsi Ming Tseng for his invaluable cooperation and suggestions in all phases of the project. Mr. Jorge Calvo is also thanked for his participation in the project, expesially for assisting in the testing operation.

The author would also like to thank Mrs. Terri Demeris and Mrs. Stephanie George for the efficient typing of this thesis.

The author wishes to dedicate this thesis to all the people who put an effort into its accomplishment, and very especially to his family. This thesis is also dedicated to Irene Saba and her family.

TABLE OF CONTENTS

LIST OF FIGURES

CHAPTER 1

INTRODUCTION

Up to date a vast amount of research has focused on the behavior of concrete subjected to monotonic loading conditions. Various investigators have obtained experimental stress-strain curves for uniaxial, biaxial and triaxial monotonic loading and a great variety of mathematical models based on these curves have been derived. In many cases the proposed models predict the behavior of concrete within acceptable limits of accuracy. In contrast to this little has been done in relation to the behavior of concrete under cyclic loading. There is a substantial lack of experimental data due to which the actual response of concrete under this type of loading is not well known. Practically all the experiments of this type have dealt with uniaxial cyclic loading conditions, while reliable data for behavior of concrete under cyclic multiaxial loadings is completely lacking. Understanding of such a behavior is essential for an adequate design of all concrete structures subjected to biaxial or triaxial cyclically varying stresses. Many structures such as slabs, thin shells and shear walls can be idealized as being in two-dimensional states of stress. Therefore, biaxial stress is an important special case.

The main objective of the present investigation is to study the behavior of concrete under biaxial cyclic stresses generated by the application of repeated loadings under uniaxial strain confinement.

For this purpose square concrete plates were subjected to two loading phases: (1) initial confining phase where the specimen is loaded horizontally to a predetermined stress value and (2) application of cyclic vertical stress during which the horizontal strain imposed in phase 1 is kept constant. Uniaxial cyclic tests were also performed mainly to offer a comparative basis for the biaxial cyclic tests. Behavior of concrete under monotonically increasing biaxial stresses is also investigated. These tests were performed following the same technique as in the biaxial cyclic tests except for the fact that vertical stress was applied monotonically. In these tests, principal stresses vary non-proportionally. Results are compared with those of previous investigations where concrete is subjected to biaxial stresses which increase proportionally (constant stress ratio). The biaxial monotonic tests serve also as a complement to the biaxial cyclic tests.

A brief review of the major experimental work done up to date dealing with the behavior of concrete under uniaxial cyclic and biaxial monotonic loading is presented in Chapter 2. In uniaxial cyclic loading three basic investigations performed by the following authors are reviewed: Sinha, Gerstle and Tulin (15), 1964; Karsan and Jirsa (7), 1969, and Shah and Chandra (13), 1970. In biaxial monotonic loading, results obtained by Kupfer et al. (8), Liu et al. (9) and other investigators are reviewed. Chapter 3 provides a detailed description of the test specimens and equipment utilized for the investigation, as well as types of tests performed and experimental techniques.

In Chapter 4, test results are presented and the data analysis is performed. Finally, in Chapter 5, the testing procedure is summarized and conclusions are given. Suggestions for further research on the behavior of concrete under biaxial cyclically varying stresses are also given.

CHAPTER 2

REVIEW OF CONCRETE BEHAVIOR UNDER UNIAXIAL CYCLIC LOADING AND BIAXIAL MONOTONIC STRESS

2.1 Uniaxial Cyclic Loading

Up to date, investigations into the behavior of concrete under cyclic loading have been aimed towards studying the response of concrete under uniaxial cyclic stress (7,13,15). This section attempts to outline, based on previously performed experiments, the basic behavioral characteristics of concrete subjected to uniaxial cyclic loading. The background material presented here constitutes an important prelude to the cyclic experiments conducted and a basis for evaluating the behavior exhibited in the present experiments. The results of three basic investigations carried out by the following authors are reviewed: Sinha, Gerstle and Tulin (15), 1964; Karsan and Jirsa (7), 1969, and Shah and Chandra (13), 1970.

2.1.1 Envelope, Unloading and Reloading Curves

It's been seen that under uniaxial cyclic loading concrete exhibits a hysteretic behavior characterized by non-overlapping unloading and reloading curves. If a specimen is repeatedly cycled between zero and progressively increasing stress levels, and strain is sufficiently increased after each unload-reload cycle, the stress strain curve decreases in slope after each cycle following the trend of the previous loading branch of the curve. The curve joining the resulting broken

curves or loading branches between cycles has been defined as the envelope curve (15). See Fig. 2.1. There is controversy as to whether the envelope actually coincides with the monotonic curve. According to Sinha et al. (15), the monotonic stress strain curve falls below the envelope curve. However, Karsan and Jirsa (7), and more recently Lam (19), have found that both curves coincide. See Fig. 2.2. Karsan and Jirsa observed that the specimen could be loaded to the envelope regardless of the strain accumulated prior to a given cycle. Accumulation of strain under maximum stress levels produced failure when the envelope was reached. See Figs. 2.3 and 2.4.

In the experiments by Karsan and Jirsa (7) and Sinha et al. (15) it is seen that in cycling to the envelope curve the slopes of the reloading and unloading curves progressively decrease with the number of cycles. See Figs. 2.2 and 2.5. This degradation process has been attributed to increasing microcracking at high strain levels. The slopes of the unloading and reloading curves were, therefore, found to depend on the strain at which unloading and subsequent reloading took place.

2.1.2 Common Points

The common points have been defined as the points where reloading curves intersect unloading curves in unload-reload cycles (points B,D, F,H in Fig. 2.5). When cycling to the envelope curve the reloading curve considerably decreases in slope after the common point. This behavior has been attributed to a significant increase in microcracking. Sinha et al. (15) considered the locus of common points as a shakedown

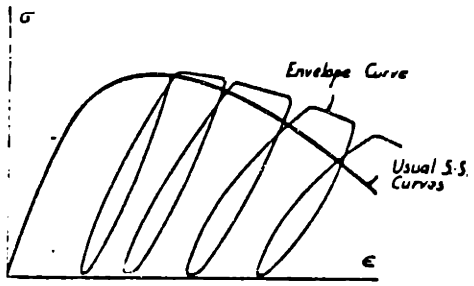

Fig. 2.1 - Envelope Curve

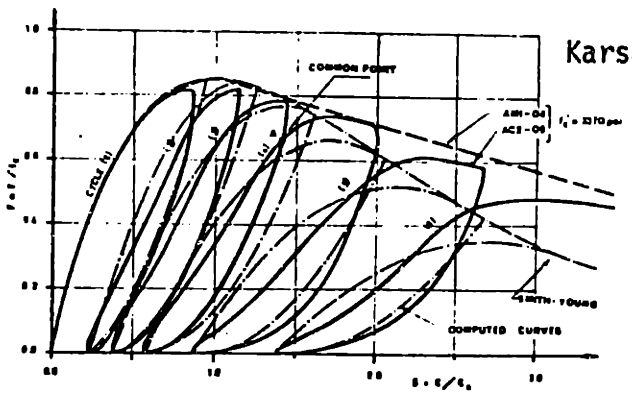

Karsan and Jirsa

Fig. 2.2 - Cyclic Loading to Envelope Curve

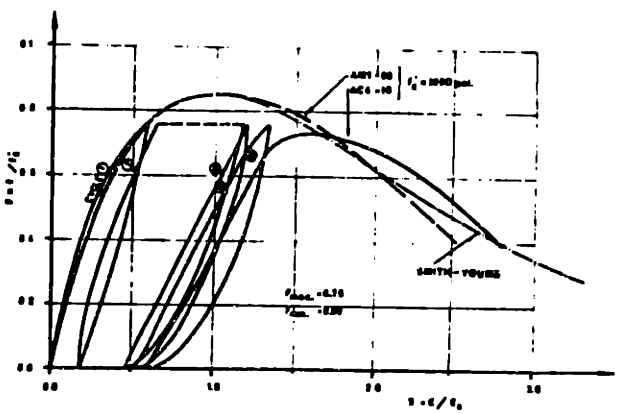

Fig. 2.3 - Comparison of Envelope Curve with Cyclic Test

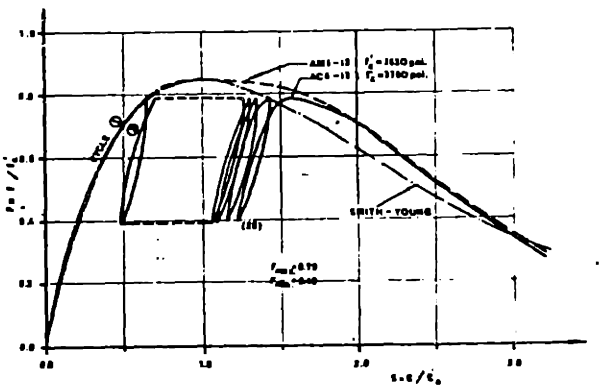

Fig. 2.4 - Comparison of Envelope Curve with Cyclic Test

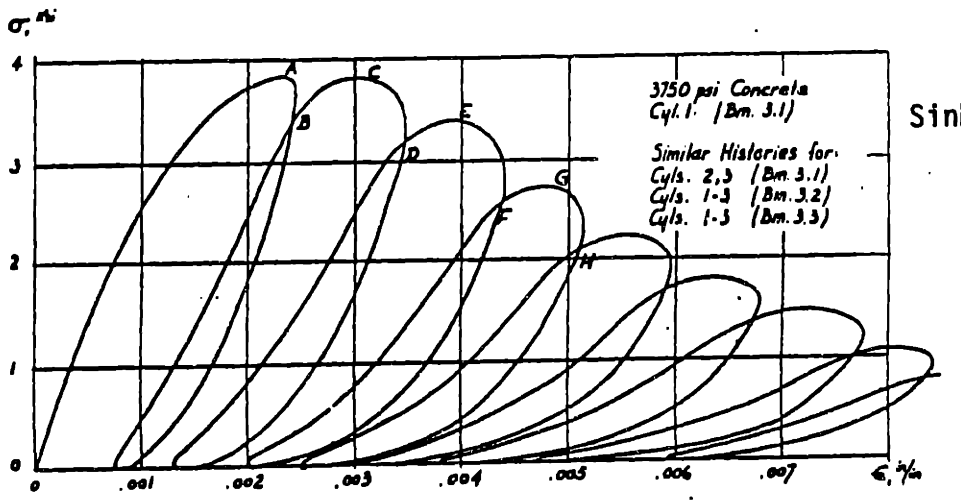

Sinha et al.

Fig. 2.5 - Cyclic Loading to Envelope Curve

limit such that stresses above the limit cause additional inelastic strains while stresses at or below this limit cause the curve to go into a closed hysteresis loop. The common points were found to depend on the minimum stress in the cycle. Karsan and Jirsa (7), however, obtained completely different results. They found that if at the common point of an unload-reload cycle the specimen is unloaded again and then reloaded the new common point falls below the first one. If the procedure is succesively repeated the common point keeps falling until it reaches a stability point. If the specimen is repeatedly cycled to this point no additional straining occurs. See Fig. 2.6. The maximum stability point was found to be equal to 0.63 f'_c. The common point location was, therefore, found to be dependent on the maximum stress and strain of the previous load cycle. Minimum stress was not found to affect the locus of common points. The locus of stability points is defined as the stability limit. The significance of the stability limit is that if concrete is subjected to repeated cycles at or below its maximum value, 0.63 f'_c, failure will not occur. The upper limit of common points is provided by the intersection points of unloading and reloading curves of cycles to the envelope curve. The maximum upper limit common point was found to be equal to 0.76 f'_c. The locus of the upper limit common points was called the common point limit. The common point limit and the stability limit obtained by Karsan and Jirsa are shown in Fig. 2.7.

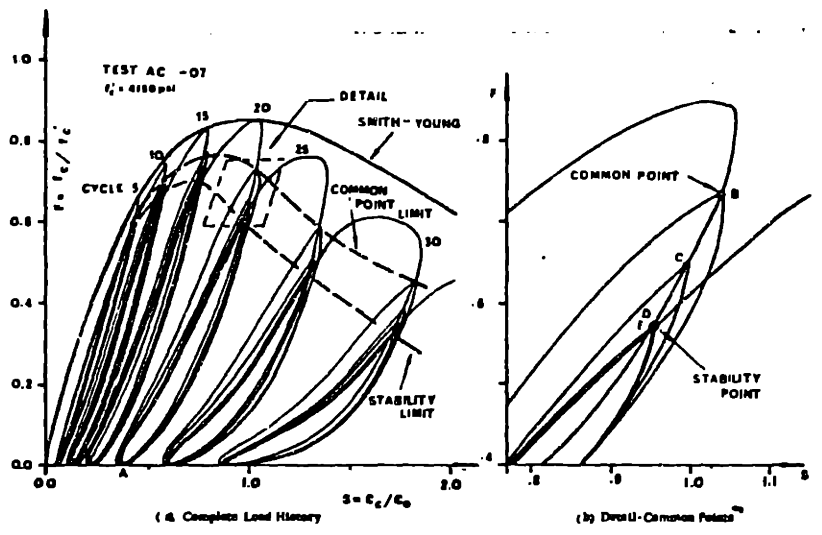

Fig. 2.6 - Variation of Common Points

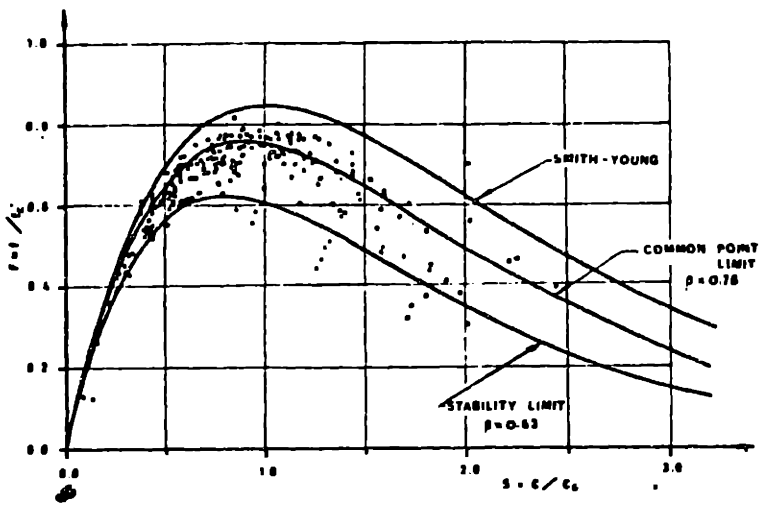

Fig. 2.7 - Common Points

2.1.3 Nonrecoverable Strains

Karsan and Jirsa (7) have defined nonrecoverable or plastic strains as those strains corresponding to zero stress level on loading or unloading stress strain curves. The ratio of plastic strain to the peak strain in uniaxial monotonic compression, ε_o, is defined as the plastic ratio S_p. Figs. 2.8 and 2.9 show loading and unloading curves corresponding to specimens subjected to different loading histories. A decline in the slopes of these curves for increasing values of S_p can be observed. The plastic ratio S_p appears to be a major variable in determining the shapes of the loading and unloading curves independently of the loading history preceding a given value of S_p.

2.1.4 Stress-Strain Relations

Sinha et al. (15) assumed that the envelope, loading and unloading curves passing through a point in the stress-strain domain are unique, i.e., independent of the previous loading history. On this basis they developed mathematical expressions for such curves. A second degree polynomial with constants depending on the concrete strength was proposed for representing the envelope curve. Unloading curves were represented by a family of second order curves while reloading curves were represented by a family of straight lines. Constants in the mathematical expressions for both types of curves are also dependent on the concrete strength.

Karsan and Jirsa (7), based on their experimental data, also developed expressions for predicting the behavior of concrete under

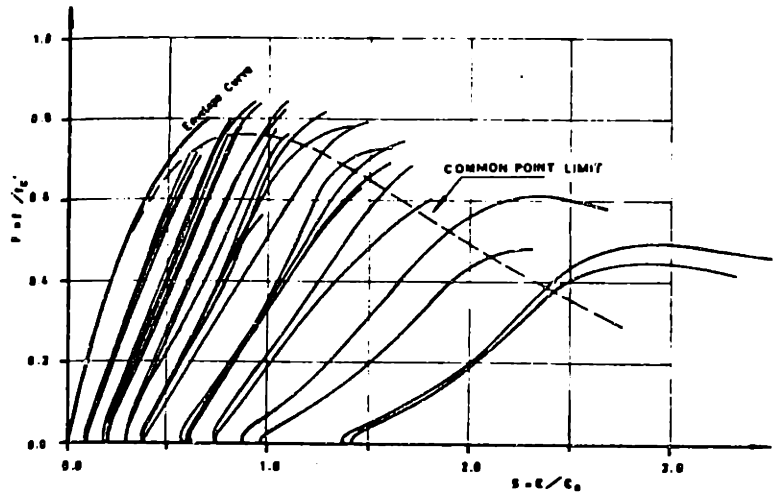

Fig. 2.8 - Loading Curves

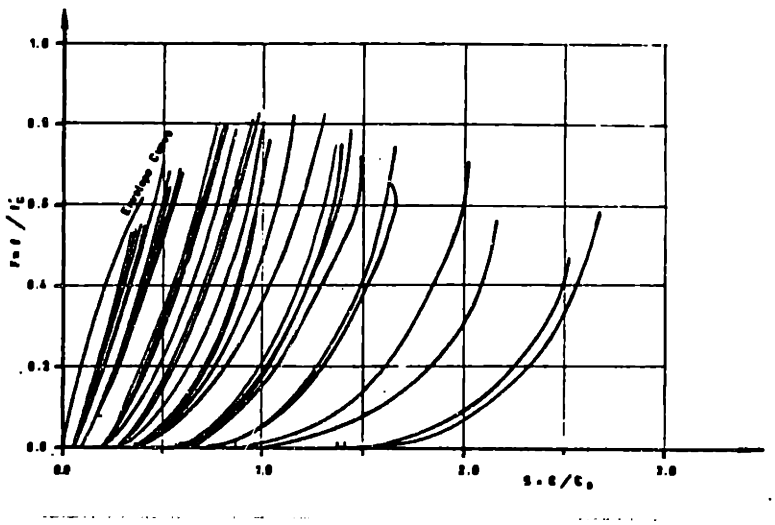

Fig. 2.9 - Unloading Curves

uniaxial cyclic loading. Their consideration of common point dependency on the maximum stress and strain of the previous cycle implied that the loading and unloading curves were not unique. The Smith-Young expression was proposed for representing the envelope curve. Loading and unloading curves in a given cycle are approximated as second degree parabolas passing through 3 points: the point on the envelope curve where unloading starts (for the unloading curve) or reloading ends (for the reloading curve), the common point and the plastic strain point. In order to define the curves this way a series of relationships were derived based on the experimental data. A relationship between the coordinates of common points as a function of the stress and strain at the peak of the previous cycle was developed, as well as three additional equations which show the relationship between plastic strains and each one of the following variables: (1) strains at common points, (2) strains at intersections of reloading curves with the envelope and (3) strains at intersections ofunloading curves with the envelope. Figure 2.10 shows the relationship between envelope strains and plastic strains.

The expressions derived by Karsan and Jirsa predict the behavior of concrete under cyclic loading more accurately than those of Sinha et al. mainly because the loading and unloading curves are not considered unique.

Karsan and Jirsa performed tests for evaluating the number of cycles to failure for cycles between fixed maximum and minimum stress levels. Experimental results and computed curves based on their expressions are shown in Figs. 2.11 and 2.12. Fig. 2.11 shows the

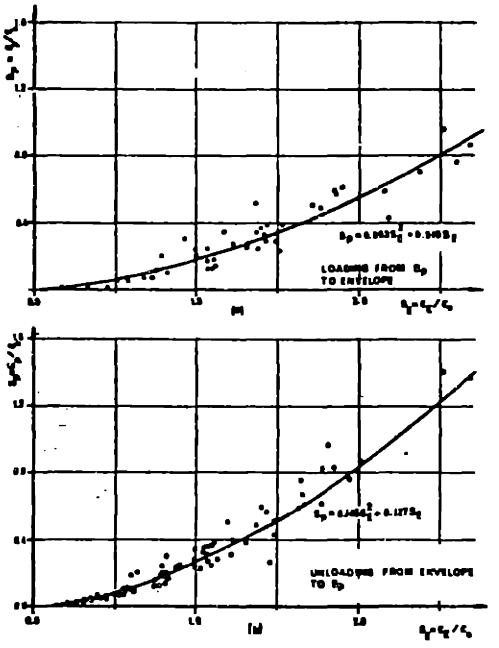

Fig. 2.10 - Relationship Between Envelope Strains and Plastic Strains

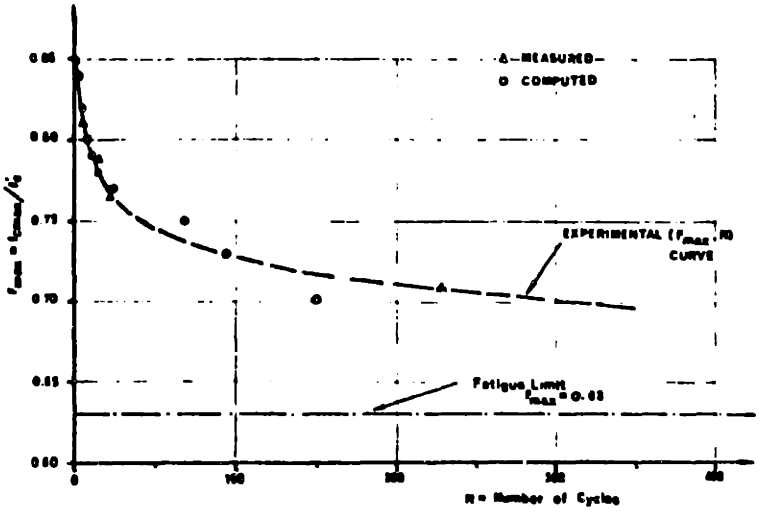

Fig. 2.11 - Number of Cycles to Failure (F_{max} = constant, F_{min} = 0)

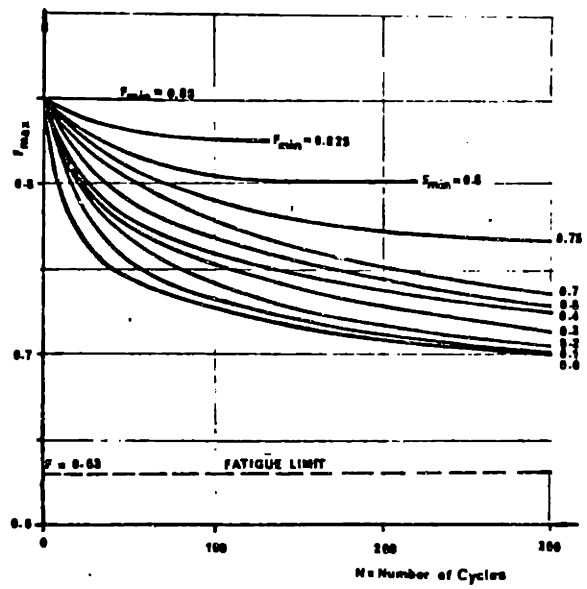

Fig. 2.12 - Number of Cycles to Failure (F_{max} = constant, $F_{min} \neq 0$)

number of cycles to failure for specimens cycled between zero minimum stress and given values of maximum stress. For a maximum stress of 0.77 f'_c the specimen failed in cycle 21 and failure was predicted in cycle 25 with the expressions proposed by Karsan and Jirsa. Assuming uniqueness of the stress strain curve, the expressions proposed by Sinha et al. predict failure after only 3 cycles. Here we see how grossly inaccurate these expressions are, which stems primarily from the uniqueness assumptions.

As seen in Figs. 2.11 and 2.12, for a given minimum stress level the number of cycles to failure decreases with increasing maximum stress.

2.1.5 Failure Mechanism

Experimental work by Shah and Chandra (13) provides a very interesting insight into the deformation behavior and failure mechanisms of concrete under uniaxial cyclic loading.

Shah and Chandra cycled both sealed paste and concrete specimens between given maximum and minimum stress levels. The minimum stress was always 10 percent of the short term strength. Maximum stress levels were 60, 70, 80 and 90 percent of the short term monotonic strength. Specimens were cycled until failure or 1000 cycles, whichever came first. Tests were carried out at a faster rate than in the tests performed by Sinna et al. (15) and Karsan and Jirsa (7). The rate of loading was about 4 to 6 cycles per minute.

The volumetric strain curves for concrete specimens subjected to cyclic stress between 10 and 90 percent of the short term ultimate strength are shown in Fig. 2.13. Failure occured after 17 cycles within a period of about 5 minutes. Each additional cycle caused volume dilation. As failure approached the rate of increase in volume dilation kept increasing as the number of cycles increased.

A similar mode of failure was observed for tests up to 80 percent of the ultimate stress. Paste specimens failed after about 157 cycles, while concrete specimens failed after 82 cycles. Incremental strains at the maximum stress level during cyclic loading are shown in Fig. 2.14. Incremental compressive strains for concrete and paste specimens were similar throughout the whole test. Incremental tensile strains for concrete specimens were as much as 6 times those for paste at failure stages. Consequently, the volume of paste specimens consolidated until failure while concrete specimens exhibited a large increase in volume before failure.

From this part of the investigation Shah and Chandra concluded that failure of concrete under cyclic stresses is caused by progressive internal microcracking rather than viscous flow of the paste. Lateral tensile strains and volumetric strains were seen to increase at a lower rate at the beginning (Stage 1) and at a faster rate towards the end (Stage 2). It was concluded that the composite nature of concrete plays a dominant role in the mode of cyclic failure because stone specimens exhibited no appreciable volumetric strains when subjected to comparable cyclic loading, while paste specimens showed volume consolidation under this type of loading.

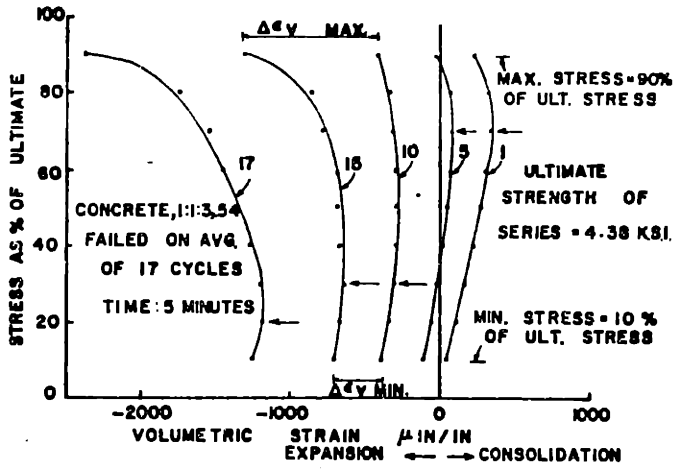

Fig. 2.13 - Volumetric Strains

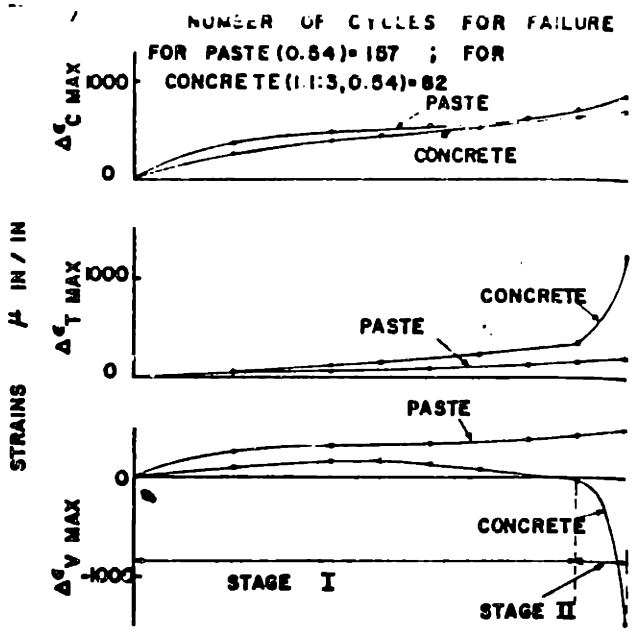

Fig. 2.14 - Behavior of Paste and Concrete Specimens that Failed Under Cyclic Load

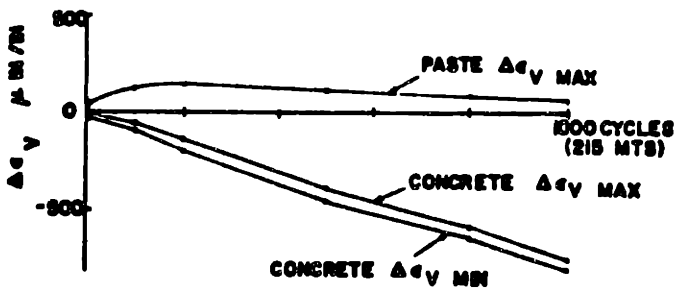

Fig. 2.15 - Behavior of Paste and Concrete Specimens Which Did Not Fail Under Cyclic Load

For cycles up to 60 and 70 percent of ultimate stress, failure did not occur after 1000 cycles. Concrete specimens showed a continuous and significant incremental volume expansion under the cyclic stresses, while incremental volumetric strains for paste specimens showed a slight tendency toward volume dilation. See Fig. 2.15. The shape of the incremental volumetric strain curve was similar to the first stage of the curves when specimens failed (Stage 1, Fig. 2.14).

Volume dilation observed in the stress-strain curves was an indicator of internal microcracking under cyclic loading. Shah and Chandra confirmed the existence of internal microcrack propagation by other means such as ultrasonic measurements and direct microscopic examination of specimens at different stages in their loading history. Two stages of crack growth were observed, corresponding to the two stages of volumetric expansion shown in Fig. 2.14. For stress levels of 70 percent and below, during which failure did not occur within the test period, a fairly stable and relatively small rate of crack growth was observed (Stage 1). This stage is externally characterized by an almost constant rate of incremental volume dilation. Stage 2 crack growth was associated with the specimens which failed (stress level of 80 percent or higher) and was characterized by a rapid increase in cracking similar to that observed in failure under monotonically increasing load. This stage is externally characterized by an increasing rate of incremental volume dilation.

2.1.6 Experiments on Mortar Specimens

Up to date, microcracking originating at the aggregate-cement paste interface has been thought to play a vital role in the behavior and degradation processes of concrete under uniaxial cyclic and monotonic loading. However, recent investigations seem to downgrade the importance of microcracking. An investigation carried out by Maher and Darwin (10) shows that the behavior of mortar under uniaxial monotonic and cyclic loading is very similar to that of concrete. The degradation processes observed for concrete under cyclic loading, such as the progressive decrease in the reloading and unloading slopes, was also exhibited by the mortar specimens. This suggests that the nonlinear behavior of concrete under uniaxial monotonic and cyclic loading may be highly controlled by the nonlinear behavior of mortar, rather than microcracking at the aggregate-cement paste interface.

2.2 Biaxial Monotonic Loading

There have been numerous investigations into the behavior of concrete under biaxial compressive stress. However, these investigations have dealt with biaxial monotonic loading, while the behavior of concrete under biaxial cyclic stress has not been investigated. This section presents the basic characteristics of the behavior of concrete under biaxial monotonic stress.

Test results vary considerably from one investigation to another, due mainly to the difficulties in developing a well-defined biaxial stress state. Different techniques have been utilized for creating

biaxial stress states on concrete. Biaxial compressive stresses $\sigma_1=\sigma_2$ can be generated by subjecting a cylindrical specimen to hydrostatic pressure in radial directions. Another technique consists in subjecting hollow cylinders to external pressure and axial compression. The most recent and popular technique consists in subjecting square concrete plates to in-plane loading (4,8,9,17). In these recent investigations brush bearing platens have been used for transmitting the loads to the specimen. The 'bristles' of the brushes consist of thin steel rods or plates and are capable of following the deformations of the concrete thereby exerting no restraint on the specimen.

In practically all biaxial compressive tests performed up to date the principal stresses have been made to increase proportionally at given stress ratios. Very little information on the behavior of concrete under biaxial nonproportional monotonic loading is available. Following is a brief review of the basic results obtained in recent biaxial tests.

2.2.1 Stress-Strain Behavior

Figs. 2.16 and 2.17 show the stress strain curves obtained by Kupfer et al. (8) for concrete subjected to biaxial compression at three different stress ratios. Fig. 2.16 shows the relationship between the three principal strains ε_1, ε_2 and ε_3, and the major principal stress σ_1, while Fig. 2.17 shows the relationship between the volumetric strain ε_v and the principal stress σ_1. The biaxial curves resemble the corresponding curves in uniaxial compression. Fig. 2.16 shows that

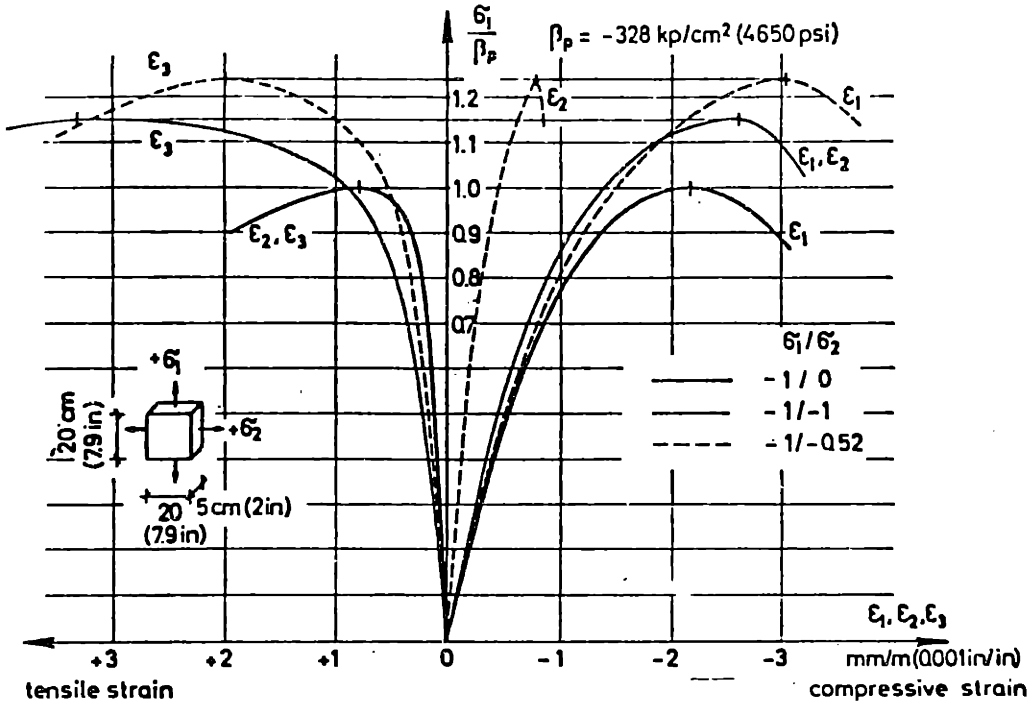

Fig. 2.16 - Stress-Strain Relationships of Concrete Under Biaxial Compression

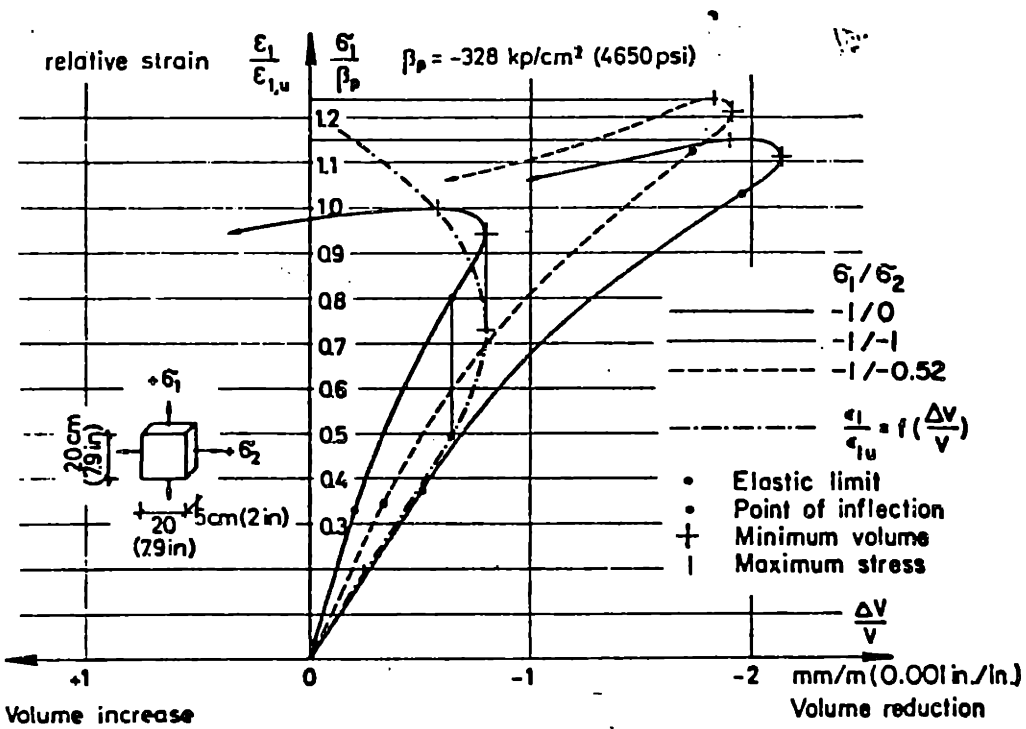

Fig. 2.17 - Volumetric Strain of Concrete Under Biaxial Compression

the stiffness of concrete in the σ_1 principal stress direction is increased by the existence of compressive stress in the σ_2 direction. In Fig. 2.17, the σ_1-ε_v curves deviate from linearity at about one third of the ultimate strength and acquire a downward concave curvature, thus revealing an increase in the rate of volumetric reduction. At about 80% or 90% of the strength the curve shows an inflection point and soon after, the concrete specimen starts dilating at the point of minimum volume. This phenomenon known as shear dilatancy has been attributed to microcracking in the third direction which is free of stress.

2.2.2 Stresses and Strains at Failure

The strength of concrete subjected to biaxial compression is significantly higher than that of concrete under uniaxial compression. The strength increase under biaxial compression is dependent on the principal stress ratio. According to the results of most investigations the maximum increase in strength occurs at a stress ratio $\sigma_1/\sigma_2 = 0.5$. However, the magnitude of this increase varies from one investigation to another. For example, Kupfer et al. (8) observed a maximum strength 27 percent higher than the uniaxial strength, for unrestrained specimens. For similar specimens, Liu et al. (9) observed a maximum strength 20 percent higher than the uniaxial strength. The stress failure envelope obtained by Kupfer et al. for concrete under biaxial compression is shown in Fig. 2.18. The stress failure envelopes obtained by Liu et al. and other investigators for this type of loading are quite similar.

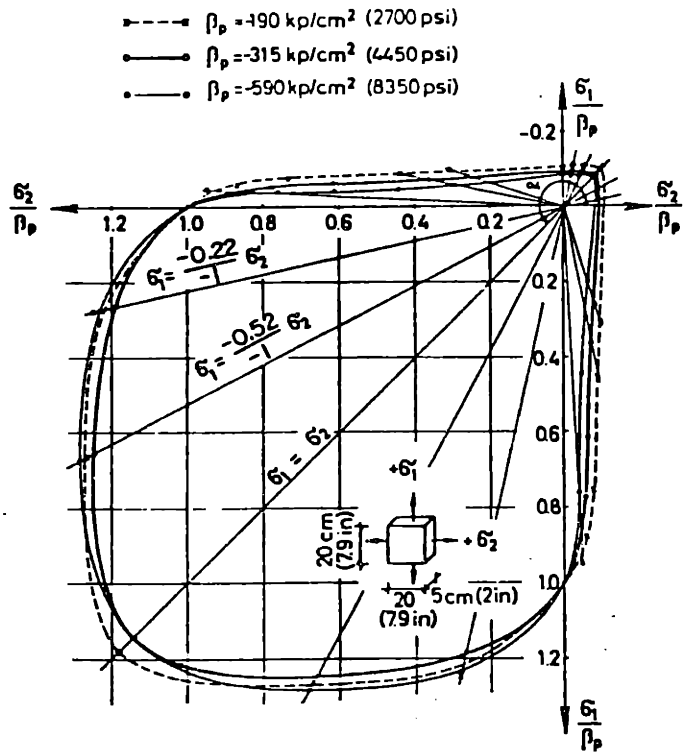

Fig. 2.18 - Biaxial Strength of Concrete

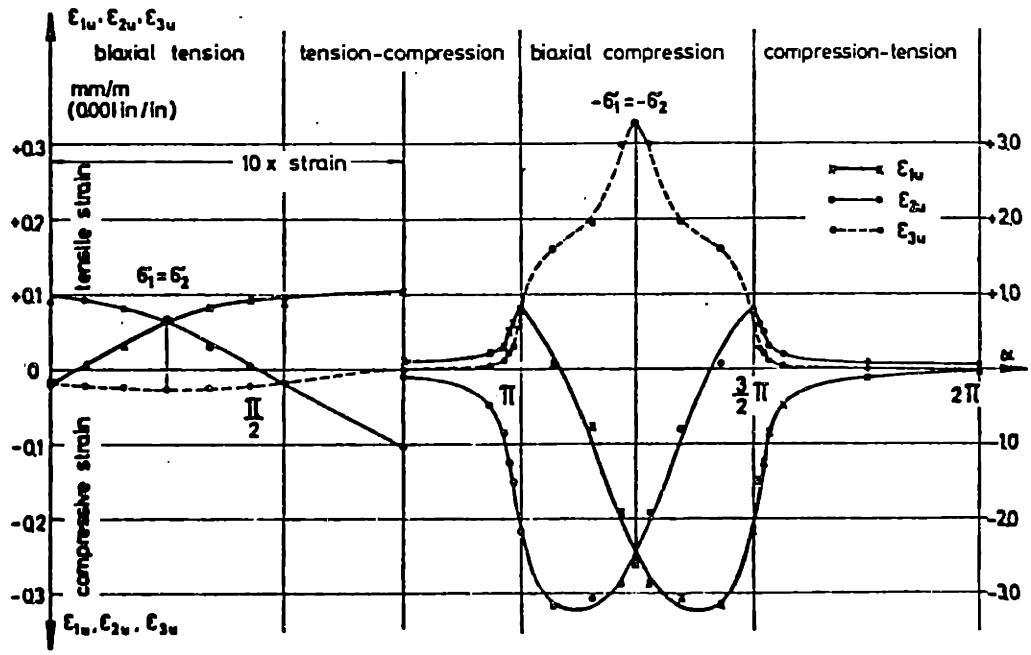

Fig. 2.19 - Failure Strains of Concrete Under Biaxial Stress States

The increase in strength and stiffness under biaxial compression has been mainly attributed to microcrack confinement in the plane of loading.

Major principal compressive strains at failure under biaxial compression are higher than in uniaxial compression. From Fig. 2.16 it is seen that the strains in the direction of the larger principal stress increase in magnitude as the stress at failure increases in magnitude. Fig. 2.19 shows the failure strains of concrete under biaxial compression as a function of the principal stress ratio, according to the tests performed by Kupfer et al. (8). At a stress ratio of 0.52, for which the maximum strength is obtained, the strain in the direction of the larger principal stress is about 36% higher than the principal compressive strain at failure in uniaxial compression, and may be considered practically the highest compressive strain at failure under biaxial loading. From the figure it is seen that the tensile strain at failure in the direction normal to the free surface of the specimen increases with the stress ratio.

2.2.3 Modes of Failure

For square concrete plates, failure in uniaxial compression occurs by splitting in the plane parallel to the load and perpendicular to the face of the specimen. Under biaxial compression failure cannot occur by separation along the line of the major load since in-plane transverse strains are prevented. Failure then occurs by splitting along planes parallel to the free surface of the specimen. However, shear modes of failure under biaxial compression have been observed by other investigators (12).

CHAPTER 3

EXPERIMENTAL PROGRAM

Square concrete plates were subjected to uniaxial and biaxial cyclic and monotonic loading. In the biaxial tests, specimens confined along the horizontal direction were subjected to cyclic or monotonic loads in the vertical direction.

This chapter describes the test specimens and equipment utilized in the investigation, as well as types of tests performed and experimental techniques.

3.1 Test Specimens

The test specimens used in the investigation were square concrete plates measuring 5" x 5" x 1". The specimens were prepared following the ANSI/ASTM C 192-76 "Standard Method of Making and Curing Concrete Test Specimens in the Laboratory".

The concrete was a blend of Type III Portland cement, Walbro pea gravel, sand and water in the following proportions by weight: water/cement = 0.67, sand/cement = 2.5 and gravel/cement = 3.5.

The concrete mix proportions were constant for all specimens.

U.S. standard sieves were used for controlling aggregate sizes. Gravel passing through the #3 sieve and retained by the #8 sieve, sand passing through the #8 sieve and cement passing through the #16 sieve were used in the mix. The maximum gravel size was 0.263 in., which is less than one third of the minimum cross-sectional dimension of the specimen (1"), as required by the ASTM Standard.

Mixing was done by hand, after which the concrete was poured into the casting molds. The molds consisted of thin plexiglass members screwed together forming 6 independent square frames, which were horizontally mounted onto 2 long rectangular plexiglass base plates (3 frames per base plate). Therefore, 6 specimens could be cast at a time. Once the concrete was poured into the molds, these were clamped on to a vibrating table which was then activated, thereby compacting the concrete. After vibration the concrete surfaces were finished with a wood float. To prevent evaporation of water from the unhardened concrete, the molds were covered with thin square plexiglass plates, after finishing the surfaces. The specimens were left to set at room temperature, and removed from the molds 20 hours later, after which they were immersed in water for approximately 3 1/2 days. The specimens were then allowed to dry for at least 12 hours at room temperature before they were prepared for strain gage installation.

The rough surfaces (those finished with the wood float) were sanded, marked and coated with EPY-150 adhesive in the area where the strain gages were to be installed, in order to provide a smooth, non-porous bonding surface. The adhesive was allowed to cure for about 5 hours before the strain gages were installed following the SR-4 application instructions. The gages were glued on to the specimen with EPY-150 Adhesive, which has a pot life of 30 minutes, cures in 12-16 hours at room temperature and has a strain limit of more than 10% at room temperature. 2 gages parallel to the vertical and horizontal directions were mounted on each square surface. Strain gage installation

took approximately 5 hours. The adhesive was allowed to cure for at least 12 hours before the lead wires were soldered to the strain gages. The wiring process took approximately 5 hours. At the seventh day after casting, the specimens were ready for testing.

Since only 6 specimens could be cast at a time, and in occasions additional specimens were needed because of tests which did not produce valid data due to test system, test equipment or operator error, a procedure was devised for having 9 specimens available for testing at a given time. The procedure consisted in casting a follow-up secondary batch (3 specimens) the day after the principal batch (6 specimens) had been cast. This batch was prepared in exactly the same way and tested at the same age as the principal batch, so that the properties of both batches coincided as much as possible at the time of testing. The secondary specimens proved extremely useful because, when not used as replacement for principal specimens, they were tested to provide additional or complementary information for a given test series.

3.2 Experimental Setup

3.2.1 Loading Equipment

A. The Automated Materials Testing System

Loading in the vertical direction was accomplished by use of the Automated Materials Testing System, hereafter referred to as the MTS. The MTS is a hydraulically operated axial test machine which can be operated manually or via an accompanying PDP-11 computer. In the

present investigation, the MTS was controlled manually because the computer was not available.

Following is a brief description of MTS components and their function in relation to the testing operation.

The MTS components considered here are:

1) Hydraulic Power Supply and Actuator
2) Load Frame
3) Transducers and Transducer Conditioners
4) Feedback Selector
5) Servo Controller
6) Digital Function Generator
7) Digital Indicator
8) Master Control Panel
9) MTS Recorder Input Controls

1) Hydraulic Power Supply and Actuator

The hydraulic power supply provides a source of hydraulic fluid under pressure for the system. The hydraulic power supply and the rest of the system are located in two different rooms. The Hydraulic Actuator is the force generating and/or positioning device in the system. Fluid under pressure coming from the hydraulic supply, is applied to one side of the piston causing it to move. The piston rod or ram is capable of applying a maximum tensile or compressive force of 50 metric tons. It's internally threaded, thus permitting a loading grip or adapter to be screwed on to it. The Hydraulic Actuator is contained in the Load Frame.

2) Load Frame

The MTS Load Frame has 4 steel columns, on which a crosshead is mounted. The crosshead position is adjustable in order to provide necessary space for the loading grips and the specimen. A loading grip can be screwed onto the load cell, which in turn is mounted on the crosshead. During a test, the actuator's ram moves while the crosshead remains static, thus imposing a given deformation and, therefore, load on the specimen.

3) Transducers and Transducer Conditioners

Transducers sense some quantity generated by the Hydraulic Actuator, such as force or linear displacement (piston stroke), and provide an output signal which represents that quantity.

The MTS load cell is a force measuring transducer that provides an output voltage having a magnitude in direct proportion to the amount of applied force. If a compressive force is applied to the cell, the output voltage is negative; a tensile force produces a positive output. Thus, the output voltage of the load cell contains information about the amount and direction of the applied force.

The Hydraulic Actuator is supplied with an internally mounted linear variable differential transformer (LVDT) to measure linear displacement.

The Transducer Conditioners supply excitation voltages to their respective transducers and condition the transducer output voltages to d-c levels suitable for use in the control portion of the system.

The conditioner units are located behind the 442 Controller panel. Each one has a Range and Zero control. The Range switch position determines the quantity of the associated variable required to produce a full-scale output signal (± 10 volts) from the Transducer Conditioner. This quantity is the operating range of the system when the conditioner is used to control the system. The 10 volt output may be used for readout as well as for system control. The quantity corresponding to the Range switch position is indicated in the main front panel (the 442 Controller panel). The Zero control introduces an electrical offset into the control loop to shift the zero or reference position of the transducer.

4) Feedback Selector

The Feedback Selector is used to select the output of a particular Transducer Conditioner for use in controlling the Hydraulic Actuator. Thus, either the force applied by the Actuator or the position of the Actuator piston can be controlled.

The Feedback Selector unit is located behind the 442 Controller panel. The Remote/Local switch on the selector selects the method of mode transfer. With the switch set to Remote position, mode transfer is accomplished by an external programming device. With the switch in the Local Position, the variable to be controlled (load, strain, or stroke) is selected by pressing the appropriate Feedback Selector button located on the 442 Controller panel. When a Feedback Select button in pressed its indicator will light.

The signal selected at the Feedback Selector is applied to the summing junction in the Servo Controller.

5) Servo Controller

The main function of the Servo Controller is to accept and compare its two main inputs, command and feedback, and to provide an output, called the error signal, which is proportional to the difference between the two inputs. The command signal, which is controlled by the Set Point and Span controls, represents the desired value of the controlled variable (load, stroke, etc.). The feedback represents the actual value as sensed by the transducer in the control loop. If the two are not equal, the resultant error signal opens the Servovalve in a direction and by an amount which causes the Actuator to correct the error. When command and feedback are equal, the error signal is reduced to zero and the Servovalve closes. The system is then in a system of equilibrium or a "null balanced" condition.

The Servo Controller unit is located behind the 442 Controller panel. Its Set Point and Span controls are both located on the Controller panel. The Set Point control provides a precise static command that adds algebraically with any dynamic commands being used. It is used to adjust the controlled variable to a particular level within the system's range of operation. Scaling is from -100% of system operating range (000 on the dial) through zero (500 on the dial). to +100% of range (1000 on the dial). Each 5 dial divisions above or below 500 add + or - 1%, respectively, to the Set Point level. The

Set Point Control is usually adjusted to zero level (500 on the dial) for automated tests.

The Span(s) control(s) are used to adjust the amplitude of command signals originating in the Function Generator or other external programming devices. The Span controls are calibrated so that the peaks of the input function drive the controlled variable to 100% of operating range when the control is set to 1000.

The DC Error position of the Meter switch allows the output of the Servo Controller (difference between command and feedback) to be indicated on the meter. It is used when adjusting the Error and Null Detectors and during hydraulic turn-on. When the meter is at null (centered), command and feedback are equal.

The Error Detector indicators light if system error exceeds their present thresholds. Pressing the Interlock Reset switch resets the Error Detectors.

6) Digital Function Generator

The Digital Function Generator provides dynamic command signals to the Servo Controller which allow the controlled variable (load, strain or stroke) to be varied in different prescribed ways with respect to time.

The panel containing the controls of the Digital Function Generator is above the 442 Controller panel. The function of the basic controls is explained briefly below.

a) Mode Switch

The Mode Switch provides for selection of one of the following control modes:

i) Remote position, used when operating with the computer.

ii) Local position, used when operating manually. Waveform output is started by pressing the Start pushbutton. The output will be continuous unless stopped by depressing the Stop at Zero, Return to Zero or Hold pushbuttons.

iii) Single Cycle position, used also when operating manually. Depressing the Start pushbutton provides a single cycle of the selected output waveform.

b) Local Stop Controls

i) Stop at Zero

If, during continuous operation in Local mode, the Stop at Zero button is depressed, the Generator will cease operation upon completion of the current cycle of the selected function. Completion of the current cycle will occur at the frequency determined by Rate 1 (for Sine and Square functions) or at rate(s) determined by Rate 1 and Rate 2 (for Ramp functions).

ii) Return to Zero

If, during continuous operation in local mode, the Return to Zero button is pressed, the generator will complete the current half-cycle of the selected Sine or Square

function or, for Ramp functions, will immediately return to zero reference at Rate 2 rate.

iii) Hold

The Hold button, when depressed, causes the waveform to hold at its current instantaneous level regardless of the function.

c) Output Zero

The Output Zero indicator lights whenever the selected function is at zero reference or the generator is in a stop condition.

d) Output Selector

The five output selector switches determine which of the following functions is to be generated: Ramp, Sine, Haver Sine, Haver Square. Depressing the Invert pushbutton and selecting one of the above functions inverts the selected function about zero reference.

The Ramp function may be combined in different ways by using the Ramp control and Breakpoint control switches.

e) Rate 1 and Rate 2

The Rate 1 switch provides frequency selection (in hz) for Sine, Haver Sine, and Haver Square functions, and time selection (in sec.) for the Ramp function. This is the time required for the controlled variable to reach 100% of operating range starting from zero reference. The Rate 2 switch also provides time selection for the Ramp function and is used with Stop to Zero, Return to Zero, Ramp control and Breakpoint control switches.

7) Digital Indicator

The MTS Digital Indicator is used as a readout device to monitor and display the voltage on one of five selectable inputs. It is located above the Digital Function Generator on the MTS Console.

The Input Select control determines which input will be monitored. Positions 1,2,3 and 4 are connected to the outputs of the system's Load, Strain and Stroke Transducer Conditioners, and the system's program source, respectively. The Input Range control selects one of the Indicator's two input ranges, 20V (0 to ± 19.99V) or 2V (0 to ± 1.999V).

8) Control Panel

The Control Panel, which is localized below the 442 Controller panel, provides centralized manual and automatic control of the following system functions: console power on/off, hydraulic pressure on/off, and the simultaneous starting and stopping of programmers and recorders.

The Panel also includes an interlock circuit which depends on normal/abnormal condition sensors, located throughout the system, to remain in a normal or "reset condition". If an abnormal condition is detected by any sensor, the interlock opens and removes hydraulic pressure from the system and also stops all programmers and recorders. In this case, the Reset pushbutton is lit, and must be pressed after correcting the abnormal condition or during normal system turn-on, in order to reset the interlock. Once this is done, hydraulic pressure may be applied to the system by pressing the Hydraulic Pressure switch. Hydraulic pressure may be removed by pressing Emergency Stop or Hydraulic Off switches.

9) MTS Recorder Input Controls

These controls are located on the 442 Controller panel. They consist of three dual-concentric switches, one switch for each input of an X-Y-Y Recorder. The Y_1 switch is not connected to the X-Y Recorder. The Load, Strain and Stroke positions of the outer concentric switch select the outputs of the Load, Strain and Stroke Transducer Conditioner Modules (±10 volts full scale). The Prog position selects the voltage signal corresponding to the variable being controlled during the test.

The inner concentric switch has the following positions: Off, - (minus), and + (plus). Off disconnects the selected signal, (-) reverses the polarity of the incoming signal and (+) does not change the polarity of the incoming signal.

B. Lateral Loading Frame

A rigid loading frame was constructed for applying loads in the horizontal direction. The frame is independent of MTS, and consists of the following.

2 vertical rectangular steel plates are welded to a horizontal rectangular base plate. Nine stiffening steel buttresses (5 for one plate and 4 for the other) are welded to both the vertical steel plates and the horizontal base plate. The buttresses are trapezoidal in form with the large base in contact with the base plate. Two threaded steel rods extend between the vertical rectangular plates. At each end they are fixed near the top of the plates by nuts and washers. The function of these rods is to increase the stiffness of the frame by reducing the displacements at specimen level due mainly to bending of the base plate.

The whole setup is supported by two aluminum I beams which are bolted to the horizontal base plate. Load is applied by means of a manually operated Duff Norton screw jack, model 1815, which has a capacity of 15 tons (≈ 33000 lb). A mechanical jack, instead of a hydraulic one, was chosen mainly because of its capability of holding loads in position without creep. The jack is an upright screw type with top plate end. The plate end has 4 equally spaced holes, two of which were used for fixing the loading brush to the jack. The lifting screw is keyed in order to prevent rotation during travel. The maximum raise or travel is 8 inches, though for this test, much less than that was required. The worm gear ratio for the jack was 24:1 (48 turns of worm for 1" raise). Such a worm gear ratio, which is smaller than the standard ratio (8:1), was chosen in order to apply and control the loading in a more precise manner. The screw jack is manually operated by a rotating handle which has an aluminum tube that fits onto the worm of the jack. The screw jack is fixed to one of the vertical rectangular plates.

The load was measured by a cylindrical aluminum load cell, which was fixed to the opposite rectangular plate. The load cell has attached strain gages and was properly calibrated so that the load values could be read on a digital strain indicator to which the gages were connected. The load signal registered by the indicator was sent to an X-Y Recorder, which plotted the values of lateral load occuring during a test. Such a procedure would have been impossible to follow if using a self contained load cell unit, where readings must be done manually by looking at a gage connected to the cell. After the test, the values would have to be

plotted, either by hand or using a computer with a plotting device. Such a procedure would be both inaccurate and time consuming. It is for these reasons that a load cell with strain gages was used. The strain gages were wired in a full bridge configuration.

The loading frame was transported to the testing site on a wagon and was placed on the MTS Load Frame platform with a crane. Four high strength wire cables clipped around shackles at both ends were used for lifting the frame. At one end the shackles were fixed to the top of the vertical rectangular plates (2 per plate) and, at the other end, all four shackles mounted onto a steel ring, which was then mounted onto the crane's hook. The frame was lifted to a given height, slided between MTS Load Frame columns into position, and then lowered onto some wooden blocks which lay on the MTS platform. The lateral loading frame was finally clamped down by using 'U' shaped clamps. The 'U' clamp was placed so that its legs rest on the aluminum beam flange and the portion near the junction rest on a small wooden block lying on the MTS platform. A long bolt was then driven between the 'U' legs and into one of the bolt circle holes in the MTS platform. Finally a nut was screwed onto the top end of the bolt and tightened until it applied pressure on the clamp, which in turn exerted pressure on the aluminum beam. This clamping procedure was followed for each one of the two aluminum beams.

A photograph of the lateral loading frame mounted on the MTS Load Frame platform is shown in Fig. 3.2. Drawings and detailing of the lateral loading frame are shown in Figs. 3.3 and 3.4.

Brushes and Adapters

The steel loading heads in contact with the 4 edges of the concrete specimens are brush-like devices with thin steel plates constituting the bristles. The bristles are flexible enough to deform laterally under applied pressure, thereby exerting no restraining lateral force on the concrete. The buckling strength of the bristles is such that the compression stresses are effectively transmitted to the concrete specimen. The brushes used in this investigation were those used before in other investigations conducted at Cornell University by Buyukozturk, Nilson and Slate (4).

The vertical loading brushes were mounted on adapters which then were screwed onto the MTS loading ram and load cell and secured into position by counterbolts. The lower brush adapter screwed to the loading ram passes through a hole in the base plate of the lateral loading frame. A swivel mechanism using a steel ball bearing was implemented for the upper vertical brush. This allowed the brush to align properly with the concrete surface during loading.

One of the horizontal loading brushes was mounted to the top plate end of the screw jack's lifting screw. The other brush was mounted on an adapter which screwed onto the load cell. This brush was also equipped with a swivel mechanism which consisted of a steel ball bearing seated between the brush and the adapter.

Fig. 3.5 shows a photograph of the brush loading platens.

3.2.2 Auxiliary Equipment and Recording Circuits

A. Strain Gages

Strain measurements in the vertical and horizontal directions were taken by means of strain gages type FAE-100N-12-SX. These are narrow grid foil gages with a polymide carrier and have a resistance of 120 ohms ± 0.2. The overall length of the gage is 1.20 inches. The suffix SX in the type nomination should be replaced by the appropriate temperature compensation number and option. Most gages had the suffix nomination 'S6EL', where 6 is the temperature compensation number and EL stands for the encapulated with leads option. The gage factor for this strain gage is GF = 2.04 ± 1%. Other gages had different temperature compensation numbers and options, and therefore different gage factors. Nevertheless the effect of the temperature compensation number is neligible since all tests were carried out at room temperature. Gages with different compensation numbers and options were used because of the unavailability of only one gage type.

For testing concrete the general rule is that the gage length be at least three times the size of the maximum aggregate. Since, the maximum aggregate measured about 0.30 in. and the grid length was 0.90 in., the requirement was satisfied. This avoids the possibility of strain gage detachment due to local failure of the aggregate or aggregate-cement paste bond.

Two gages per direction, wired in series and attached to opposite sides of the specimen, were used for measuring strains in the vertical and horizontal directions. This procedure eliminates recording of bending

strains by averaging the strains on both sides of the specimen. Vertical gages were attached near the center of the specimen, while horizontal gages were attached near the bottom, midway between the two vertical edges of the specimen. See Fig. 3.6.

The vertical and horizontal strain measurement circuits were each arranged as a half-bridge configuration consisting of two active and two dummy or compensating gages. The active gages were those attached to the test specimen, while the compensating gages were those attached to an identical but unstressed concrete specimen. The two compensating gages per direction were also wired in series and attached to the specimen in exactly the same way as the active gages. Thus, the dummy specimen for one test was later used as the test specimen for another test. The half-bridge configuration employed in the experiments had the advantage of minimizing temperature effect on strain measurements.

B. Monitoring and Plotting Equipment

Monitoring and plotting equipment included 3 digital strain indicators, 2 X-Y Recorders, and the MTS X-Y Recorder.

One of the strain indicators is a BLH 1200A model and the other two are BLH 1200B models. The three indicators were used indistinctly for measuring vertical strain, horizontal strain and horizontal load. The vertical load, applied by the MTS, was measured by the MTS load cell and internal system.

The strain indicator amplifies and measures the milivolt per volt output of strain gages and displays it in microinches per inch.

Input to the indicator was either a half-bridge configuration (for strain measurements) or a full bridge configuration (for horizontal load measurements). A grouping of three pushbuttons allow the instrument to be set for the correct bridge configuration in use. Initial gage bridge unbalance is cancelled with the Coarse and Fine Bridge Balance controls. The gage factor of the gage(s) being used (as specified by the manufacturer) is set into the instrument with the Coarse and Fine Gage Factor switches. Gages are connected to color-coded three way terminal posts.

The lead wires used for the strain measurement circuits were type STC-26V, which have an approximate resistance of 0.04 ohms/ft at 70°F. Since the length of the lead wires was small the effect of lead wire resistance on strain measurements was negligible and therefore, the Gage Factor control was not adjusted. Lead wires of the same length were located sufficiently close together to insure self-cancellation of temperature induced resistance changes.

All indicators are equipped with a Dynamic Output scope jack, which permits output of the corresponding analog signal to X-Y Recorders. Output is approximately ± 1.0V for 10000 microinches per inch.

Plotting was done by the MTS X-Y Recorder and two Houston Instrument, Series 2000, Omnigraphic X-Y Recorders. The Recorders plot the functional relationship between two external analog inputs and may be calibrated to one's choice by properly setting the voltage sensitivity knobs.

For vertical strain measurements two parallel circuits were connected to the strain indicator through the scope jack. One circuit connected to an X-Y Recorder, and the other connected to the MTS, for plotting on the MTS X-Y Recorder. Thus, two plots involving vertical strain were obtained for each test. The horizontal strain and horizontal load, when recorded, were plotted on the independent X-Y Recorders, whereas the vertical load was plotted on the MTS Recorder.

Depending on the type of test, one of the following plotting arrangements was used:

1) Uniaxial Test — Vertical load versus vertical strain on MTS Recorder, and vertical versus horizontal strain on X-Y Recorder

2) Biaxial Test — Vertical load versus vertical strain on MTS Recorder, and horizontal load versus vertical strain on X-Y Recorder

The recording circuits for each of the two cases are shown schematically in Figs. 3.7 and 3.8.

In some occasions, plotting arrangement '2' was complemented by a vertical versus horizontal load plot on an X-Y Recorder. In this case, a circuit in parallel with the existing one was connected to the horizontal load indicator through the scope jack. This circuit transmitted the horizontal load signal to an X-Y Recorder, which on the other hand, received the vertical load signal from the MTS Load Transducer Conditioner output.

3.3 Types of Tests

Biaxial testing was accomplished by subjecting square concrete plates to in-plane loading along the vertical and horizontal directions. In such a procedure, whether doing cyclic or morotonic tests, the four basic variables to be considered are the vertical and horizontal stresses and strains. The kind of biaxial test will depend on how these variables are controlled throughout the test (for example, constant horizontal strain, constant stress ratio, etc.). Thus, there may be different kinds of biaxial tests. In the present investigation, the biaxial testing procedure consisted in loading vertically while keeping the horizontal strain constant and equal to a prescribed value. These tests are referred to, in the present context, as "confined tests", meaning biaxial tests carried out at constant lateral (horizontal) strain. Most confined tests were cyclic but also some were monotonic. It is important to notice that, in the cyclic case, the confined test is actually a biaxial cyclic test in the sense that, as the vertical stress increases and decreases, the horizontal stress also increases and decreases. This is due to the Poisson effect. Under vertical loading the specimen tends to expand laterally, but cannot do so due to the confinement. Consequently, there is an increase in horizontal stress to compensate for the effect. When the specimen is unloaded vertically, its tendency to expand laterally decreases, thus leading to a decrease in horizontal stress.

A total of 30 specimens were tested in four different series:

1) Monotonic Loading to Failure
2) Cycles to the Envelope Curve
3) Cycles to Prescribed Values of Vertical Stress
4) Cycles Between Fixed Maximum and Minimum Stresses

Each Test Series was performed on both unconfined specimens and specimens under different levels of confinement, in order to assess the effects of confinement on the behavior of concrete for the given Test Series. Levels of confinement refer to values of constant lateral (horizontal) strain. In general, the imposed values of constant lateral strain in each Series were those corresponding to loads of about 20%, 40%, and 60% of the concrete compressive strength. Such a strength was determined by performing simple uniaxial compression tests on 2 or more specimens of the batch and averaging the individual strength values. All the specimens of a given batch (principal plus secondary) were subjected in general to the same Test Series.

The notation for specimens is of the form X. Y, where X denotes the batch number, and Y denotes the individual specimen number within the X batch. A 'prime' to the right of the batch number X is used for denoting the corresponding secondary batch. For example, specimen 4!3 is the third specimen of the secondary batch 4!

Besides from the vertical stress-vertical strain curve obtained in all tests, the interactions between vertical strain and horizontal strain in unconfined tests, and horizontal stress and vertical strain in confined tests, were also recorded. Thus, complete stress-strain histories were obtained in each test.

Following is a description of each Test Series. In the individual test description for each Test Series, '$\sigma_{h\ in}$' is the value of horizontal stress applied to the specimen before loading vertically and 'ε_{hc}' is the corresponding value of horizontal strain, which was kept constant while vertical load was applied. 'F_c'' and 'ε_o' are the stress and strain at the peak of the uniaxial compression curve for the batch. Only those tests producing applicable data are listed.

3.3.1 Series 1 - Monotonic Loading to Failure

Both confined and unconfined specimens were tested monotonically to failure by progressively increasing the vertical strain, while keeping the horizontal strain constant in the case of confined tests. In these tests, the horizontal stress increases due to the confinement and, therefore, both vertical and horizontal stresses increase monotonically. It should be noted, however, that these types of biaxial tests are in essence different to those which have been carried out by other investigators, because the ratio of vertical to horizontal stress is not kept constant throughout the test. Thus, a new type of biaxial monotonic loading history is introduced, which allows to establish the effect of uniaxial confinement on the stress-strain behavior of concrete subjected to monotonic loading.

The individual tests carried out in this Series are shown below:

Specimen	Test
1.1	Unconfined Monotonic
1.5*	Confined Monotonic $\sigma_{h\ in} = 0.07\ f'_c \quad \varepsilon_{hc} = 0.02\varepsilon_o$
2.1	Unconfined Monotonic
2.2	Unconfined Monotonic
2.3	Confined Monotonic $\sigma_{h\ in} = 0.40\ f'_c \quad \varepsilon_{hc} = 0.20\varepsilon_o$
2.4	Confined Monotonic $\sigma_{h\ in} = 0.60\ f'_c \quad \varepsilon_{hc} = 0.34\varepsilon_o$

*In this test ε_{hc} was not kept constant.

3.3.2 Series 2 - Cycles to the Envelope Curve

Previous investigators (7,15) have introduced the concept of the envelope curve in uniaxial cyclic loading as one to which eventually all stress-strain paths lead to upon increasing strain at any given point during the test. The envelope curve has been said to coincide with the simple monotonic stress strain curve (7,19). An envelope to the stress-strain curve for biaxial cyclic loading may also be defined.

The criterion for determining the point at which to unload in order to reach the envelope is as follows. Initially the specimen is loaded vertically up to a given value of vertical strain, then unloaded to zero and reloaded up to the point where the stress-strain path

would seem to be following the trend of the previous loading portion of the stress strain curve. Such a procedure is followed to the end until failure occurs. This same procedure was followed for both unconfined specimens and specimens under different levels of confinement.

The tests provide very interesting information regarding the behavior of concrete subjected to vertical stress cycles of progressively increasing amplitude, while confined at different levels of lateral strain. As explained before, the confined specimens were actually subjected to biaxial cyclic stresses and the complete stress-strain history was recorded. The effects of the confinement on the cyclic behavior may be established by comparison of the stress-strain curves, as well as envelopes, corresponding to the different confinement levels (including zero confinement).

The individual tests for this Series are:

Specimen	Test
4.1	Unconfined Monotonic
4.2	Unconfined Monotonic
4.1	Unconfined Monotonic
4.4	Unconfined Cyclic
4.5	Unconfined Cyclic
4.6	Confined Cyclic $\sigma_{h\ in} = 0.20\ f'_c$, $\varepsilon_{hc} = 0.08\varepsilon_o$
4.2	Confined Cyclic $\sigma_{h\ in} = 0.40\ f'_c$, $\varepsilon_{hc} = 0.15\varepsilon_o$
4.3	Confined Cyclic $\sigma_{h\ in} = 0.60\ f'_c$, $\varepsilon_{hc} = 0.27\varepsilon_o$

Specimen	Test
5.2	Unconfined Cyclic
5.3	Confined Cyclic $\sigma_{h\ in} = 0.18\ f'_c$, $\varepsilon_{hc} = 0.06\ \varepsilon_o$
5'2	Confined Cyclic $\sigma_{h\ in} = 0.37\ f'_c$, $\varepsilon_{hc} = 0.22\ \varepsilon_o$
5'3	Confined Cyclic $\sigma_{h\ in} = 0.55\ f'_c$, $\varepsilon_{hc} = 0.36\ \varepsilon_o$

The corresponding unconfined monotonic tests for Batches 5 and 5' were performed on specimens 5.1 and 5'1.

3.3.3 Series 3 - Cycles to Prescribed Values of Vertical Stress

Unconfined specimens and specimens under different levels of lateral confinement were all subjected to the same vertical stress history, after which the confined specimens were loaded monotonically to failure. The resulting stress-strain curves were studied and compared in order to assess the effect of confinement on strain accumulation.

The individual tests for this Series are shown in the following table.

Specimen	Test
5.1	Unconfined Monotonic
5!1	Unconfined Monotonic
5.2	Unconfined Cyclic
5.4	Confined Cyclic $\sigma_{h\ in} = 0.18\ f'_c$, $\varepsilon_{hc} = 0.06\varepsilon_o$
5.5	Confined Cyclic $\sigma_{h\ in} = 0.37\ f'_c$, $\varepsilon_{hc} = 0.17\varepsilon_o$
5.6	Confined Cyclic $\sigma_{h\ in} = 0.55\ f'_c$, $\varepsilon_{hc} = 0.27\varepsilon_o$

Note: Specimen 5.2 has been stated in Series 2 and 3 because it both defined an envelope curve and was used for setting the vertical stress history in Series 3.

3.3.4 Series 4 - Cycles Between Fixed Maximum and Minimum Stresses

Confined specimens were cycled between zero and constant maximum vertical stress levels a number of times equal to that required for failure of an unconfined specimen cycled between zero and a stress of $0.82\ f'_c$.

After the required number of cycles was performed, the confined specimens were loaded monotonically to failure. These tests provide useful information regarding the effects of confinement on stress-strain behavior of concrete subjected to repeated vertical stress cycles of constant amplitude.

The individual tests in this Series were the following:

Specimen	Test
6.1	Unconfined Monotonic
6'.1	Unconfined Monotonic
6.6	Unconfined Cyclic
6.3	Confined Cyclic $\sigma_{h\ in} = 0.24\ f'_c$, $\varepsilon_{hc} = 0.11\ \varepsilon_o$
6.4	Confined Cyclic $\sigma_{h\ in} = 0.48\ f'_c$, $\varepsilon_{hc} = 0.30\ \varepsilon_o$
6.5	Confined Cyclic $\sigma_{h\ in} = 0.72\ f'_c$, $\varepsilon_{hc} = 0.50\ \varepsilon_o$

3.4 Test Operation

This section describes the procedures followed in carrying out the tests, as well as the main problems encountered and how they were solved.

One of the most difficult parts of a testing procedure is imposing the desired stress and strain fields on the specimen. The present tests require that the specimen be subjected to uniform normal stress and strain distributions in the directions of loading. There are many factors which may adversely affect such a distribution. One of them is the lateral restraint imposed by solid bearing platens on the concrete specimen, due to which shear stresses are introduced in the regions of the specimen adjacent to the platens. This problem was solved by using

brush-like loading heads where the bristles are capable of deforming laterally thus eliminating the friction between specimen and loading heads. Another important factor is the alignment between the specimen and the loading brushes. Errors in the alignment introduce small bending moments and, therefore, non-uniform stress and strain distributions across the specimen thickness. Since a perfect alignment is impossible to achieve small deviations of strain from uniformity should be expected. This is the reason for using two strain gages per loading direction, one on each side of the specimen. The gages are hooked up to the indicator in such a way that the average strain is recorded, which is the strain existing at specimen mid-thickness.

Another source of non-uniform strain distribution is the roughness of the concrete edge surfaces in contact with the loading brushes. Due to small irregularities in these surfaces the loading brushes are not initially in full contact with the specimen. This becomes evident in the uniaxial compression test when load versus displacement is plotted. At low load levels large displacements are plotted which actually do not correspond to strains of the central or core region of the specimen but rather to localized cracking at the edge regions of the specimen in contact with the brushes. The observed behavior may also be due to the existence of weaker concrete layers in the edge regions. At higher load levels the brushes came into full contact with the specimen and normal behavior is established as evidenced by an increase in the slope of the load-displacement curve.

The existence of the weak or 'soft' edge regions influences the behavior of the concrete under confined compression. If the specimen is initially confined at a given strain in the horizontal direction and subsequently loaded in the vertical direction it tends to expand laterally, but, since it is restrained, the 'soft' zones at the vertical edges crush or deform which results in an overall lengthening of the 'core' zone in the horizontal direction. The opposite effect occurs upon vertical unloading, where the specimen tends to regain ts initial state such that the soft zones expand while the core zone contracts. The expansion and contraction of the core region is recorded by the horizontal strain gages installed in the central region of the specimen. To compensate for this effect, the lateral loading jack was activated during vertical loading and unloading so that the horizontal strain in the core region remained constant and equal to its initial value. During vertical loading the jack was activated in its loading direction to counteract tensile strain increments in the core region, while during vertical unloading the jack was activated in its unloading direction to counteract compressive strain increments in the same region. Therefore, at all times during a test the horizontal strain in the core region remained constant, thus simulating a perfectly confined compression test.

The general testing procedure consisted in the basic phases listed below. Each phase is explained in more detail after the list.

Phases

1) Hydraulic Oil Warmup
2) Recording Circuit Setup
3) Instrument Balancing and Calibration
4) Setting of MTS Panel Controls
5) Positioning of the MTS Loading Ram
6) Specimen Collocation and Alignment
7) Initial Confinement
8) Test Initiation
9) Test Operation
10) Test Termination

1) Hydraulic Oil Warmup. It is convenient to warm up the hydraulic oil of the MTS before testing in order to obtain a more stable response from the loading ram during the test. Instructions for warm up are given in the MTS instruction manual. The warm up phase may be skipped if the hydraulic oil is already warm.

2) Recording Circuit Setup. This phase consists in setting up the strain measurement circuit according to the type of test to be performed, as shown in Figs. 3.7 (uniaxial tests) and 3.8 (biaxial tests).

3) Instrument Balancing and Calibration. Strain indicators are balanced and the appropriate gage factors are set into the instruments according to the corresponding indicator instruction manual. The strain voltage in the MTS, displayed by the MTS Digital Indicator (at position

2 of its Input Select control), should be zeroed by adjusting the zero control of the MTS Strain Transducer Conditioner. Fluctuations about zero of ± 0.010 V are normal.

Calibration of the recorders is usually done before this phase. However, this may not always be possible, and sometimes, if it is, a calibration check at this point is advised. Calibration of the non-MTS X-Y Recorders is done easily by adjusting the Attenuator and Cal/Var switches on the Recorder so that the pen displaces the desired distance for a given reading of the digital indicator. This reading may be introduced by properly turning the Coarse and Fine Bridge Balance controls. The gage factor of the indicator during calibration must be equal to that at which it will be set during the test. The MTS X-Y Recorder cannot be calibrated in the same way as the other X-Y Recorders. For strain recording a jumper circuit had to be introduced in the Strain Transducer Conditioner module in order to obtain the correct signal amplification for driving the MTS Recorder. For each axis one of five sensitivity ranges may be selected with the '% of Range/In. Cm.' switch and no variable adjustment is possible. Calibration of the strain axis is done by introducing a reading in the corresponding indicator as previously explained and measuring the displacement of the pen at different sensitivity ranges. The range which yields the most suitable pen displacement is selected and scaling is done according to the indicator reading corresponding to such a displacement. Once all calibrations have been performed the strain indicators should be re-balanced and the voltage sensitivity knobs set to zero input.

4) Setting of MTS Panel Controls. The MTS may be operated under three different control modes: stroke (displacement), strain and load. The strain and load control modes were found to be very unstable under local (manual) control. Therefore, all tests were carried out under stroke control. The command signal was provided by the function generator. Since the test was operated manually (without use of the computer) the Control Mode switch on the generator was set to the Local position. The Ramp-Invert function of the Function Generator was chosen so that the stroke varied linearly with time. The desired stroke rate was determined by using the Rate 1 and Rate 2 switches of the Function Generator. When used with the Ramp function, Rate 1 is the time in seconds required for the controlled variable (in this case, stroke) to reach 100% of operating range starting from zero reference. See the following figure:

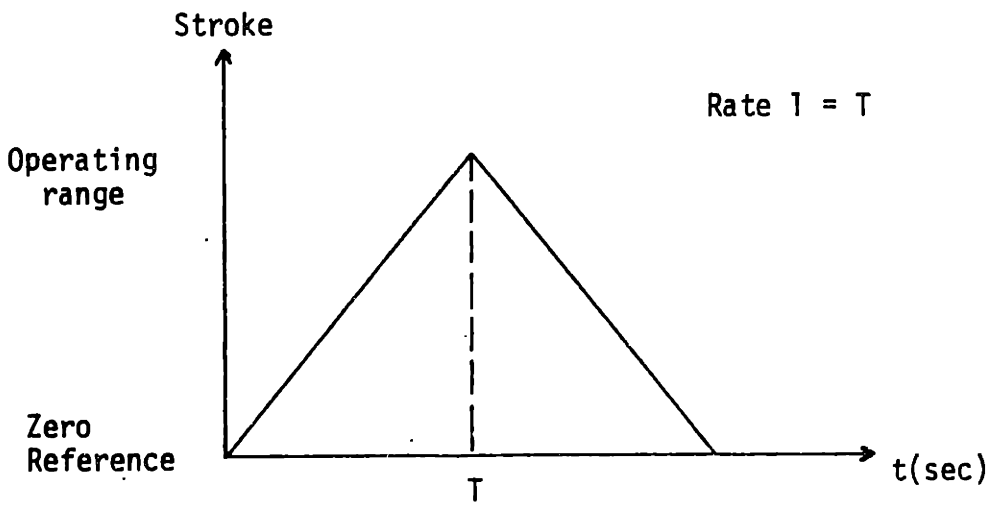

The operating range is selected with the Range switch of the Stroke Transducer Conditioner and is indicated in the main front panel. In this investigation the chosen range was equal to ± 10 mm.

The amplitude of the Ramp function may be controlled by setting the Span 1 control to a given percentage of the operating range. At such a percentage of operating range the function reverses direction and returns to zero reference.

A more direct way of controlling the amplitude of the function is by using the Return to Zero pushbutton of the Function Generator. If, during continuous operation in Local mode, Return to Zero is pressed, the generator will immediately return to zero reference at Rate 2 rate. Once zero reference is reached, the Output Zero indicator lights. The function may be generated again by pressing the Start pushbutton. The procedure described above can be done successively in such a way as to produce any desired cyclic history. This is the advantage of using the Local mode over the Remote mode (with the computer). One can make decisions during the test as to when to unload and reload according to the current circumstances, as for example in loading to the envelope curve. However, on the other hand, if, for example, many cycles to the same predetermined stress level are to be carried out the procedure becomes tiresome and it is clearly better to use the computer (if available).

The stroke rate imposed in the monotonic uniaxial and biaxial tests was such that failure occured in about 15 to 20 minutes. Rate 1 was set at 7900 seconds at a span setting of 100%. Rates 1 and 2 in the

cyclic tests to the envelope were each equal to 240 seconds at an average of about 5 1/2 minutes per load-unload cycle. Rates 1 and 2 in the cyclic tests to prescribed values of vertical stress were equal to 360 seconds at an average of about 4 minutes per cycle. The tests in Series 4 were carried out at a higher rate. Rates 1 and 2 were equal to 180 seconds at an approximate average of 2.5 minutes per cycle.

For read-out and recording purposes the load and strain ranges were set to 25K and 10%FS Range, respectively, in all tests. The MTS Recorder input controls were set as follows:

Y_1 Off

Y_2 Load (-)

X Strain (+)

In most tests, a '% of Range/In .' of 10 was selected for both X and Y axes. At these percentages the X (strain) scale was about 940 με/in./in. at a strain gage factor of 2.04 and the Y (load) scale was 5500 lb/in.

5) Positioning of the MTS Loading Ram. Positioning of the ram must always be done in stroke control. The stroke range used for control of the ram during testing was ± 10 mm. However, a higher stroke range, ± 100mm, is required to bring the ram from its lowest position up to a level which is less than 10mm below that required for testing the specimen. Once the ram has been brought to within less than 10mm from testing level at a range of ± 100mm, the hydraulics are turned off, the range is switched to ± 10mm and the hydraulics are turned on again. This whole procedure must be done without the specimen in place to avoid its accidental damage. The specific steps which must be followed to position the ram according

to the procedure mentioned above, if the hydraulics are initially off, are the following:

1) Set the Remote/Local switch of the Feedback Selector to Local
2) Press the Stroke button on the main panel and set the range to ± 100mm by using the Range switch in the Stroke Transducer Conditioner
3) Press Interlock Reset on the Controller panel
4) Monitor DC Error on the Controller meter
5) Null the meter using the Set Point control
6) Push Reset on the Control Panel
7) Push Hydraulic Pressure, first Low, then High
8) Using the Set Point control bring the ram within ± 10mm of required testing level. This level may be approximately judged by the relative position of the lower brush screwed into the ram, with respect to the vertical brushes.
9) Turn the Hydraulics off by pressing Hydraulic Pressure Low then Hydraulic Off.
10) Switch to a stroke range of ± 10mm
11) Repeat steps (3) to (7)

6) Specimen Collocation and Alignment. Once the previous steps have been performed the specimen is placed on the lower brush and the Set Point control is turned slowly to bring the specimen up to a level where it is almost touching the upper brush screwed into the MTS load cell. The specimen is then carefully aligned with the brushes, after which the Set Point control is slowly reactivated so that a small pressure is applied to the specimen, as monitored in the MTS Digital

Indicator (at position 1 of its Input Select control). In the present tests an initial vertical load not higher than about 110 lbs was applied (reading of 0.02 in the DVM, at a range of 25 tons). The Set Point control need not be at 500 for manual testing.

7) Initial Confinement. This phase is present only in the biaxial tests. Once the specimen is under slight vertical pressure, the horizontal confinement is applied. In this phase, the lateral loading jack is activated manually and horizontal stress is slowly applied to the specimen until it reaches a predetermined level as indicated by the strain indicator to which the lateral load cell is connected. The imposed horizontal strain, read from the corresponding strain indicator, is to be kept constant throughout the remainder of the test. It should be noted that due to the Poisson effect vertical stress and strain may build up during the confining phase. The resulting vertical strain is shown by the corresponding strain indicator. Its value is recorded for later calculations of real strain, and the indicator is then re-balanced to zero reading. Thus, upon subsequent vertical loading the indicator will register the increments of vertical strain starting from the initially deformed configuration.

8) Test Initiation. The voltage sensitivity knobs of the X-Y Recorders are properly set and the recorder pens are lowered to their initial position. The test is initiated by pressing the Start pushbutton of the Function Generator.

9) Test Operation. The procedures to be followed during the test vary according to the type of test. In monotonic uniaxial tests no extra operative procedure is required. During confined monotonic tests the operator must activate the lateral loading jack in its loading direction as described at the beginning of this Section so that the initially imposed horizontal strain as indicated by the corresponding strain indicator remains constant.

The procedure for carrying out the confined cyclic tests is a little more complicated and may require 2 operators. The levels of load or strain at which unloadings and reloadings must occur may be determined either during or before the test. In this last case it is advisable to mark those levels on the plotting paper. During loading, while one operator activates the screw jack in order to maintain a constant horizontal strain the other must monitor the stress-strain curve which is being simultaneously plotted. Whenever the curve reaches the desired level, the Return to Zero pushbutton is depressed, which immediately causes unloading of the specimen. During unloading the screw jack must be activated in its unloading direction as described previously. Whenever it is wished to reload the specimen the Start pushbutton on the Function Generator should be pressed. This procedure is carried on successively until all the cycles have been completed. Uniaxial cyclic tests are carried out under the same procedure except that no horizontal loading is involved..

10) Test Termination. One may wish to terminate the test before failure or once failure has occured. In either case this is achieved by pressing the Hold pushbutton of the Function Generator, which causes the ram to stop and hold at its current instantaneous level. Then the Set Point control is used for lowering the ram and unloading the specimen vertically. If the test is biaxial the lateral loading jack is activated in its unloading direction until the specimen is free.

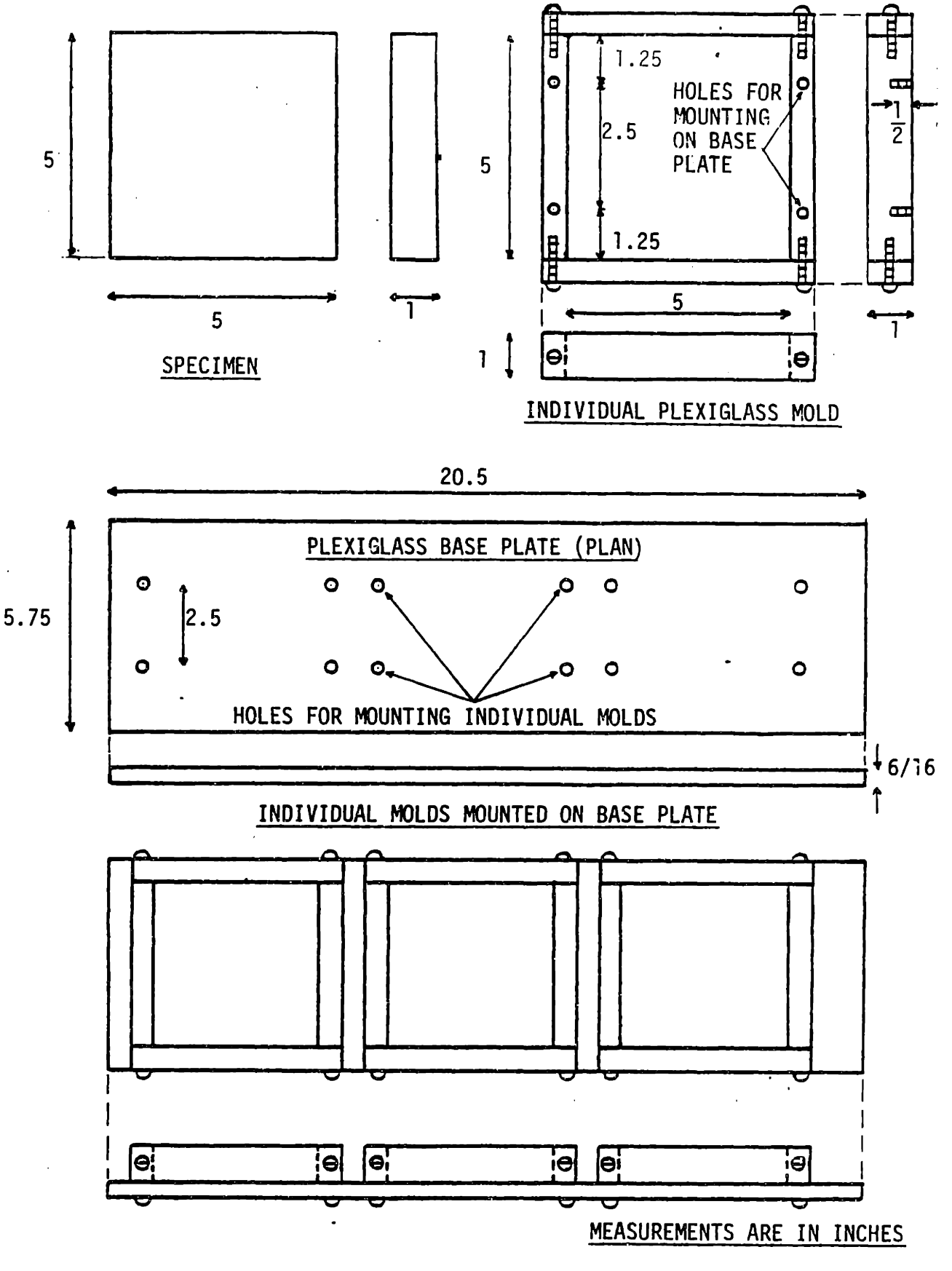

Fig. 3.1 - Specimen and Molds

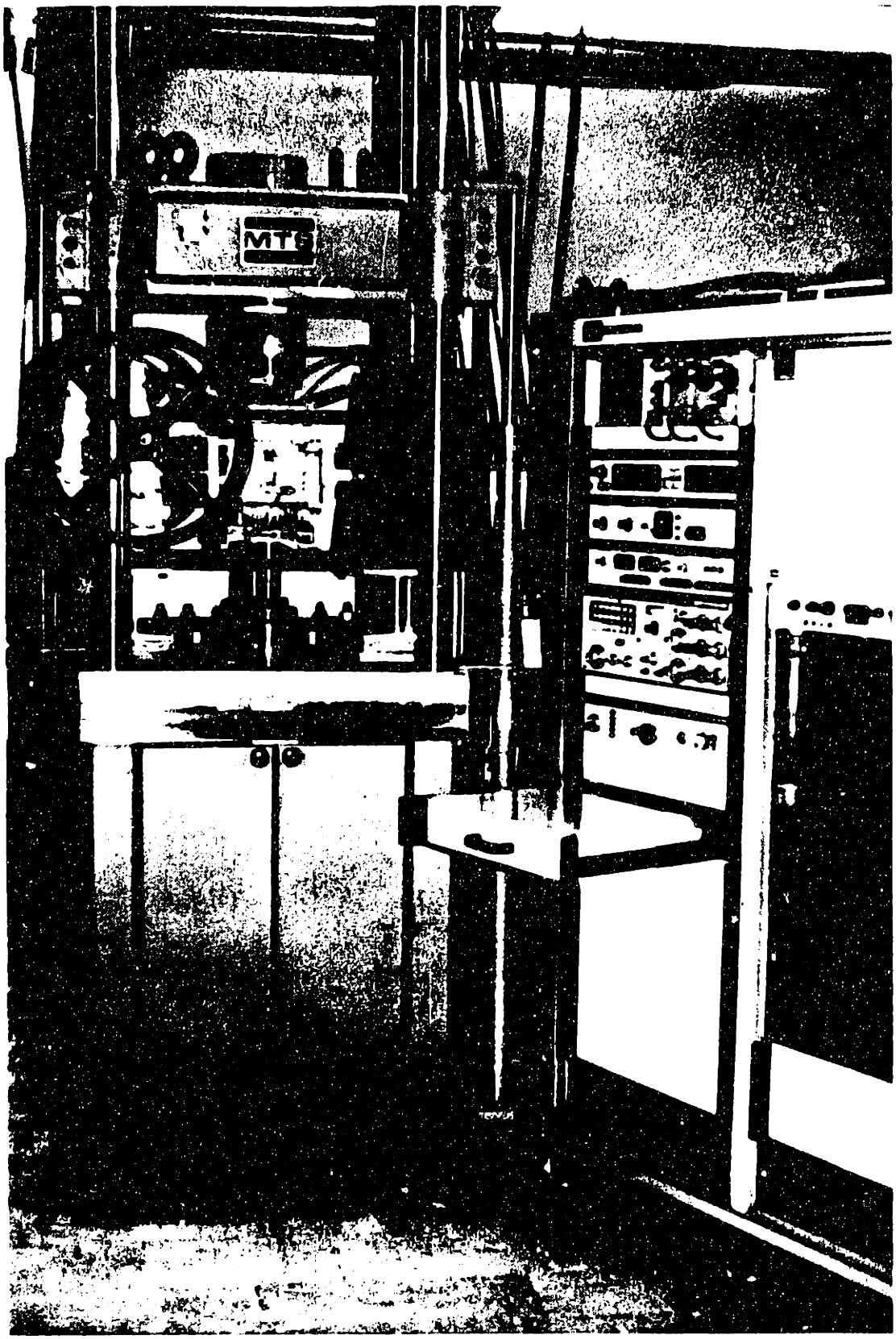

Fig. 3.2 Lateral Loading Frame on MTS Platform

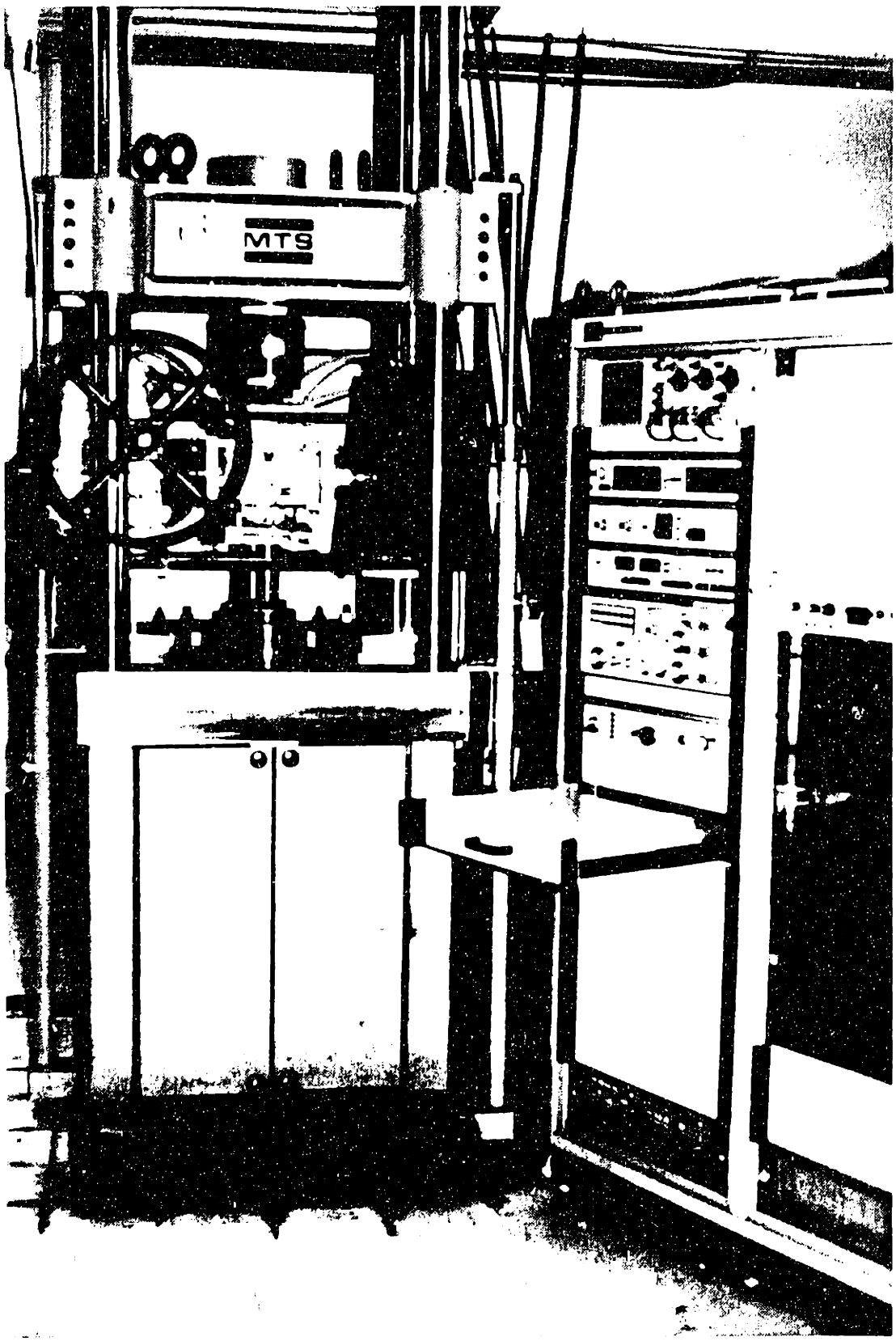

Fig. 3.2 Lateral Loading Frame on MTS Platform

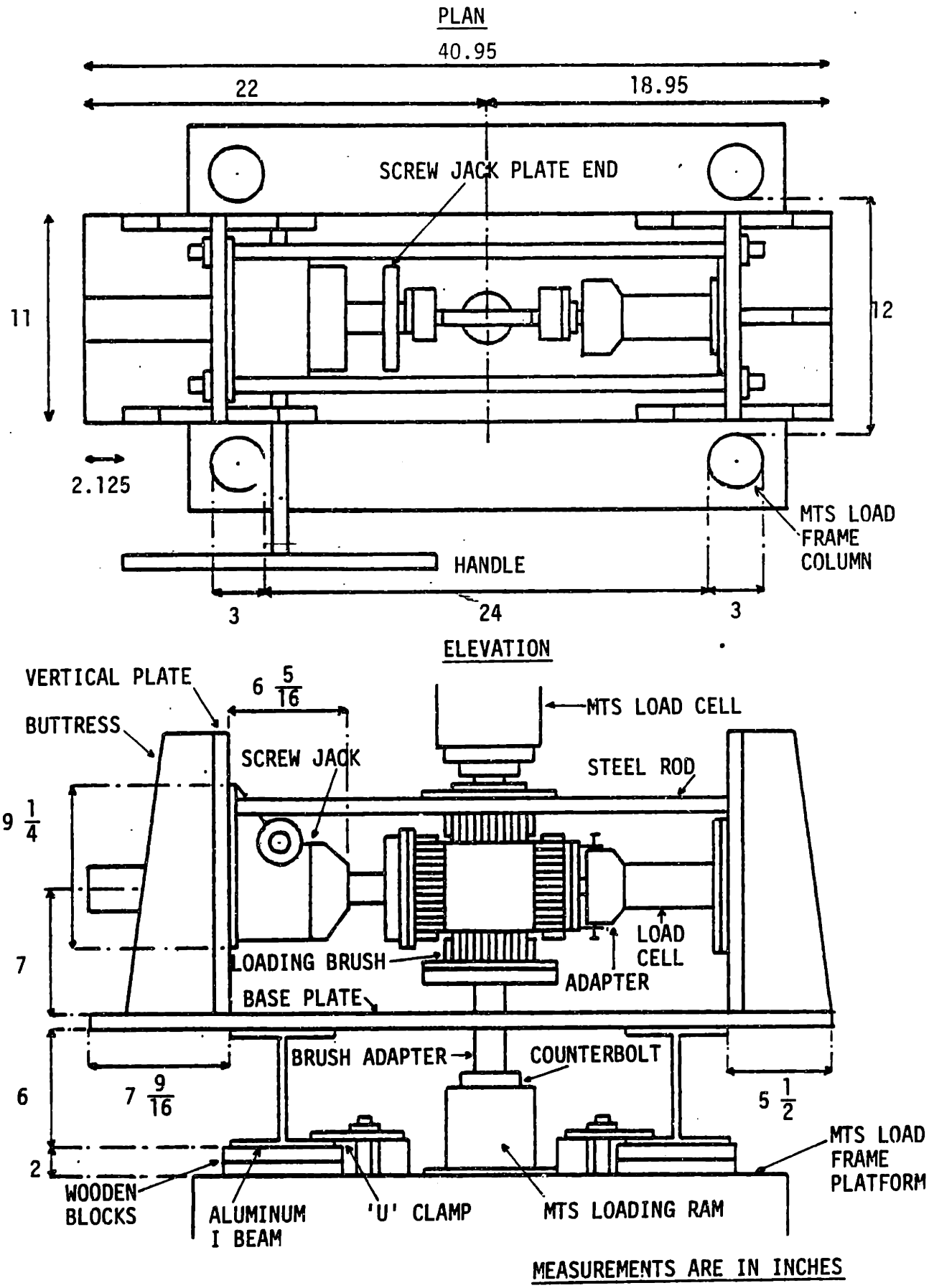

FIG. 3.3 - Lateral Loading Frame on MTS Platform

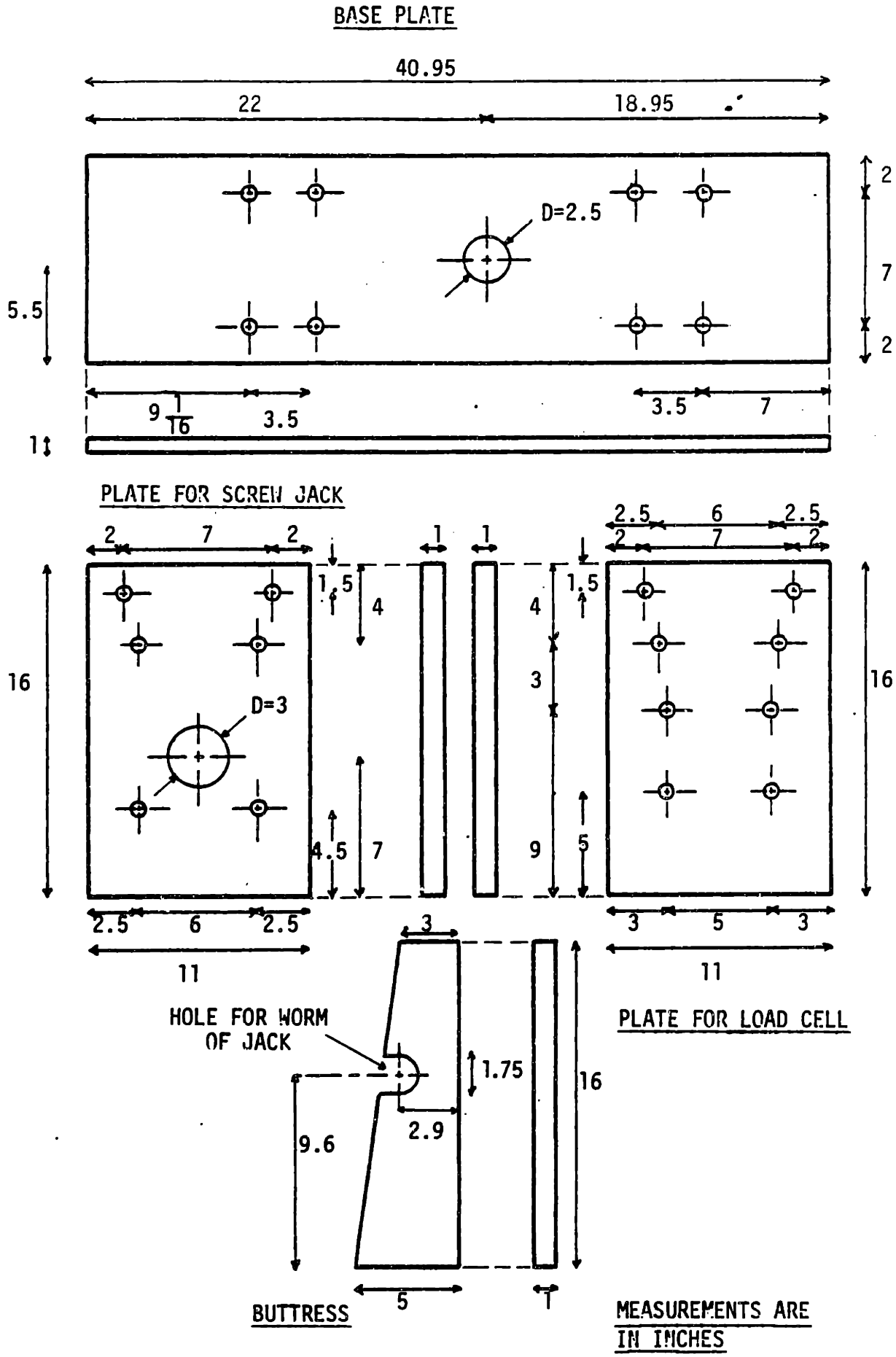

Fig. 3.4 Lateral Loading Frame Steel Plates

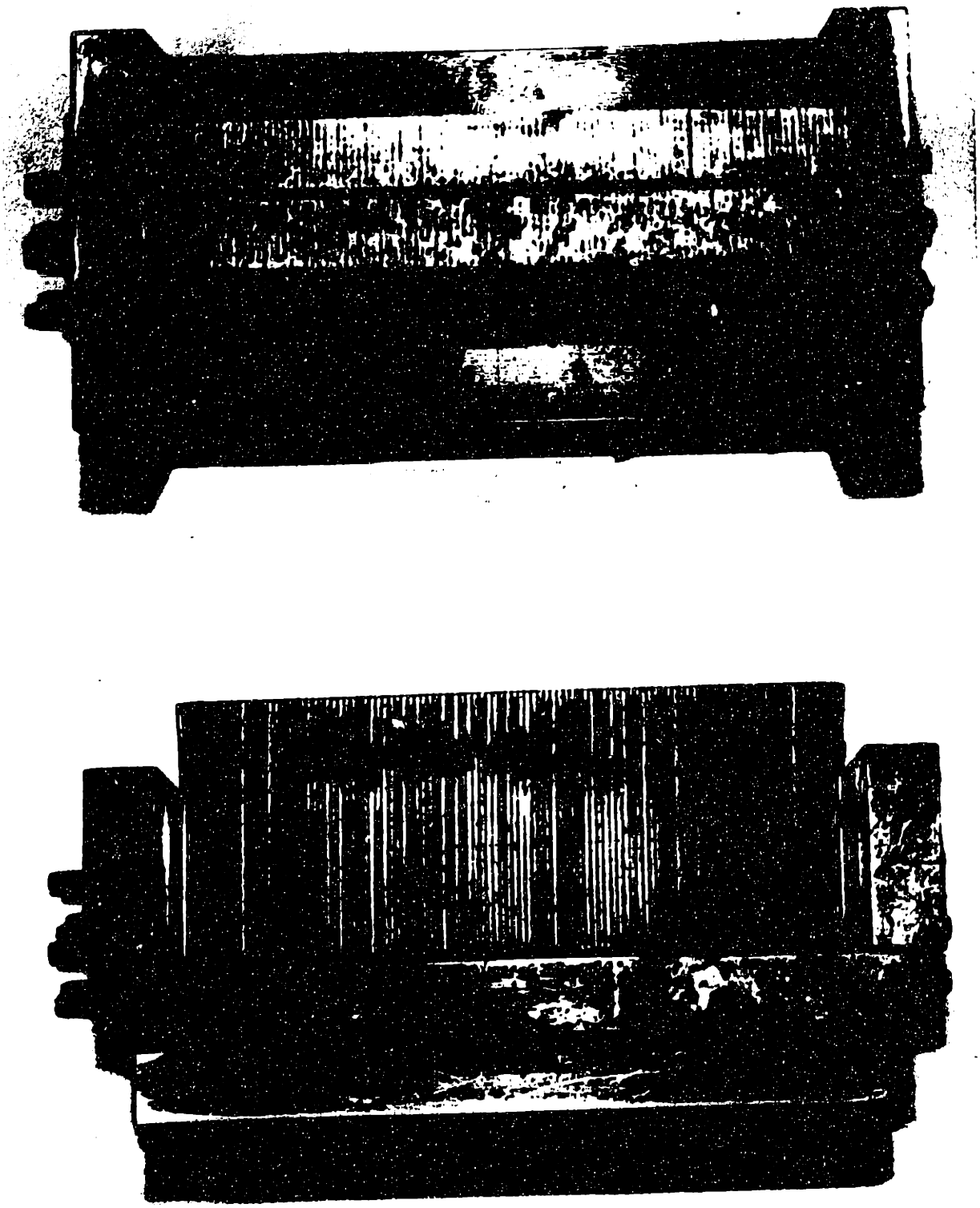

Fig. 3.5 Brush Bearing Platens

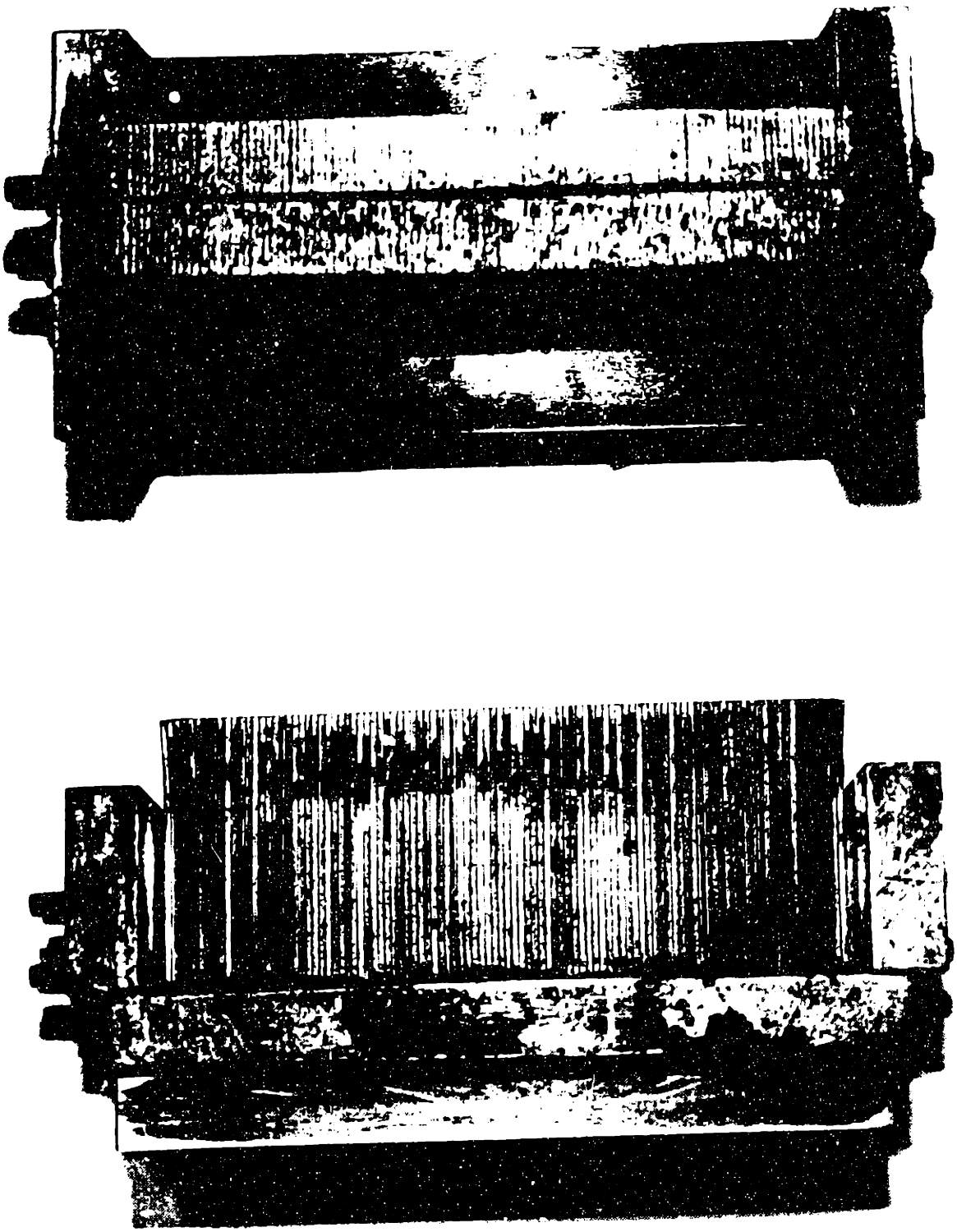

Fig. 3.5 Brush Bearing Platens

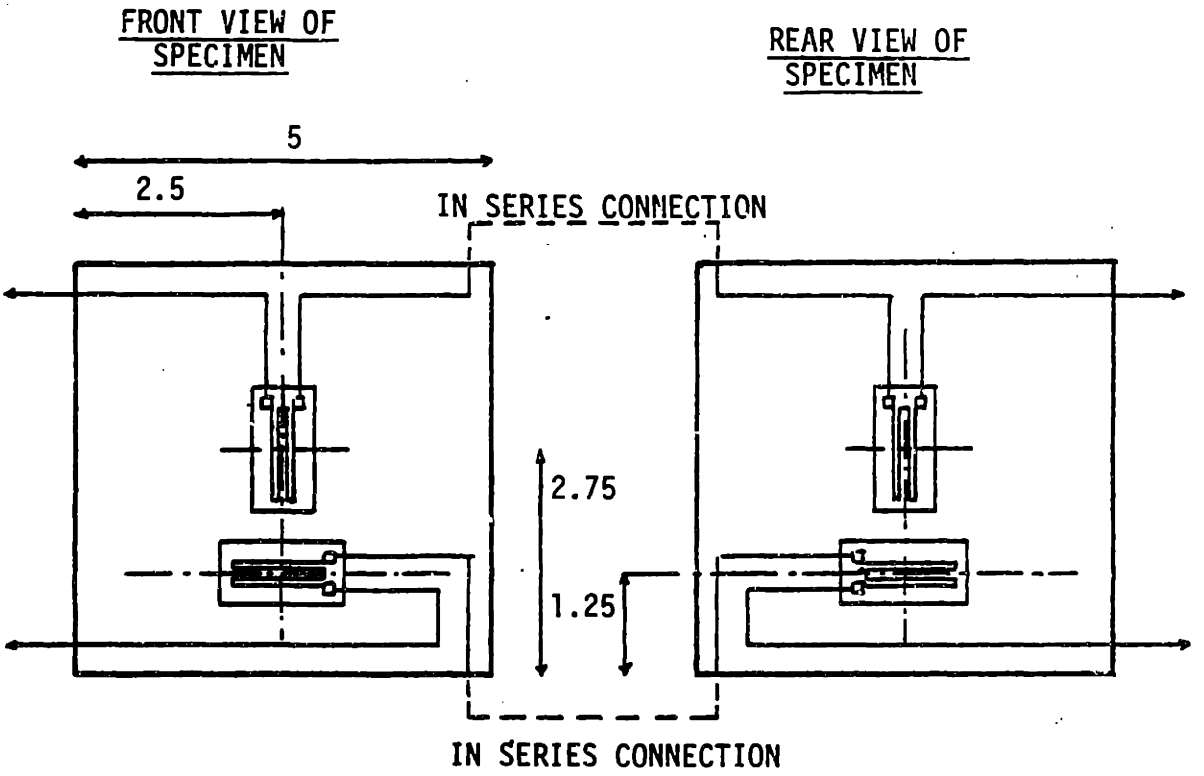

Fig. 3.6 - Position and Wiring of Strain Gages

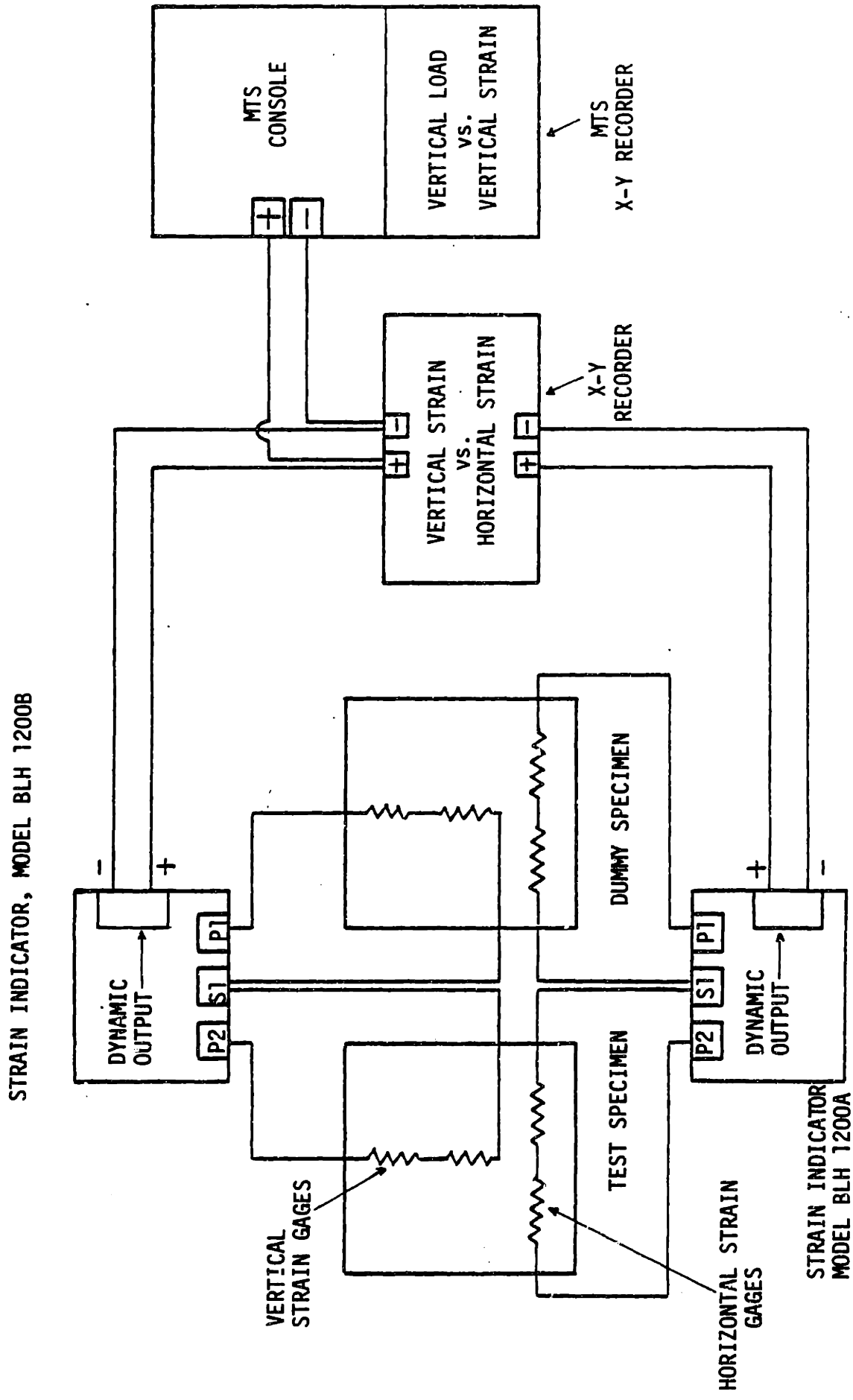

Fig. 3.7 - Strain Measurement Circuit for Uniaxial Tests

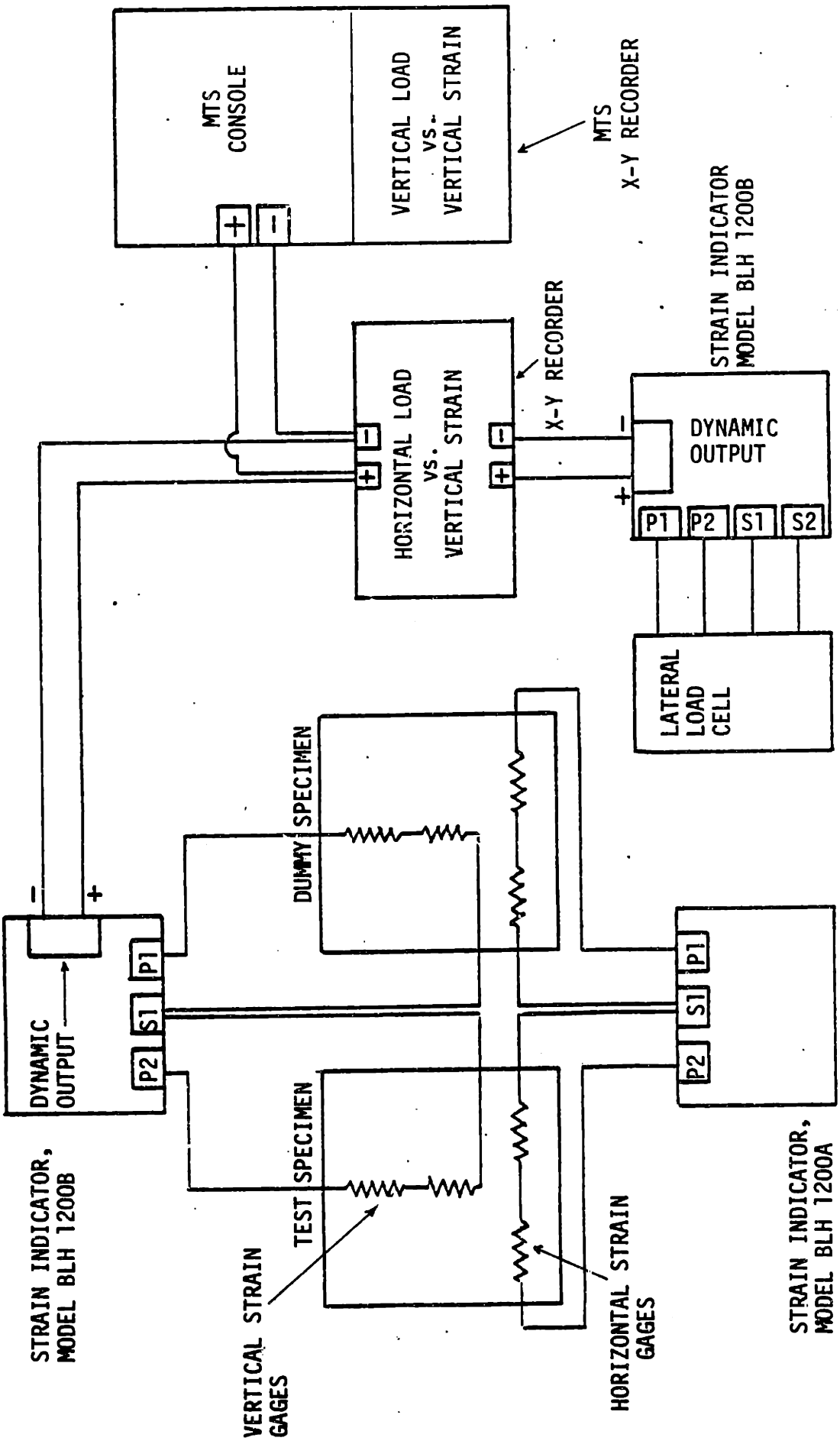

Fig. 3.8 - Strain Measurement Circuit for Biaxial Tests

CHAPTER 4

TEST RESULTS AND DATA ANALYSIS

4.1 Test Series 1 - Monotonic Loading to Failure

Biaxial testing consisted here in increasing the vertical strain monotonically while keeping the horizontal strain constant and equal to a prescribed value. Monotonic uniaxial tests were also carried out in order to assess basic behavior and properties of concrete under uniaxial loading and provide a basis against which the biaxial tests can be compared.

4.1.1 Uniaxial Tests

Uniaxial compression tests were performed on specimens 1.1, 2.1 and 2.2. For each uniaxial test a vertical stress-vertical strain curve (σ_v-ε_v) and a vertical strain-horizontal strain curve (ε_v-ε_h) were simultaneously recorded. See Figs. 4.1, 4.2 and 4.7. Descriptive parameters of the behavior, obtained from the recorded curves, are shown in the table below. Parameters for batch 2 were obtained by averaging those of specimens 2.1 and 2.2.

	Batch	
Concept	1	2
f'_c (psi)	4015	3550
ε_o (με/in)	3243	2500
ε_{vf} (με/in)	3431	3185
E (psi)	2.3×10^6	2.3×10^6
σ_{vy}	$0.55\ f'_c$	$0.50\ f'_c$
ν_{in}	0.20	0.20

Table 4.1

where

f'_c = peak stress or strength under uniaxial compression

ε_o = vertical strain corresponding to peak stress

ε_{vf} = vertical strain at failure

E = initial modulus of elasticity

σ_{vy} = elastic or proportional limit

ν_{in} = initial Poisson ratio

Results of the uniaxial tests reasonably agree with those reported in the literature. For example, the value of the initial Poisson ratio (ν=0.20) coincides with that obtained in previous investigations. The elastic limit, σ_{vy}, was approximately equal to half the compressive strength. From the ε_v-ε_h curve in Fig. 4.2 it can be seen that the tangent Poisson ratio $\nu=d\varepsilon_h/d\varepsilon_v$ (inverse slope of the curve) is initially constant up to a value of vertical strain equal to 0.67 f'_c, after which it starts increasing. This stress is known as the initiation stress and is associated with a substantial increase in bond cracking. Shah and Chandra (14) have determined experimentally a value of 0.55 f'_c for the initiation stress. However different investigators have quoted different values for this parameter. For example, Kupfer et al (8) have recorded initiation stress values of approximately 0.80 f'_c. If the values given by Kupfer et al and Shah and Chandra are averaged the resulting percentage of initiation stress is equal to that obtained in this investigation. It should be noted that the initiation stress (0.67 f'_c) is higher than the elastic limit (0.50 f'_c). Such a result was also obtained by Kupfer et al (8), where the elastic limit was about 0.35 f'_c. Since the σ_v-ε_v curve becomes non-linear at a

stress lower than the initiation stress, this seems to indicate that the decrease in tangent modulus ($d\sigma_v/d\varepsilon_v$) at early stages of the uniaxial compression test is not related to micorcracking but rather to plastic slip. This is the first of several cases in the present investigation where a feature of inelastic behavior traditionally attributed to microcracking at the aggregate mortar interface may actually be related to plastic flow of the cement paste or, in general, nonlinear behavior of the mortar. Supporting evidence of this concept is found in recent research work by Maher and Darwin (10) dealing with the behavior of mortar under uniaxial monotonic and cyclic loading. Results obtained in this investigation (10) show that cement paste and mortar are not elastic as supposed in the past and their nonlinearity dominates the nonlinear behavior of concrete. Under monotonic loading it is seen that mortar is initially linear elastic and starts exhibiting inelastic behavior at about half of its compressive strength. This tentatively explains why in the present investigation the concrete starts exhibiting inelastic behavior before significant microcracking takes place.

Volumetric strain is given by the simple expression

$$\varepsilon_{vol} = \varepsilon_v + 2\varepsilon_h \; ; \quad \varepsilon_h = \nu\, \varepsilon_v$$

$$\therefore \quad \varepsilon_{vol} = \varepsilon_v\,(1+2\nu) \tag{4.1}$$

where

ε_{vol} = volumetric strain

ε_v = compressive vertical strain; $\varepsilon_v > 0$

ε_h = tensile horizontal strain; $\varepsilon_h < 0$

ν = Poisson ratio

Equation 4.1 is valid for linear behavior, where ν remains constant. However, it may be applied in incremental form after initiation stress, where the tangent Poisson ratio $\nu = d\varepsilon_h/d\varepsilon_v$ is dependent on the value of stress or strain.

$$d\varepsilon_{vol} = d\varepsilon_v (1 + 2\nu); \quad \nu = \frac{d\varepsilon_h}{d\varepsilon_v} \tag{4.2}$$

where

$d\varepsilon_{vol}$ = differential increment of volumetric strain
$d\varepsilon_v$ = differential increment of vertical strain
$d\varepsilon_h$ = differential increment of horizontal strain
ν = tangent Poisson ratio

Once intiation stress has occurred, horizontal strain continuously increases at a faster rate than vertical strain, which implies an increase of the tangent Poisson ratio (see Fig. 4.2), and a progressive decrease in the rate of volumetric reduction (see Eq. 4.2). This process continues up to a point where the differential increase in volume $d\varepsilon_{vol}$ is equal to zero and the volume of compressed concrete starts to increase rather than to decrease (the tangent Poisson ratio becomes -1/2; see Eq. 4.2). The stress at which this occurs and which corresponds to the minimum volumetric strain is known as the critical stress, and is characterized by a sharp increase in mortar cracking bridging the bond cracks. As in the case of initiation stress, different investigators have obtained different values for the critical stress. For example,

Shah and Chandra (14) report a value of critical stress equal to about 0.70 f'_c; from the tests performed by Kupfer et al (8), it is seen that critical stress occurs at about 0.95 f'_c. In the present investigation, it is seen from the recorded curves that the critical stress is equal to about 0.92 f'_c, and therefore practically coincides with the percentage value of Kupfer et al. Inspection of the specimen surface during testing verified this result, since visible cracking was observed only towards the end of the test, just before failure.

Failure occured suddenly once peak stress was attained. Thus, a very limited portion, and sometimes no portion at all, of the descending branch of the σ_v-ε_v curve was recorded. This phenomenon is related to the sudden release of energy of the MTS loading frame at peak stress. Another factor which does not allow post peak strain recording is the propagation of cracks through the concrete area covered by the strain gages. Failure occurred by splitting in the plane paralell to the load and perpendicular to the free faces of the specimen. This mode of failure has been observed by other investigators, e.g., Kupfer et al (8), Liu et al (9), etc.

4.1.2 Biaxial Tests

Biaxial monotonic tests were performed on specimens 1.5, 2.3 and 2.4. Biaxial tests 2.3 and 2.4 consisted of two basic phases:

1) Application of horizontal confining strain

2) Vertical loading under the imposed horizontal confinement

Phase 1 consisted basically in loading uniaxially in the horizontal direction up to a predetermined value of horizontal stress σ_{hin}. Phase 2

consisted in loading vertically while keeping the initially applied horizontal strain ε_{hc} constant. This second phase was the actual biaxial part of the test. While vertical stress is applied the concrete tends to expand laterally, but, since it cannot do so due to the confinement, there is an increase in horizontal stress $\Delta\sigma_h$. Thus, the stresses in both directions progressively increase until failure. It should be noted that both stresses increase in a non-proportional manner, and not at a constant ratio as in most of the biaxial tests performed up to date. Therefore the test provides useful information on the behavior of concrete under monotonic nonproportional biaxial loading.

The initial confining conditions for each test are shown in Table 4.2.

	Test		
Concept	2.3	2.4	1.5
σ_{hin}/f'_c	0.40	0.60	0.07
ε_{hc} (με/in.)	517 (0.20 ε_o)	870 (0.34 ε_o)	80 (0.02 ε_o)

Table 4.2

where

σ_{hin} = initial horizontal confining stress

ε_{hc} = horizontal strain corresponding to σ_{hin}. This strain is kept constant in tests 2.3 and 2.4

ε_o = strain corresponding to peak stress in the uniaxial compression test

For each biaxial test a vertical stress-vertical strain curve (σ_v-ε_v) and a horizontal stress-vertical strain curve (σ_h-ε_v) were simultaneously recorded. An additional ε_v-ε_h curve was recorded

for specimen 1.5 since this biaxial test was not carried out at constant lateral strain. See Figs. 4.3, 4.4, 4.5, 4.6, 4.7, 4.8 and 4.9.

Stress-Strain Behavior

The parameters which have been obtained from the recorded curves in order to describe the behavior are shown in the Table below. The corresponding uniaxial data has been included for comparison with the biaxial data. Stresses and strains at failure are not included since they are discussed in the next section.

	Uniaxial	2.3	2.4	Uniaxial	1.5
Concept	Batch 2	$\sigma_{hin}=0.40f'_c$ $\varepsilon_{hc}=517\,\mu\varepsilon/in$	$\sigma_{hin}=0.60f'_c$ $\varepsilon_{hc}=870\,\mu\varepsilon/in$	Batch 1	$\sigma_{hin}=0.07f'_c$ $\varepsilon_{hc}=80\,\mu\varepsilon/in$
E_{ef} (psi)	2.3×10^6	2.6×10^6	2.0×10^6	2.3×10^6	2.3×10^6
σ_{vy}/f'_c	0.50	0.47	0.85	0.55	0.71
$(\Delta\sigma_h/\Delta\varepsilon_v)_{in}$ (psi/με/in)	-	0.22	0.14	-	0.011
$(\Delta\sigma_h/\sigma_v)_{in}$	-	0.083	0.073	-	0.005

Table 4.3

where

E_{ef} = effective modulus: initial slope of the σ_v-ε_v curve. In the uniaxial compression test it is equal to E

σ_{vy} = elastic limit: the value of vertical stress at which the σ_v-ε_v curve becomes non-linear

$(\Delta\sigma_h/\Delta\varepsilon_v)_{in}$ = initial 'cross' modulus: initial slope of the σ_h-ε_v curve

$(\Delta\sigma_h/\sigma_v)_{in}$ = initial ratio of horizontal to vertical stress increments

$\Delta\sigma_h$ refers to the increase in horizontal stress above the initial value σ_{hin} during confined compression. It should be noted that the initial lateral confining phase introduces a tensile strain in the vertical direction ε_{vin} due to the Poisson effect. The subsequent vertical loading phase introduces compressive strain increments $\Delta\varepsilon_v$ starting from the initially deformed configuration. The vertical strain axis of the stress strain curve is scaled according to these increments normalized with respect to ε_o. The actual vertical strain at any point along the axis is obtained by subtracting the initial vertical tensile strain from the corresponding increment. All the stress strain curves of the confined tests carried out in this investigation should be interpreted this way. The initial vertical strain in each confined test is indicated in the Figure containing the stress strain curve. The initial vertical stress is practically equal to zero.

By inspection of the stress-strain curves we can see that for all the biaxial tests there is an initial region (limited by σ_{vy}) where the

stress and strain increments are linearly related. The following discussion is aimed at explaining the observed behavior in this region.

Elastic Behavior

Since stress and strain increments vary linearly, the stress-strain behavior might be explained by using a linear elastic isotropic stress strain law. We apply this law to the behavior once confinement has been applied and the specimen is being loaded vertically. Thus it must be formulated in terms of stress and strain increments with respect to the initial confining conditions σ_{hin}, ϵ_{hc}, ϵ_{vin}. The linear elastic isotropic stress-strain law can therefore be expressed as:

$$\Delta\epsilon_v = \frac{1}{E}(\sigma_v - \nu\Delta\sigma_h) \qquad (4.3)$$

$$\Delta\epsilon_h = \frac{1}{E}(\Delta\sigma_h - \nu\sigma_v) \qquad (4.4)$$

where

$\Delta\epsilon_v$ = compressive vertical strain increment (w/r to ϵ_{vin})

$\Delta\epsilon_h$ = horizontal strain increment (w/r to ϵ_{hc})

σ_v = vertical stress ($\sigma_{vin} = 0$)

$\Delta\sigma_h$ = increment of horizontal stress (w/r to σ_{hin})

E = modulus of elasticity

ν = Poisson ratio

Since the horizontal strain was not allowed to vary, $\Delta\epsilon_h=0$ (for tests 2.3 and 2.4). Substituting $\Delta\epsilon_h=0$ in eq. 4.4, we obtain the following relationship between vertical and horizontal stress increments:

$$\frac{\Delta\sigma_h}{\sigma_v} = \nu \tag{4.5}$$

Considering ν=0.20 according to the uniaxial compression test for this batch (see Table 4.1), we have that:

$$\frac{\Delta\sigma_h}{\sigma_v} = 0.20 \tag{4.6}$$

However, this expected relationship is not satisifed as can be seen from the data in Table 4.3

For test 2.3 $$\frac{\Delta\sigma_h}{\sigma_v} = 0.083 \tag{4.7}$$

For test 2.4 $$\frac{\Delta\sigma_h}{\sigma_v} = 0.073 \tag{4.8}$$

As can be seen, the ratio between horizontal and vertical stress increments in the early stages of the test is considerably less than that predicted by linear elastic isotropic theory.

The reason for this is the following. Once the initial confining phase has been performed, the concrete can no longer be considered an isotropic material but rather a stress induced orthotropic one, since properties of the concrete in the vertical and horizontal directions are not the same. Also the confining phase induces formation of microcracks, which tend to align horizontally parallel to the direction of confining stress. This preferred crack orientation may contribute to the difference between properties in the vertical and horizontal directions, if microcracking is significant. Thus it is believed that an orthotropic

stress-strain law can explain the behavior more realistically. Formulating the orthotropic model, again in terms of stress and strain increments:

$$\Delta\varepsilon_v = \frac{\sigma_v}{E_v} - \nu_{vh}\frac{\Delta\sigma_h}{E_h} \tag{4.9}$$

$$\Delta\varepsilon_h = \frac{\Delta\sigma_h}{E_h} - \nu_{hv}\frac{\sigma_v}{E_v} \tag{4.10}$$

where

E_v = elastic modulus in the vertical direction

E_h = elastic modulus in the horizontal direction

$\nu_{vh} = \frac{\delta\varepsilon_v}{\delta\varepsilon_h}$ = horizontal Poisson ratio: ratio between vertical and horizontal strain increments due to a horizontal stress increment $\Delta\sigma_h$

$\nu_{hv} = \frac{\delta\varepsilon_h}{\delta\varepsilon_v}$ = vertical Poisson ratio: ratio between horizontal and vertical strain increments due to a vertical stress increment σ_v

Notice that this formulation is total since it's intended to model the behavior in the elastic range. However, Eqs. 4.9 and 4.10 may be used in incremental form ($d(\Delta\underset{\sim}{\varepsilon}) = \underset{\sim}{D}\, d(\Delta\underset{\sim}{\sigma})$) in the region of inelastic (nonlinear) behavior (for values of $\sigma_v > \sigma_{vy}$), with the orthotropic parameters varying according to the current values of stress and strain. Incrementally linear (tangential) orthotropic stress strain laws for modelling the behavior of concrete under biaxial stresses have been used

by other investigators such as Darwin and Pecknold (6).

It is very important to realize that the values of the orthotropic parameters in Eqs. 4.9 and 4.10 depend on the initial confining conditions σ_{hin} and ε_{hc}. In order to gain insight into the physical meaning of the orthotropic parameters and realize how they are affected by the initial confining conditions, we will analyze the superposition implied by the orthotropic stress strain relations (Eqs. 4.9 and 4.10).

The initial state consists in the specimen subjected to the initial confining conditions, before any vertical load has been applied.

Initial State

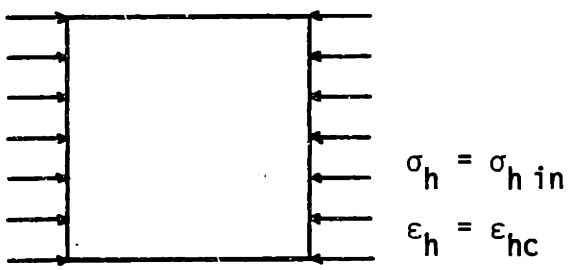

We now suppose that a vertical stress increment $\Delta\sigma_v$ is applied while keeping the horizontal strain constant, which leads to an increase in horizontal stress, $\Delta\sigma_h$. The final state, consisting in the specimen subjected to the new total stresses and strains is illustrated below.

The final state is reached by superimposing causes and effects on the initial state. See Systems 1 and 2.

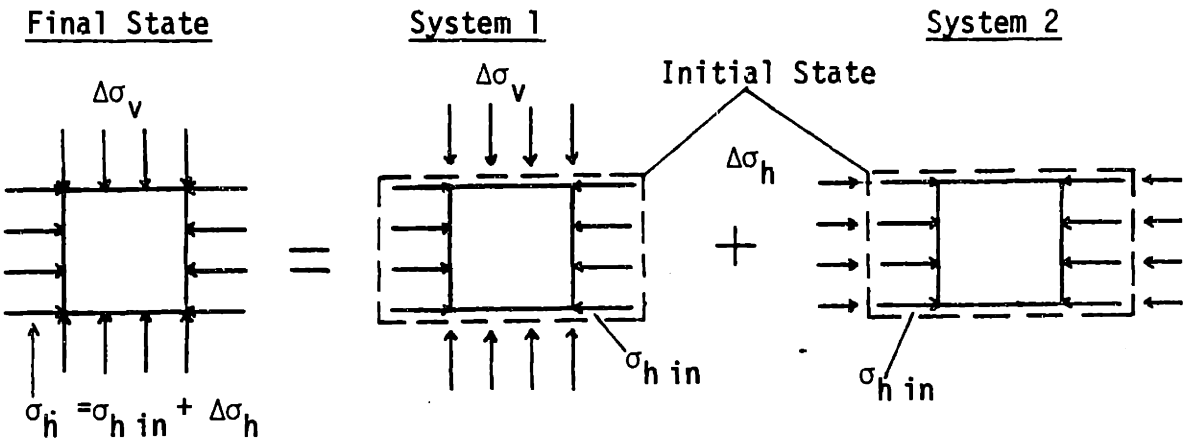

$\Delta\varepsilon_v = \Delta\varepsilon_{v1} + \Delta\varepsilon_{v2}$ $\quad \Delta\varepsilon_{v1} = \Delta\sigma_v/E_v$ $\quad \Delta\varepsilon_{v2} = \Delta\varepsilon_{h2}\,\nu_{vh}$

$\Delta\varepsilon_h = \Delta\varepsilon_{h1} + \Delta\varepsilon_{h2} = 0$ $\quad \Delta\varepsilon_{h1} = \Delta\varepsilon_{v1}\,\nu_{hv}$ $\quad \Delta\varepsilon_{h2} = \Delta\sigma_h/E_h$

System 1 consists in applying a vertical stress increment $\Delta\sigma_v$ to the specimen while the horizontal stress σ_{hin} remains constant. This might be considered as the 2-D analog of axial loading under "hydrostatic" or confining pressure. The Poisson ratio ν_{hv} at such a state of stress and strain must be lower than that corresponding to the pure uniaxial loading condition, among other reasons because the resulting increment of tensile

horizontal strain, $\Delta\varepsilon_h$, is not associated with microcracking (the net horizontal strain, $\varepsilon_{hc} + \Delta\varepsilon_h$, remains compressive). Concrete is an inelastic material, and as such, its material constants are generally dependent on the state of stress and strain. Unfortunately no research work has focused on the specific problem of determining the value of the Poisson ratio at different values of uniaxial confining stress. However, some authors such as Palaniswamy and Shah (11) have investigated the stress strain behavior of concrete cylinders subjected to axial loading under constant biaxial lateral stress (hydrostatic pressure). It is seen that under axial load the lateral strains initially are highly inhibited due to the confining pressure, which implies the existence of very low Poisson ratios. An analogous behavior is expected to exist under uniaxial confining stress (System 1). Though reduction of the Poisson ratio in this case is probably not as pronounced as in biaxial confinement, ν_{hv} can still be considered lower than the uniaxial Poisson ratio ν. The vertical modulus E_v in System 1 would apparently also be different from the initial uniaxial modulus E, due to the initial confining conditions. However, the experimental data seems to indicate that E_v is not significantly affected with respect to the initial uniaxial modulus by the confining conditions σ_{hin} and ε_{hc}. This is discussed later when the effective modulus is analyzed.

System 2 can be considered as a uniaxial loading situation with material constants E_h and ν_{vh}. Hence, ν_{vh} can be taken as the initial uniaxial Poisson ratio ν, if σ_{hin} is lower than initiation stress, and E_h can be considered equal to the tangent modulus (slope) of the uniaxial

σ_v-ε_v curve at the value of initial horizontal stress σ_{hin}. It might be assumed that E_h and ν_{vh} will vary as loading progresses according to the current stress and strain states. However this is not so for values of $\sigma_v < \sigma_{vy}$, where total stress and strain increments are linearly related, as observed in the recorded stress-strain curves.

Setting $\Delta\varepsilon_h$=0 because of confinement in Eq. 4.10 we obtain the following expression for the ratio of stress increments:

$$\frac{\Delta\sigma_h}{\sigma_v} = \nu_{hv} \frac{E_h}{E_v} \tag{4.11}$$

The fact that the observed ratio $\Delta\sigma_h/\sigma_v$ is lower than that predicted by linear elastic isotropic theory ($\Delta\sigma_h/\sigma_v$ = 0.20) can now be explained by applying the orthotropic relation (Eq. 4.11), where, on the basis of the previous discussion, ν_{hv} is lower than ν, E_v is approximately equal to E, and E_h is equal to or smaller than E.

From Table 4.3 it is seen that the ratio $\Delta\sigma_h/\sigma_v$ decreases as the initial lateral confining stress increases from 0.40 f'_c to 0.60 f'_c. Other tests, 4.6, 4'.2, 4'.3, under similar initial conditions exhibit the same behavior. These tests also reveal that the ratio $\Delta\sigma_h/\sigma_v$ for an initial confining stress σ_{hin}= 0.40f'_c is equal to that for a confining stress σ_{hin}= 0.20 f'_c.

On the other hand, the values of the effective modulus E_{ef} have been found to increase very little with respect to the uniaxial modulus E and coincide among each other for values of initial confining stress equal to 0.20f'_c, 0.40f'_c and 0.60f'_c. See Tables 4.3 and 4.6.

The effective modulus of test 2.4 is not considered to be representative because of excessive strain recordings due probably to alignment problems. From the orthotropic stress-strain relations, Eqs. 4.9 and 4.10, the relationship between vertical stress and vertical strain is given by:

$$\Delta\sigma_v = \frac{E_v}{1-\nu_{vh}\nu_{hv}} \varepsilon_v$$

$$\rightarrow \qquad \frac{E_v}{1-\nu_{vh}\nu_{hv}} = E_{ef} \qquad (4.12)$$

Since E_{ef} for all biaxial tests is practically the same as the initial uniaxial modulus E, the value of E_v must be practically equal to E, independently of the initial horizontal stress σ_{hin}, and the product $\nu_{vh}\nu_{hv}$ must be small compared to one. This last requirement is obviously satisfied since ν_{hv} is smaller than the uniaxial Poisson ratio ν, as discussed before, and ν_{vh} is probably equal to the initial uniaxial value ν=0.20. Hence, the product of both ratios is considerably smaller than 1 and E_{ef}, as computed by Eq. 4.12, is therefore equal to E, thus justifying the experimental data. It should be noticed that at different levels of confinement the Poisson ratio ν_{hv} may undergo small changes. While the effective modulus E_{ef} is quite insensitive to these changes by virtue of the relationship expressed in Eq. 4.12, the ratio $\Delta\sigma_h/\sigma_v$ may be affected by them to a certain degree (see Eq. 4.11). Since $\Delta\sigma_h/\sigma_v$ also depends on E_v and E_h, and we have considered E_v not to vary at the different confinement levels, it's the modulus E_h which is believed to influence most the

decrease of $\Delta\sigma_h/\sigma_v$ at increasing values of σ_{hin}. E_h may be considered practically equal to the uniaxial tangent modulus at the value of initial horizontal stress σ_{hin}. Therefore E_h is practically equal to the initial uniaxial elastic modulus E, for values of σ_{hin} below the uniaxial elastic limit, ($\simeq 0.50f'_c$, see Table 4.1), while it progressively decreases and depends on the value of σ_{hin} for values of σ_{hin} higher than the elastic limit.

It is significant that the initial portion of the biaxial loading phase is linear, particularly in the case of $\sigma_{hin}=0.60f'_c$ ($> .50f'_c$), where the concrete at the end of the confining phase has already undergone plastic deformation. Thus, initially, the effect of the biaxial loading phase is to induce an "elastic" (linear) behavior where the elastic parameters E_v, E_h, ν_{vh}, ν_{hv} remain constant and depend only on the initial loading conditions (stresses and strains at the end of the confining phase). Notice that for $\sigma_{hin}=0.60f'_c$, E_h remains constant throughout the initial portion of the biaxial loading phase, whereas it would continuously decrease under further uniaxial loading.

Values of the cross modulus $\Delta\sigma_h/\Delta\varepsilon_v$ are shown in Table 4.3. The cross modulus is the initial slope of the σ_h-ε_v curve, and thus represents the increase in horizontal stress per unit vertical strain increment during confined loading. It is not an independent quantity and can be expressed in terms of the effective modulus E_{ef} and the ratio $\Delta\sigma_h/\sigma_v$. From the orthotropic stress-strain relations (Eq. 4.9 and 4.10):

$$C = \frac{\Delta\sigma_h}{\Delta\varepsilon_v} = \frac{E_h\nu_{hv}}{1-\nu_{vh}\nu_{hv}} \qquad C = \text{cross modulus} \qquad (4.13)$$

$$C = E_{ef} \frac{\Delta\sigma_h}{\sigma_v} \tag{4.14}$$

Since E_{ef} does not vary at different confinement levels and $\Delta\sigma_h/\sigma_v$ does, C varies at these levels according to the variations in $\Delta\sigma_h/\sigma_v$.

It should be noted that the four orthotropic parameters E_v, E_h, ν_{vh} and ν_{hv} cannot be absolutely determined from the experimental data because there are only two independent equations and four unknowns. Therefore, assumptions must be made on two of the parameters and the other two can be obtained by substituting the observed experimental values of the effective modulus and ratio $\Delta\sigma_h/\sigma_v$ in Eqs. 4.11 and 4.12 and solving for the unknowns.

Inelastic Behavior

Table 4.3 contains the values of vertical stress σ_{vy} at which the σ_v-ε_v curve becomes nonlinear. Nonlinearity is characterized by a progressive decrease of the tangent effective modulus until failure. This is true for both uniaxial and biaxial tests. However the mechanism of inelastic behavior is different for both cases. Under uniaxial loading inelastic behavior at high stress is related to microcrack propagation, whereas under biaxial loading microcracking is inhibited and inelastic straining is caused primarily by plastic slip. The tangent effective stiffness at high stress levels is higher in the biaxial case than in the uniaxial one. This can be seen by comparing the uniaxial and confined curves in Figs. 4.3 and 4.7. On the other hand, the strength of concrete under biaxial loading was found to increase considerably with respect to the uniaxial strength f'_c. Stresses and strains at failure are discussed in

the next section.

By inspection of Figs. 4.6 and 4.8 it is seen that the σ_h-ε_v curves remain approximately linear throughout the test. However, a slight increase in slope can be detected at approximately the strain value ε_v corresponding to the vertical stress limit σ_{vy}. Since the cross modulus slightly increases and the tangent effective modulus progressively decreases after σ_{vy}, the value of the ratio $d(\Delta\sigma_h)/d\sigma_v$ progressively increases in this region ($d(\Delta\sigma_h)/d\sigma_v = (C/E_{ef})_{tan}$). This may be explained physically as follows. Since $E_{ef_{tan}}$ progressively decreases, a given vertical stress increment $d\sigma_v$ produces every time higher vertical strain increments which, due to the Poisson ratio $\nu_{hv_{tan}}$, tend to produce every time higher horizontal strain increments. Since these progressively increasing increments are not allowed to occur due to the confinement, progressively higher horizontal stress increments are produced. Thus, the ratio $d(\Delta\sigma_h)/d\sigma_v$ continuously increases.

Stresses and Strains at Failure

Values of vertical and horizontal stresses and strains at the peak of the σ_v-ε_v curve, for biaxial tests 2.3, 2.4 and 1.5 are shown in Table 4.4. Stresses and strains are normalized with respect to the f'_c and ε_o values of the corresponding batch.

.	Initial Conditions		Stresses at Peak		Strains at Peak		Initial Stress Ratio	Stress Ratio at Peak
Test	σ_{hin}/f'_c	ϵ_{hc} ($\mu\epsilon$/in)	σ_{vp}/f'_c	σ_{hp}/f'_c	ϵ_{vp}/ϵ_o	ϵ_{hp}/ϵ_o	$\sigma_{hin}/\sigma_{vin}$	σ_{hp}/σ_{vp}
2.3	0.40	517($0.20\epsilon_o$)	1.43	0.65	1.23	0.20	∞	0.46
2.4	0.60	870($0.34\epsilon_o$)	1.40	0.75	1.19	0.34	∞	0.54
1.5	0.07	80($0.02\epsilon_o$)	1.17	0.11	1.13	-0.19	∞	0.10

Table 4.4

where:

σ_{hin} = initial horizontal stress
ϵ_{hc} = horizontal strain corresponding to σ_{hin}; kept constant in tests 2.3 and 2.4
σ_{vp} = peak vertical stress
σ_{hp} = peak horizontal stress (occurs simultaneously with σ_{vp})
ϵ_{vp} = vertical strain at σ_{vp}
ϵ_{hp} = horizontal strain at σ_{vp}
ϵ_o = principal compressive strain at peak stress in the uniaxial compression test

It should be emphasized that the principal stress ratio varies throughout the tests (non-proportional loading) unlike most previous investigations where the stress ratio was maintained constant (proportional loading).

For tests 2.3 and 2.4 the stress ratio σ_h/σ_v varied from ∞ at the beginning of vertical loading (where $\sigma_v=0$) to 0.46 and 0.54 at failure, respectively. For test 1.5 the stress ratio varied from ∞ to 0.10; however the horizontal strain was not kept constant.

Based on the data of Table 4.4, 2 failure envelopes were constructed, one in terms of principal stresses at failure and the other in terms of principal strains at failure. See Figs. 4.10(a) and 4.10(b). Axes of the plots are normalized with respect to f'_c and ϵ_o. Based on the data from the corresponding stress-strain curves, the principal stress and principal strain paths are drawn on the same figures.

It is a well known fact that under biaxial compression concrete exhibits an increase in strength. The magnitude of this increase varies from one investigation to another and has been reported for constant stress ratio tests. Even within this type of biaxial test the increase in strength reported by different investigators varies considerably. The experimental technique has been a factor influencing the results (e.g., bearing platens which eliminate the friction, etc.). Kupfer et al (8) report a maximum strength of 1.27 f'_c for $\sigma_1/\sigma_2 = 0.5$, in the case of unrestrained specimens. For restrained specimens there is an increase of 0.48 f'_c for the same ratio. Liu, Nilson and Slate (9) have found somewhat lower increases in uniaxial strength, approximately 0.20 f'_c for

σ_1/σ_2=0.5. The brush-like loading heads used in their investigation for eliminating friction were the same used in the present investigation. In the present work, a maximum increase in strength of 0.43 f'_c was obtained, somewhat higher than in the investigations mentioned before. This increase in strength could not have been influenced by lateral restraint on the concrete because brushes for eliminating friction were used. Also the concrete mix was standard and the uniaxial strength was within the usual range for this type of investigation. The main difference between the present tests and the tests previously mentioned lies in the stress and strain paths (or stress-strain path). It is therefore apparent that the strength of concrete under biaxial compression is path dependent. Therefore no one stress failure envelope may be considered unique, and a general failure criterion based only on critical stress values is unrealistic. However, it is significant that the increase of 0.43f'_c occurred at a current stress ratio of about 0.50, which is the ratio at which specimens under biaxial proportional loading exhibit their maximum strength.

Vertical strains at failure were up to 23% higher than the uniaxial peak strain ε_o, and therefore did not vary over a wide range of values, thus exhibiting a tendency similar to that observed in previous biaxial tests (8,16). However, the strain states at failure (expressed in terms of ε_o) in the present investigation do not coincide with those of previous investigations. Following the same line of reasoning as above it appears that the strains at failure are also path dependent and a failure criterion based on critical strain states is not valid either.

It is seen from the previous observations that a failure criterion for concrete under biaxial compression should not be based on critical stress states only or critical strain states only, but rather on critical stress-strain states. For example, failure does not occur at the points where the stress paths in Fig. 4.10(a) intersect the classical envelope curve because at such points the strains are not the same as those of the constant stress ratio tests due to the difference in the stress-strain paths leading to the points. Thus, the concrete in the present tests can withstand further loading and eventually fail at a given combination of stresses and strains. Therefore it is appropriate to consider all the variables in a failure criterion rather than only stresses or strains, although it is obvious that such a formulation is extremely complex and would require much more experimental data. The formulation would require an investigation into the uniqueness, not of stress or strain states at failure, but rather of stress-strain states at failure, which means that concrete will fail upon attainment of critical stress strain states independently of the stress-strain paths leading to them. Such a uniqueness property is studied on the basis of the results of Test Series 1, 2 and 3.

Failure Mode. In the biaxial tests, failure occurred suddenly at the peak of the stress strain curve, as in the uniaxial tests. A shear mode of failure was observed with a major crack running perpendicular to the major loading direction (vertical in this case), at about specimen mid-height and in a plane forming an angle of about 25 degrees to the free surfaces of the specimen. This type of failure under biaxial compression was also observed by Rosenthal and Glucklich (12). However, other investigators such as Liu, Nilson and Slate (9), report a tensile splitting mode of failure in a plane parallel to the plane of the specimen. The reason for this discrepancy might be that in the present tests tensile strains in the direction normal to the free surface are inhibited. This is because the in-plane horizontal strain remains constant and therefore does not induce significant out of plane tensile strain increments.

4.2 Test Series 2 - Cycles to the Envelope Curve

In this series, biaxial testing consisted in cycling the vertical stress between zero and successively higher levels corresponding to the envelope curve, while maintaining a constant horizontal strain. The specimens were cycled up to failure. Other tests were also performed in this Series such as uniaxial monotonic and uniaxial cyclic tests, in order to provide basic and auxiliary data for comparative purposes.

Uniaxial Tests

Uniaxial compression tests were performed on 3 specimens, 4.1, 4.2,

and 4'.1 . The procedure followed here was the same as that followed in Series 1. For each uniaxial test, a vertical stress-vertical strain curve (σ_v-ε_v) and a vertical strain-horizontal strain curve (ε_v-ε_h) were simultaneously recorded. Basic parameters obtained from the uniaxial tests are shown in Table 4.5.

Concept	Batch 4
f'_c (psi)	3575
ε_o ($\mu\varepsilon$/in)	3431
E (psi)	2.1×10^6
ν	0.25

Table 4.5

Meaning of each variable is the same as for Table 4.1.

Cyclic Tests

Two uniaxial cyclic tests, 4.4 and 4.5, and 3 biaxial cyclic tests, 4.6, 4'.2 and 4'.3 , were performed. For the biaxial tests the same basic phases described in Section 4.1.2 were applied, i.e., the initial confining phase and vertical loading and unloading under confinement (constant horizontal strain). When vertical loading increases the concrete tends to expand laterally due to the Poisson effect; since it cannot do so due to the confinement there is an increase in horizontal stress. When vertical loading decreases the tendency of the concrete to expand laterally is reduced, thus leading to a decrease in horizontal stress. In such a way,

stresses in both directions alternately increase and decrease and thus constitute a biaxial cyclic stress field. The stresses increase and decrease in a non-proportional manner.

For each uniaxial cyclic test a vertical stress-vertical strain curve (σ_v-ε_v) and a vertical strain-horizontal strain curve (ε_v-ε_h) were simultaneously recorded. See Figs. 4.12 and 4.13. For each biaxial cyclic test, a σ_v-ε_v curve and a σ_h-ε_v curve were recorded. See Figs. 4.14-4.19.

Data for each of the tests is provided in the Table below.

	Test				
Concept	4.4	4.5	4.6	4'.2	4'.3
σ_{hin}/f'_c	0	0	0.20	0.40	0.60
ε_{hc} ($\mu\varepsilon$/in)	0	0	260($0.08\varepsilon_o$)	500($0.15\varepsilon_o$)	935($0.27\varepsilon_o$)
E_{ef} (psi)	2.11×10^6	1.80×10^6	2.22×10^6	2.22×10^6	2.22×10^6
σ_{vp}/f'_c	1.03	0.90	1.25	1.31	1.48
$\varepsilon_{vp}/\varepsilon_o$	0.95	0.92	1.29	1.25	1.20
σ_{hp}/f'_c	0	0	0.37	0.46	0.53
$\varepsilon_{hp}/\varepsilon_o$	-0.71	-0.42	0.08	0.15	0.27
σ_{hp}/σ_{vp}	0	0	0.30	0.35	0.36

Table 4.6

where

σ_{hin} = initial horizontal confining stress

ε_{hc} = horizontal strain kept constant during test

E_{ef} = effective modulus (initial slope of the σ_v-ε_v curve)

σ_{vp} = peak vertical stress

ε_{vp} = vertical strain at σ_{vp}

σ_{hp} = horizontal stress at σ_{vp}

ε_{hp} = horizontal strain at σ_{vp}

4.2.1 Uniaxial Cyclic Tests

σ_v-ε_v Curve

General behavior exhibited in this test resembles that observed in other uniaxial cyclic tests carried out by different investigators (7, 15). The concrete exhibits a typical hysteretic behavior, where the area within the hysteresis loops, representing the energy dissipated during a cycle, becomes bigger as vertical strain increases. In the present tests the cycles were performed in the region before peak stress, due to limitations of the test equipment. It is believed, however, that this is the region of most interest because actual concrete structures are in most cases subjected to stresses and strains below the peak values. However, works by other investigators such as Karsan and Jirsa (7) and Sinha et al (15) deal mainly with cycles after peak stress.

The envelope curve was found to coincide with the monotonic σ_v-ε_v curve. The reloading curves may be considered fairly linear along most of their length up to the common points. After the first load-unload cycle there is an increase in the slope of the reloading curve with respect to that of the initial loading branch. This shows that compaction of the material occurs during the first cycle, inducing a stiffer behavior upon reloading. As cycling proceeds the slopes of the reloading curves continuously

decrease (degradation of elastic moduli). After the intersection with the unloading curve at the common points, the reloading curve progressively decreases in slope accumulating inelastic strain. The unloading curves are initially mildly non-linear (near the unloading point) with a slope that does not vary much across the different cycles. However, the latter portion of the curve (approaching zero stress) presents a marked curvature which increases with the number of cycles.

ε_v-ε_h Curve

The ε_v-ε_h curve shows an interesting relationship between vertical and horizontal strains during cyclic loading. See Fig. 4.13. Each point on the curve represents a strain state. It is assumed that the strain in the direction normal to the free surface of the specimen is equal to the in-plane horizontal strain. Thus, the volumetric strain $\varepsilon_{vol} = \varepsilon_v + 2\varepsilon_h$ is known at any point during the test and the whole curve represents the entire strain history. The upper peaks of the curve represent the points at which unloading takes place while the lower peaks correspond to the points at which reloading occurs. When unloading takes place the curve does not return on the initial loading path as can be seen in Fig. 4.13. The abrupt change in slope at this point indicates that horizontal strains during unloading are recovered at a much slower rate (w/r to vertical strains) than that at which they are produced during the previous loading phase. Thus, inelastic behavior is higher in the horizontal direction than in the vertical direction, which corresponds to the direction of loading. The unloading curve is fairly linear along most of its portion and exhibits a

gradual decrease in slope as it approaches the lower peak. The coordinates of this peak correspond to the vertical and horizontal plastic or non-recoverable strains. The reloading curve originating at the lower peak does not follow the same path as the unloading curve. It is initially 'stiffer' but eventually decreases in slope until it intersects the unloading curve at a point that will be defined as the common strain point. The path thus traced by the material strain states during an unload-reload cycle resembles a hysteresis loop. At any point of the curve, the inverse slope represents the tangent or incremental Poisson ratio $d\varepsilon_h/d\varepsilon_v$.

It is interesting to note that the common strain points do not coincide with the common points of the σ_v-ε_v curve, as one might be led to suspect. The value of ε_v at the latter points practically coincides with the strain at which unloading occures and thus represents a limit value after which additional inelastic vertical strain takes place. However, at this point the common strain point has been surpassed and there has been a net increase in horizontal strain with respect to that existing at the moment of unloading. Thus, a net increase in volumetric strain with respect to that existing at the unloading point, has already occurred by the time the common point of the σ_v-ε_v curve has been reached.

When loading progresses after an unload-reload cycle, the path traced by the ε_v-ε_h curve follows a trend similar to that of the previous loading portion of the curve. This occurs for every interval between cycles, thus resulting in a series of broken curves which may be joined in a smooth upper envelope curve. On the other hand, the lower peaks,

representing the values of plastic strain in the vertical and horizontal directions, may also be joined to form a smooth lower envelope curve. The envelope curves are indicated in Fig. 4.13, and may be of considerable importance. Possibly the region defined by both curves is the region within which all possible strain states under uniaxial loading lie, regardless of the stress path. The upper envelope would thus be an upper bound possibly coinciding with the monotonic ε_v-ε_h curve. The lower envelope, if unique, represents the locus of all possible plastic strain states upon completion of unloadings to zero stress, and thus constitutes a lower bound to any arbitrary cyclic strain history. This envelope will be defined as the plastic strain curve and the slope at any point may be interpreted as the ratio of vertical to horizontal plastic strain increments due to a reload-unload cycle. See the Figure below.

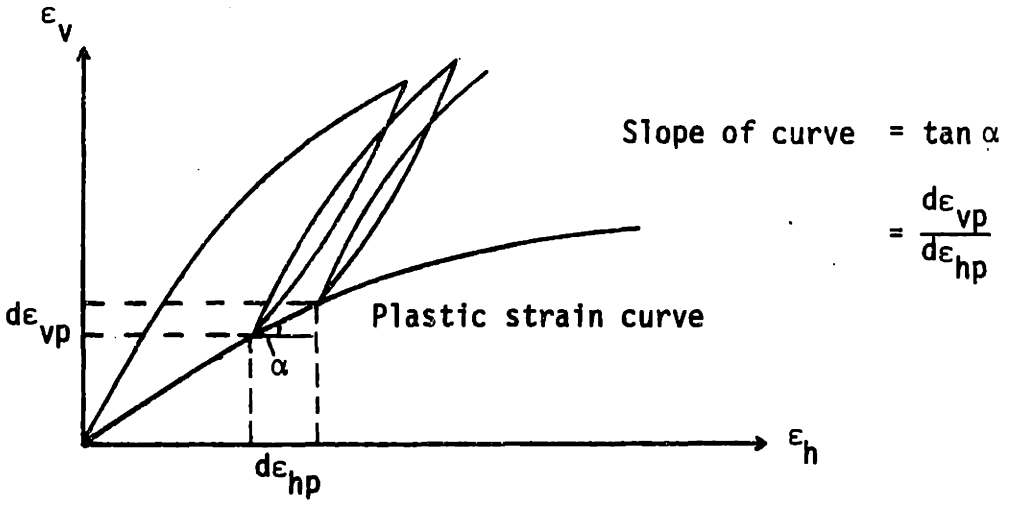

Plastic Strain Curve

The fact that the slope of the curve continuously decreases means that the horizontal plastic strain increases faster than the vertical plastic strain as cycling progresses.

Uniqueness of the upper and lower envelope curves implies that if at any point within the region defined by these curves, the strains continuously increase, they will reach and follow the path defined by the upper envelope whereas if the concrete is completely unloaded the strains will decrease until they reach a point on the plastic strain curve. Not enough tests were performed to conclusively verify the uniqueness of the upper and lower envelopes. A comparison of the envelopes in Fig. 4.13, with those corresponding to the uniaxial cyclic test 5.2 (see Fig. 4.24) shows that the plastic-strain curves coincide; however the upper envelopes do not, for reasons described in Section 4.3.1.

4.2.2 Biaxial Cyclic Tests

σ_v-ε_v Curve

A comparative analysis of the vertical stress strain behavior of concrete under confined cyclic loading is presented next. The discussion is based on the σ_v-ε_v curves of tests 4.6, 4'.2 and 4'.3, which are shown in Figs. 4.14, 4.16 and 4.18.

The same general behavioral pattern can be observed in all 3 tests, where the confined specimens exhibit a hysteretic behavior similar to that observed for specimens under uniaxial cyclic loading. The envelope curve formed by joining the peaks of the cycles, has the same initial slope in all the confined tests, which is slightly higher than the

initial modulus in uniaxial loading due to the Poisson effect. This has been discussed previously (see Section 4.1.2). At higher strain levels, however, the envelope curve rises higher for higher levels of lateral confinement. See Fig. 4.20.

Unloading Curves

In most of their portion the unloading curves are mildly non-linear with a slope which does not vary much across the different cycles, but in their final portion, as they approach zero vertical stress, there is a marked decrease in slope, which is more pronounced for unloadings beginning at higher strain levels, $\Delta\varepsilon_{vun}$. Unloading curves corresponding to different tests (including the uniaxial test) and starting at the same strain level ($\Delta\varepsilon_{vun}$) were found to overlap when superimposed at their lowest point (σ_v=0), the only difference being in their length, which is greater for tests at higher confinement levels, where unloading occurs at higher values of stress. Therefore the unloading curves appear to be basically non-dependent on the level of confinement, and a major criterion for determining their shape is the value of strain at which unloading occurs ($\Delta\varepsilon_{vun}$).

Reloading Curves

The reloading curves are practically linear throughout most of their portion until they intersect the unloading curves at the common points. In all confined tests the slopes of the first reloading curves are higher than the slope of the initial loading branch due to the stiffening or hardening effect produced by load reversals, as observed in the uniaxial cyclic test. Similar to the observed behavior in this test,

the reloading slopes progressively decrease as the number of cycles increases. A comparison of reloading curves corresponding to different tests and starting at the same values of vertical strain shows that they coincide in slope up to the common points, regardless of the level of confinement (including zero confinement). This should be partly expected since the initial effective modulus underconfined monotonic loading is unaffected by the confinement (see Section 4.1.2) and the reloading process may be viewed as a monotonic loading situation starting at a given value of vertical plastic strain. Thus, apparently, the reloading curves are, in their linear portion, non-dependent on the level of confinement and can be defined on the basis of plastic strain $\Delta\varepsilon_{vp}$ at which they originate. An important factor influencing the slopes of both reloading and unloading curves is the initial elastic modulus of the concrete. However this effect was not studied in the present investigation.

After the common point the reloading curve gradually decreases in slope, exhibiting a behavior similar to that observed in uniaxial cyclic tests. The common point location increases with increasing confinement. It can be observed that the decrease in slope of the reloading curve after the common point is less pronounced at higher confinement levels. This is partly responsible for the fact that the envelope curve rises higher at higher confinement levels.

Plastic Strains

Nonrecoverable or plastic strains are those corresponding to a zero stress level on the unloading stress-strain curve.

Fig. 4.22 shows the relationship between the plastic strains and the strains at unloading $\Delta\varepsilon_{vun}$, for all cyclic tests, including the uniaxial one. According to this figure the plastic strain increments appear to be dependent mainly on the vertical strain at unloading and are not significantly affected by the stresses and strains in the horizontal direction. Only at values of $\Delta\varepsilon_{vun}/\varepsilon_o$ higher than 0.60 do the plastic strains in the confined tests appear to be slightly reduced with respect to those in the unconfined tests. However the difference is not significant and for practical purposes unique values may be considered. For comparison the curve obtained by Karsan and Jirsa (7) based on their uniaxial cyclic tests is shown on the same figure. It coincides initially with the data obtained in this investigation for low values of $\Delta\varepsilon_{vun}/\varepsilon_o$. At higher values there is some deviation which may be due to the difference in experimental techniques, form and size of specimen, etc.

General Discussion

It is very significant that the basic features of concrete behavior under uniaxial cyclic loading are also found in the biaxial cyclic tests. Such features include the initial compaction of the material upon the first load-unload cycle and the subsequent degradation of elastic moduli as cycling proceeds. Compaction induces an increase in slope of the first reloading curve with respect to the initial elastic modulus and the

degradation of elastic moduli is manifested by the continuous decline in the slopes of the reloading and unloading curves throughout the test. This last phenomenon, in the uniaxial cyclic tests, has been traditionally attributed to continuous microcrack propagation (originating at the aggregate-mortar interface). However since the same behavior is exhibited in the biaxial tests, where microcrack formation and propagation is highly inhibited, it appears that such behavior cannot be entirely attributed to microcracking. This is more so, considering that the reloading and unloading curves originating at given values of vertical strain have actually the same slopes in both uniaxial and biaxial tests. Therefore, since the described degradation process cannot be explained by microcracking the only other mechanism which can explain it is the nonlinear behavior of the mortar. This is confirmed by results obtained in recent research work (10) which show that the behavior of mortar under uniaxial cyclic compression is very similar to that of concrete under uniaxial cyclic loading. The behavioral patterns exhibited by the mortar are the same as those observed for concrete in the present uniaxial and biaxial cyclic tests. It therefore follows that the behavior of concrete under cyclic (and monotonic) loading is mostly dominated by nonlinear behavior of the mortar. There are, in turn, two basic mechanisms which may govern the nonlinear behavior of the mortar: 1) microcracking originating at the sand-cement paste interface and 2) plastic flow of the cement paste. However, previous investigations (14) have shown that under uniaxial loading, microcracking at the sand-cement paste interface is very limited, at least in the ascending branch

of the stress-strain curve. Under biaxial loading such microcracking should therefore be practically non-existent. Therefore the nonlinear behavior of mortar, and therefore of concrete, under uniaxial and biaxial cyclic loading before peak stress, appears to be mainly influenced by the nonlinear behavior of the cement paste. Previous investigations (10) have actually shown that the process of degradation of cement paste under uniaxial monotonic and cyclic loading is similar to that of mortar and concrete, and other investigators are presently doing research in this field.

Thus far we have discussed the similarities in behavior of concrete under uniaxial and biaxial cyclic stress. The difference in behavior is seen at high stress levels in the reloading portions of the cycles, where the concrete exhibits a stiffer behavior at higher confinement levels. The strength of concrete also increases with the confinement. The benefitial effects of biaxial stress on stiffness and strength should be expected since they have been observed previously in monotonic biaxial tests.

The fact that the reloading and unloading curves as well as the plastic strains present certain uniqueness properties may facilitate the mathematical modeling of the confined cyclic behavior in the principal direction of loading (in this case, vertical). A procedure similar to that followed by Karsan and Jirsa (7) could be applied for cyclic loading at different confinement levels if the envelope and the common point curve (that which joins all common points) for each confinement level are considered unique, which cannot be conclusively established on the basis of the present tests. However it is felt that the cyclic envelope does

not appreciably deviate from the corresponding biaxial monotonic curve. Unfortunately, the cyclic envelopes of tests 4'.2 and 4'.3 cannot be compared with full confidence to the biaxial monotonic curves of tests 2.3 and 2.4, due to the fact that the concrete of batch 4 is more ductile than that of batch 2 (see values of ε_o in Tables 4.1 and 4.5). For example, if the monotonic curve of test 2.3 (Fig. 4.3) is superimposed on the cyclic curve of test 4'.2 (Fig. 4.16), it is seen that initially they coincide, but at higher stress values the cyclic envelope falls below the monotonic curve. However, it is encouraging that the uniaxial cyclic envelope of test 4.4 coincides with the uniaxial monotonic curve. It is thus likely that the same behavior extends to the biaxial case where at a given confinement level, the cyclic envelope coincides with the corresponding monotonic curve.

σ_h-ε_v Curve

The σ_h-ε_v curve corresponding to tests 4.6, 4'.2 and 4'.3 (σ_{hin}= 0.20, 0.40 and 0.60f'_c, respectively) are shown in Figs. 4.15, 4.17 and 4.19. The point on the vertical axis where each curve starts has been arbitrarily selected and given the value of the initial horizontal stress σ_{hin}. Scaling of the vertical axis is done starting from this initial point.

The upper peaks of the curve correspond to points at which horizontal stress ceases to increase and starts decreasing while at the lower peaks horizontal stress ceases to decrease and starts increasing. These peaks coincide with the upper and lower peaks of the σ_v-ε_v curve. Thus, the alternating increase and decrease of vertical stress

is associated with a corresponding increase and decrease of horizontal stress, as should be expected by virtue of the Poisson effect. If two lines are drawn, one joining the upper peaks and the other joining the lower peaks, we will obtain for each σ_h-ε_v curve an upper and lower envelope. Two envelopes can also be defined for each σ_v-ε_v curve, an upper envelope joining the peaks of the cycles and a lower envelope which joins the points corresponding to zero vertical stress.

In all cyclic tests the σ_v-ε_v upper envelope continuously rises, i.e., the vertical stress at which unloading takes place is successively higher, while the lower envelope is a horizontal line coinciding with the σ_v=0 line ('x' axis), i.e., the specimen is unloaded to zero vertical stress in each cycle. One might expect a similar behavior in the horizontal direction, i.e., successively increasing values of maximum horizontal stress (peak stress of cycle) and unloading to the same value of initial horizontal stress. However, this is not the case as seen in Figs. 4.15, 4.17 and 4.19. For example, in Fig. 4.19, which corresponds to the test at the highest confinement level (σ_{hin}=0.60f'_c, ε_{hc}=935 με/in), the upper envelope initially rises in an approximate linear manner, after which it decreases in slope and starts descending. Therefore, during the last few cycles progressively increasing values of peak vertical stress are associated with progressively decreasing values of peak horizontal stress. This phenomenon is less marked in test 4'.2 (σ_{hin}=0.40f'_c, ε_{hc}=500 με/in), and in test 4.6 (σ_{hin}=0.20f'_c, ε_{hc}=260 με/in) there is no descending branch. It is thus clear that this behavior is influenced by the level of confinement. It can also be seen that the

lower envelope in curves 4'.2, 4'.3 and 4.6 falls below the level of initial horizontal stress, and each time the specimen is unloaded to zero vertical stress the horizontal stress decreases to a lower value. This phenomenon is more pronounced at increasing levels of lateral confinement.

Comparing the envelope curves at the different confinement levels we see that for higher confinement levels the σ_v-ε_v upper envelope is higher, while both the upper and lower σ_h-ε_v envelopes are lower with respect to the initial horizontal confining stress. See Figs. 4.20 & 4.21. The region bounded by both envelopes seems to rotate and expand for higher confinement levels.

It is significant that the upper envelope coincides in its initial linear portion with the biaxial monotonic σ_h-ε_v curve corresponding to the same initial confining conditions. This can be seen by comparing the monotonic curves in Fig. 4.6 with the envelopes of the σ_h-ε_v curves in Fig. 4.21. However, after a few cycles the cyclic envelope clearly falls below the corresponding monotonic curve.

As seen in Figs. 4.15, 4.17 and 4.19, the unloading branches of the σ_h-ε_v curve do not follow the paths of the previous loading branches, and in successive unloadings the minimum horizontal stress drops to progressively decreasing values, which may be considerably lower than the initial horizontal stress σ_{hin} depending on the confinement level. This behavior indicates that even though the horizontal strain ε_{hc} is maintained constant there is some inelastic behavior in the horizontal direction. This can be most easily understood by considering Fig. 4.11.

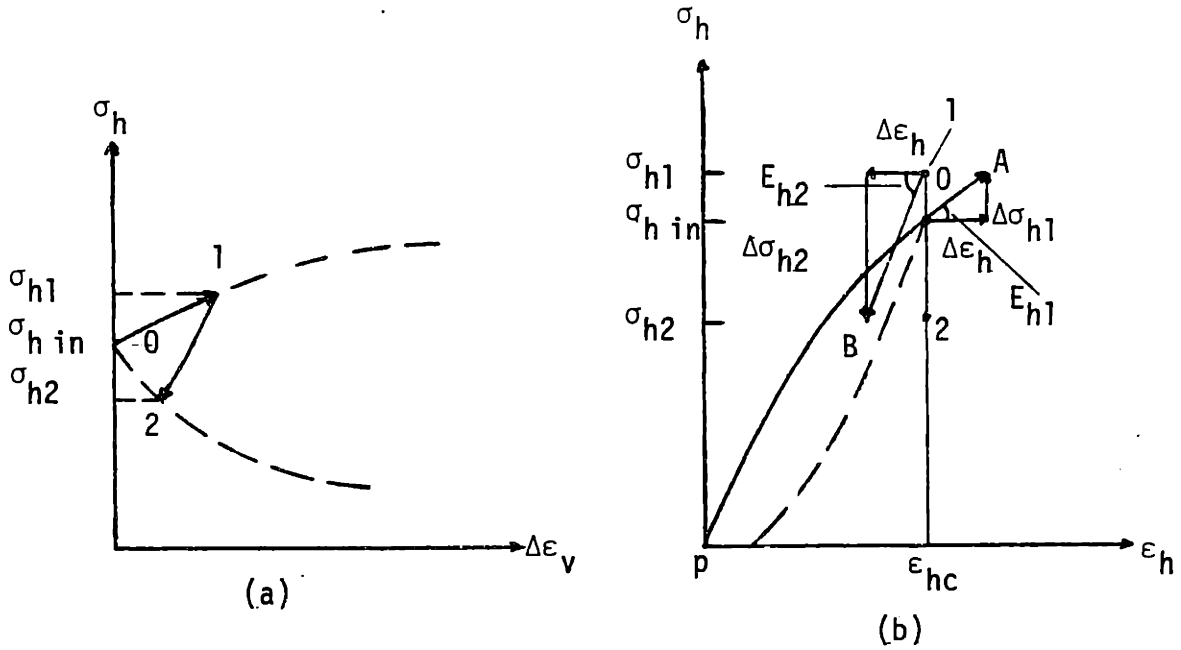

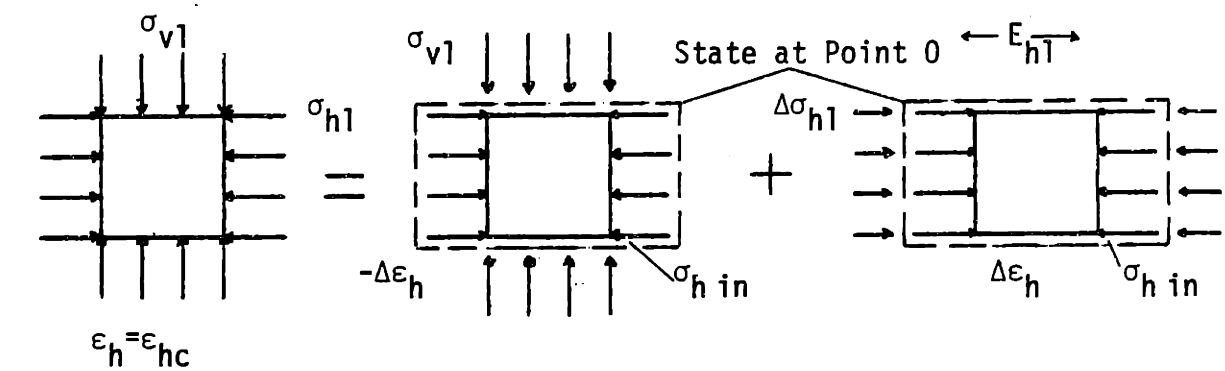

(c) Loading Process

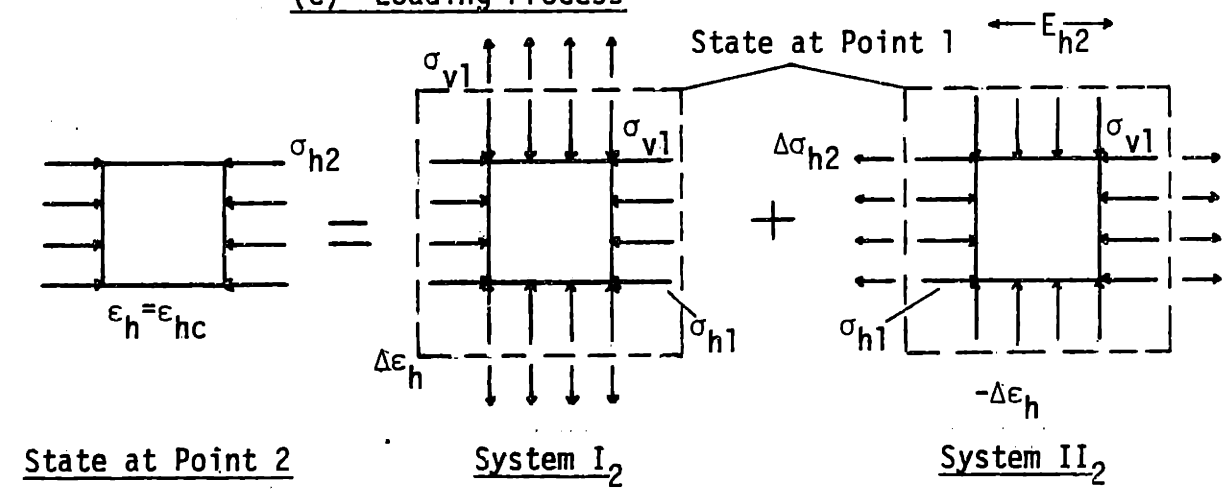

(d) Unloading Process

Fig. 4.11 - Analysis of Horizontal Stress Variation Under Confined Cyclic Loading

First of all we must consider the initial phase of the biaxial test, which consists in applying the horizontal confining strain ε_{hc}. This is a uniaxial loading process with a stress-strain curve as shown in Fig. 4.11(b) (path PO). If ε_{hc} is sufficiently high the concrete will have undergone some plastic deformation and point O will be located on the nonlinear portion of the curve. Once the initial state (Point O) is reached vertical stress is applied to the specimen.

Let us consider the first load-unload cycle in a given confined test, shown as path O12 in Fig. 4.11(a). For simplicity we assume the loading and unloading curves to be linear. The confined specimen is loaded vertically giving rise to an increment of horizontal stress $\Delta\sigma_{h1}$. The σ_h-ε_v path corresponding to this process is the loading curve O1. This loading process may be expressed as the superposition of 2 systems as shown in Fig. 4.11(c). One system (I_1) consists in applying the increment of vertical stress σ_{v1} at constant horizontal stress σ_{hin}, thus producing a compressive vertical strain increment and a tensile horizontal strain increment $-\Delta\varepsilon_h$. The second system (II_1) consists in applying a horizontal stress increment $\Delta\sigma_{h1}$, such that it produces an equal and opposite horizontal strain increment $\Delta\varepsilon_h$, in order to comply with the condition that ε_h remains constant. The stress-strain path corresponding to this system is shown in Fig. 4.11(b) as path OA. As seen in the figure, the modulus E_{h1} to be considered is the tangent modulus of the stress strain curve at the initial state, Point O. The actual state after loading, obtained by superimposing systems I_1 and II_1, is shown as Point 1 in the same figure. Note that there has been an increase in horizontal stress $\Delta\sigma_{h1}$, but no net increase in horizontal strain ε_{hc} due to the

confinement.

Unloading now takes place and the σ_h-ε_v path corresponding to this process is the curve 12 in Fig. 4.11(a). The unloading process may also be expressed as the superposition of two systems, as shown in Fig. 4.11(d). One system (I_2) consists in removing the vertical stress σ_{v1} at constant horizontal stress σ_{h1}, thus producing a tensile vertical strain increment and a compressive horizontal strain increment $\Delta\varepsilon_h$. The second system (II_2) consists in unloading horizontally by an amount $\Delta\sigma_{h2}$ at constant vertical stress so as to produce a horizontal tensile strain increment $-\Delta\varepsilon_h$, in order to enforce the confinement condition. This strain increment for the purpose of the present analysis is considered to be equal in magnitude to that of the loading process. The stress-strain path corresponding to system II_2 is shown in Fig. 4.11(b), as path 1B . The key fact to be recognized is that the horizontal unloading process in System II_2 is not elastic since ε_{hc}, if sufficiently high, is not fully recoverable. Thus unloading must occur at a modulus higher than the tangent loading modulus E_{h1} and approximately equal to that which would be expected if unloading occured at Point 0 of the σ_h-ε_h curve (see dashed line).

This and the fact that the slopes of the σ_h-ε_v curve are directly proportional to the values of the E_h moduli, explain why the loading and unloading curves in Fig. 4.11(a) do not coincide. Furthermore, since the unloading modulus E_{h2} is higher than the loading modulus E_{h1} and the horizontal strain increments $\Delta\varepsilon_h$ are considered equal under loading and unloading, it follows that the decrease in horizontal stress upon

unloading is higher than the increase in horizontal stress upon loading. See Fig. 4.11(b). This explains why in a load (reload)-unload cycle, as shown in Fig. 4.11(a), the horizontal stress drops below its initial value (in this case, σ_{hin}). The present analysis may be extended to any load-unload cycle in the test, where the initial horizontal stress is the stress at the lower peak where reloading begins, and the final horizontal stress is the stress at the following lower peak where unloading is completed. Such an analysis would explain why the branches of reload-unload cycles in the σ_h-ε_v curve do not follow the same path and why the horizontal stress drops to lower values as cycling proceeds.

The major assumption in the analysis was that horizontal strain increments $\Delta\varepsilon_h$ produced in systems I_1 (loading) and I_2 (unloading) are equal and opposite. Considering that the strain increments are due to the Poisson effect as measured by the Poisson ratio ν_{hv}, we have thus implicitly assumed that this ratio is the same under loading and unloading conditions and that there has been no accumulation of vertical plastic strain in the cycle since $\Delta\varepsilon_h = \nu_{hv}\,\Delta\varepsilon_v$. This last implicit assumption is not entirely correct for cycles at higher strain levels as can be seen in the σ_v-ε_v curves, where the vertical strain increment $\Delta\varepsilon_v$, produced by a reloading process is not entirely recoverable upon unloading. See the figure below.

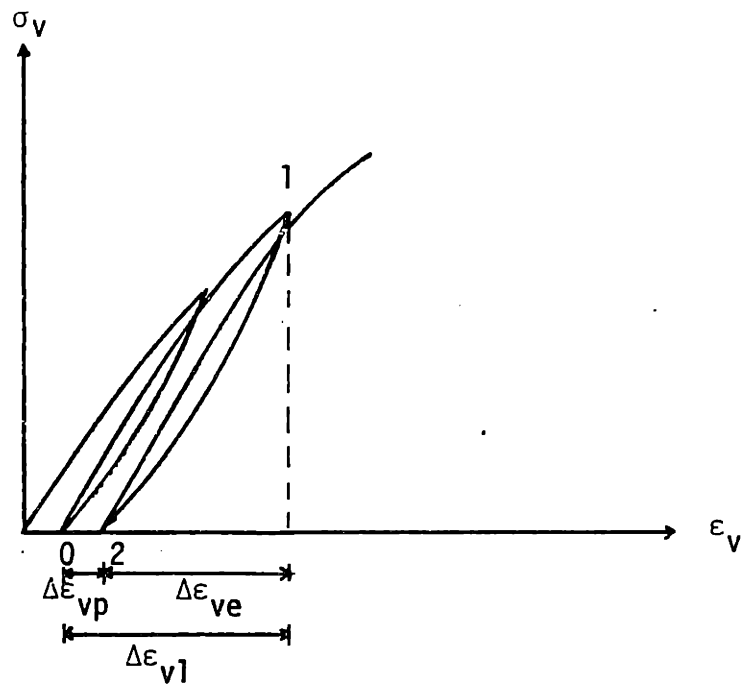

$\Delta\varepsilon_{v1} = \Delta\varepsilon_{ve} + \Delta\varepsilon_{vp}$

$\Delta\varepsilon_{v1} \equiv$ vertical strain increment in a reloading process 01

$\Delta\varepsilon_{ve} \equiv$ recoverable vertical strain

$\Delta\varepsilon_{vp} \equiv$ plastic vertical strain increment

However, from inspection of σ_v-ε_v curves, Figs. 4.14, 4.16 and 4.18, it is seen that most of the vertical strain produced in a reloading process is recovered upon unloading, so there is no major error involved in the assumption of fully recoverable strain in a reload-unload cycle for the purpose of the previous analysis. On the other hand it is reasonable to assume that the Poisson ratio ν_{hv} at loading does not vary significantly from that at unloading, since both processes take place in the presence of in-plane compressive strain fields which inhibit microcracking and induce similar Poisson behavior.

If the unloading curves of tests 4'.2 and 4'.3 originating at given values of vertical strain are superimposed at their origin it is seen that they coincide throughout most of their length. Only towards their end the unloading curves of test 4'.2 have a slightly less pronounced curvature than those of test 4'.3. So practically we can consider the unloading curves originating at given values of vertical strain to be the same for both tests. It should be recalled that a similar behavior was observed for the σ_v-ε_v unloading curves which were found to depend mainly on the vertical strain at unloading regardless of the confinement level.

In the previous analysis it was seen that the slope of the σ_h-ε_v unloading curve was related to the slope of the uniaxial unloading curve originating at the value of the confining strain ε_{hc}. If the strain ε_{hc} is in the plastic region the σ_h-ε_h unloading curve will have practically the same initial slope independently of the value of ε_{hc} by virtue of what was said previously that the initial slopes of unloading curves do not vary much across the cycles. Therefore we should expect similar σ_h-ε_v unloading curves for tests at confinement levels where ε_{hc} is in the plastic range. This is why the unloading curves corresponding to tests at confinement levels of ε_{hc}=500με/in (σ_{hin}=0.40f'_c) and ε_{hc}=935με/in (σ_{hin}=0.60f'_c) are practically the same for unloadings originating at given values of vertical strain. If ε_{hc} is so small that no plastic deformation has occurred, the σ_h-ε_h curve of Fig. 4.11(b) is still in its linear portion and it should be expected that upon unloading it will follow closely the initial loading path. Thus the slope Eh of this unloading

curve is lower than the slope of any unloading curve in the plastic region, and therefore the corresponding σ_h-ε_v unloading curves should have a lower slope than those at higher confinement levels, which is exactly what happens in the case of the confined test 4.4 at ε_{hc}=260με/in and σ_{hin}=0.20f'_c. See Fig. 4.15 and compare with Figs. 4.17 and 4.19.

The higher decrease of horizontal stress with respect to σ_{hin} at higher confinement levels is related to the initial slope of the σ_h-ε_v curve and the slopes of its unloading curves. For example, the initial σ_h-ε_v slope of test 4.6 (σ_{hin}=0.20f'_c) and 4'.2 (σ_{hin}=0.40f'_c) coincide since the initial confining stress in both tests is lower than the elastic limit but the slopes of the unloading curves are higher in test 4'.2. Thus the decrease of stress below the initial confining value σ_{hin} at the end of the first load-unload cycle is higher in test 4'.2. In the case of tests 4'.2 (σ_{hin}=0.40f'_c) and 4'.3 (σ_{hin}=0.60f'_c) their unloading curves have the same slope as discussed before, but the initial slope of the loading curve in test 4'.3 is lower because σ_{hin}=0.60f'_c, which is higher than the uniaxial elastic limit. Therefore, at the end of the first load-unload cycle the horizontal stress decreases more with respect to σ_{hin} in test 4'.3.

A peculiar characteristic of the σ_h-ε_v reloading curves is that they initially coincide with the unloading curves in the unload-reload cycles. This behavior completely differs from that exhibited in the vertical direction as shown in the σ_v-ε_v curves, where the reloading curves do not follow the same path as the unloading curves. The reason for this behavior in the horizontal direction may be related to the fact

that stress in this direction does not drop to zero at the end of each cycle and thus reloading occurs at a relatively high value of stress. From uniaxial cyclic loading experiments (7) it can be seen that if reloading in a given cycle occurs at a relatively high value of stress the reloading curve tends to follow more closely the unloading curve thus exhibiting a highly reduced hysteretic behavior. Since behavior in the horizontal direction is related to the uniaxial cyclic behavior, it follows that the σ_h-ε_v reloading curve would tend to follow the path of the unloading curve in an unload reload cycle. At a certain percentage of the horizontal stress existing at the moment of unloading the reloading curve starts declining in slope and tends to regain the initial loading slope existing at the beginning of the test. Thus if unloading does not occur again the reloading curve will apparently continue its course at a slope equal to the initial one. Thus, one should not consider the upper envelope, which in tests 4'.2 and 4'.3 has a descending portion, as the path which the reloading curve would follow upon monotonic loading. The envelope should be viewed only as the curve joining the peaks of the cyclic curve. The envelope has a descending portion because the cyclic peaks occur at progressively lower values of horizontal stress, which is partly due to the fact that reloading occurs every time at lower values of horizontal stress.

The fact that the slope of the reloading curve at each peak is equal to the initial loading slope and thus equal to the slope of the corresponding monotonic curve may be viewed as a tendency of the concrete to behave after reloading as if no previous cycling had occurred.

The major difference at higher strain levels is that this behavior occurs at lower values of horizontal stress than those of the monotonic curve mainly because the reloading process begins at lower values of horizontal stress. This behavior exhibited by the σ_h-ε_v reloading curve is similar to that of its σ_v-ε_v counterpart, where after the common point the slope of the reloading curve starts declining and the curve becomes tangent to an envelope curve which is probably equal to the monotonic curve, thus showing that the concrete starts exhibiting a σ_v-ε_v behavior as if no previous cycling had occurred.

It should be noted that in test 4.6 at $\sigma_{hin}=0.20f'_c$ the upper σ_h-ε_v envelope is a straight line and thus may be considered as coinciding with the corresponding biaxial monotonic curve. In this case the upper peaks do not decrease, which is partly due to the fact that reloading begins at more or less the same values of horizontal stress in different cycles.

Stresses and Strains at Failure

Values of vertical and horizontal stresses and strains at the peak of the σ_v-ε_v curve for cyclic tests 4.4, 4.5, 4.6, 4!2 and 4!3 are shown in Table 4.6. Based on the data of this Table peak stresses and strains are plotted on Figs. 4.10(a) and 4.10(b) respectively, for comparison with the data obtained in the biaxial monotonic tests.

It is remarkable that the strains at failure in the biaxial cyclic tests practically lie on the strain failure envelope corresponding to the monotonic tests (see Fig. 4.10(b)). On the other hand, stresses at failure in the biaxial cyclic tests show in general good agreement with the monotonic stress failure envelope considering the experimental error and other involved random variables. This would seem to point out that failure of concrete occurs at given combinations of stress and strain regardless of the previous stress-strain path. This means that there is a correspondence of points on both envelopes such that concrete will fail if at any point along its stress-strain path it attains any one of the stress-strain states represented by a pair of envelope points. Notice that this path need not necessarily be one attained under a confined compression test, however being that the envelopes are constructed on the basis of these tests. Moreover the pair of envelopes obtained in these tests actually represent a limited set of stress-strain states at failure. It is easy to conceive that other envelopes can be obtained for other types of tests. For example, the stress and strain failure envelopes obtained for concrete subjected to biaxial compression at a constant principal stress ratio (see Kupfer, et al. (8))

do not coincide with those obtained in this investigation. However, the uniqueness properties expressed above might also be applied to this and other sets of envelopes obtained under different circumstances. Integrating these envelopes and including the effect of the strain in the third direction, the total failure criterion for concrete under biaxial compressive loading would be based on a unique five-dimensional stress-strain surface. Thus, concrete would fail if at any point along its stress-strain path it attained any one of the stress-strain states represented by a point on the envelope surface regardless of the previous stress-strain path, be it cyclic, monotonic or any other combination thereof. In this context failure has been understood as the inability of concrete to carry additional stress beyond the current level, and not as total collapse, which may occur at lower stress and higher strain values in the softening or descending branch.

The failure mode exhibited in the confined cyclic tests of the present Series, as well as of Series 3 and 4, is the same as that observed in the confined monotonic tests of Series 1 (see Section 4.1.2).

4.3 Test Series 3 - Cycles to Prescribed Values of Vertical Stress

In this Series unconfined specimens and specimens under different confinement levels were subjected to the same vertical stress history, after which the confined specimens were loaded monotonically to failure.

Uniaxial data for the batch tested in this Series is given in Table 4.7.

Concept	Batch 5
f'_c(psi)	5225
ε_o($\mu\varepsilon$/in)	3822
E(psi)	2.12×10^6
ν	0.25

Table 4.7

Meaning of each variable is the same as in Table 4.1

The levels of vertical stress to which the specimens were loaded in the cycles are given in the following Table:

Cycle No.	Max. σ_v/f'_c
1	0.37
2	0.55
3	0.68
4	0.80
5	0.91
6	0.97
7	1.00

Table 4.8

One uniaxial cyclic test, 5.2, and three biaxial cyclic tests, 5.4, 5.5 and 5.6, each at a different confinement level, were performed. In the uniaxial cyclic test a σ_v-ε_v curve and a ε_v-ε_h curve were simultaneously recorded. See Figs. 4.23 and 4.24. For each biaxial cyclic test a σ_v-ε_v curve and a σ_h-ε_v curve were simultaneously recorded. See Figs. 4.25 - 4.28.

Based on the curves, the data shown in the Table below was obtained.

	Test			
Concept	5.2	5.4	5.5	5.6
$\sigma_{h\,in}/f'_c$	0	0.18	0.37	0.55
$\varepsilon_{hc}(\mu\varepsilon/in.)$	0	215	650	1050
E_{ef} (psi)	2.12×10^6	2.49	3.25	2.22
σ_{vp}/f'_c	1.0	1.36	1.53	1.42
$\varepsilon_{vp}/\varepsilon_o$	1.0	1.34	1.11	1.17
σ_{hp}/f'_c	0	0.44	0.68	0.68
$\varepsilon_{hp}/\varepsilon_o$	0.71	0.06	0.17	0.27
σ_{hp}/σ_{vp}	0	0.32	0.44	0.48

Table 4.9

Meaning of each variable is the same as in Table 4.6

Test 5.2 was actually used in determining the uniaxial properties of the batch since it was considered to be more representative than the monotonic uniaxial tests.

4.3.1 Uniaxial Cyclic Test

σ_v-ε_v Curve

The uniaxially cycled specimen in this Series exhibits a very similar behavior to that of the specimen in Series 2 (test 4.4, Fig. 4.12). Reloading curves in both tests starting at given values of vertical (plastic) strain coincide in slope up to the common points of test 4.4, and the unloading curves in these tests starting at given values of vertical strain, overlap when superimposed at σ_v=0. Since the strength of the batch in this Series is higher than that of batch 4, but the initial elastic modulus E is the same, the slopes of the unloading and reloading curves originating at given values of vertical strain do not seem to be affected by the strength of the specimen, and appear to depend mainly on the initial elastic modulus E.

It should be noted that the stress levels to which the specimen was cycled were such that the curve became tangent to its envelope curve.

ε_v-ε_h Curve

If this curve is compared to that of the uniaxial cyclic test of Series 2 (test 4.4, Fig. 4.13), we can see that the upper envelope falls below that of test 4.4, but the lower envelopes coincide. The reason

for the discrepancy in the upper envelope is related to the fact that the tangent Poisson ratio (inverse slope of the curve) starts varying at a given percentage of the uniaxial strength f'_c. Since f'_c is higher in this batch the vertical strain at which the ε_v-ε_h curve becomes non-linear is higher than that at which nonlinearity occurs in the ε_v-ε_h curve of test 4.4. On the other hand, it is very significant that the lower envelopes in both tests coincide, in spite of the difference in strength and stiffness at high stress levels. This result strengthens the notion of uniqueness of the plastic strain curve, which implies that at a given value of vertical plastic strain there will always be one and only one corresponding horizontal plastic strain, independently of the previous stress-strain paths. This may be very useful for modeling plastic behavior of concrete under uniaxial loading. Physically speaking, the concept is appealing since vertical and horizontal strains are always intrinsically related through the Poisson effect. Thus it is not difficult to imagine that a plastic vertical strain will automatically imply a horizontal plastic strain.

4.3.2 Biaxial Cyclic Tests

σ_v-ε_v Curve

The σ_v-ε_v curves of tests 5.4, and 5.6 are shown in Figs. 4.25 and 4.26. The initial slopes of the curves of tests 5.4 ($\sigma_{h\ in.} = 0.18\ f'_c$) and 5.6 ($\sigma_{h\ in.} = 0.55\ f'_c$) are similar and somewhat higher than the uniaxial modulus E, as in the previously discussed Test Series. The curve of test 5.5 ($\sigma_{h\ in.} = 0.37\ f'_c$) exhibits a much higher slope than

the other curves, which is most probably due to the fact that the specimen was actually stiffer and stronger than the others and hence cannot be considered as representative of the batch. It can be seen that the envelope to this curve is significantly higher than those of the other tests, which should not be expected. Therefore, the discussion will be limited to tests 5.4 and 5.6.

The effect of the confinement in cyclic tests can most easily be appreciated by subjecting confined and unconfined specimens to the same vertical stress history. It is seen that strains, both total and plastic, accumulated under the same levels of applied vertical stress are highly reduced in the confined tests. The total strain accumulated by the specimens confined at 0.18 f'_c and 0.55 f'_c, upon completion of the cycles, was 70% of that corresponding to the unconfined specimen. The accumulated plastic strain in the confined tests was only 46% of that in the unconfined test. Also the ratio of total to plastic strain is considerably lower in the confined tests, thus indicating a more elastic behavior of concrete under confinement.

The curves of tests 5.4 and 5.6, when superimposed, show a very good agreement. Reloadings take place up to about the same values of vertical strain, and therefore the envelopes to both curves practically coincide throughout the cyclic portion of the test. The only difference between curves exsits in the subsequent monotonic branches where the curve of the test at lower confinement falls below that of the test at higher confinement, as should be expected according to the results of Test Series 2. Behavior of the reloading and unloading curves follows a

pattern similar to that of tests in Series 2. The shapes and slopes of these curves in regions previously specified do not vary with confinement. The curves of test 5.4 show a slight descrepancy with respect to those of tests 5.6 and 5.2, but that is due mainly to a difference in initial effective modulus. The reloading slopes in the biaxial tests do not vary much from one cycle to another because cycling takes place in a small strain range. The same trend is exhibited by the unloading curves.

A biaxial cyclic test to the envelope of the type performed in the previous Series, was carried out at an initial confining stress $\sigma_{h\ in} = 0.20\ f'_c$ on one of the specimens of the batch for the present Series (test 5.3). If the curve of this test is compared to that of test 5.4 ($\sigma_{h\ in} = 0.18\ f'_c$) it is seen that the envelopes to both curves coincide initially, after which the envelope of test 5.4 falls slightly below that of test 5.3 because the levels of vertical stress are not sufficient to allow for the curve to reach the envelope, and, at the end, the monotonic portion of the curve of test 5.4 becomes perfectly tangent to the envelope of test 5.3 and failure occurs at very similar values of stress and strain. This reinforces the notion of a unique envelope curve which may be reached under different loading histories, therefore, adding validity to the supposition that the cyclic curve possesses an envelope such that if at any point during a test the strain is monotonically increased the stress-strain curve will eventually reach and follow the path of this envelope, which perhaps coincides with the corresponding monotonic curve.

Plastic Strains. Fig. 4.29 shows the relationship between vertical plastic strains and strains at unloading $\Delta\varepsilon_{vun}$ for cyclic tests 5.2, 5.4 and 5.6. Similar results to those obtained in Series 2 are obtained here. The plastic strains appear to be uniquely defined on the basis of the value of vertical strain at unloading without having the confinement influence the results significantly. Comparison of Figs. 4.29 and 4.22 shows that the points corresponding to the present test Series fall in the same region as those corresponding to test Series 2, in spite of the difference in batch strength as well as stiffness at high strain levels. This supports the idea of uniqueness of the relationship between plastic strains and strains at unloading. However, it should be emphasized that the relationship is valid for unloadings originating at the envelope curve because it is expected that if unloading occurs at the same strain level but at a much lower value of stress, the recoverable strain increment will be much smaller thus rendering a higher plastic strain.

σ_h-ε_v Curve

The σ_h-ε_v curves of tests 5.4 and 5.6 are shown in Figs. 4.27 and 4.28 respectively. The general behavior exhibited here is analogous to that observed in the biaxial cyclic tests of Test Series 2 (cycles to the envelope curve). Here again, at higher confinement levels, the rise of the upper envelope above $\sigma_{h\ in.}$ is lower, with the envelope exhibiting a descending portion in test 5.6, and the descent of the lower envelope below $\sigma_{h\ in.}$ is higher.

Since cycling is performed within a small strain range, the reload-unload curves are much closer than in the case of cycles to the envelope curve (previous Test Series). It is important to realize that the re-loading curves tend to regain a slope at the peaks equal to that of the initial loading portion of the curve, just as observed in the previous Series. However, in test 5.6 for example, since cycling was not performed to the σ_v-ε_v envelope, sufficient vertical strain in a given cycle was not developed, so the slope of the reloading curve did not decrease enough and thus the slope at some peaks is higher than the initial loading slope. Very interesting is the behavior upon monotonic loading. As seen in Fig. 4.28, in the last cycle, when vertical strain is increased monotonically the reloading curve gradually decreases in slope, adopts the initial loading slope, and continues its course at that same slope, thus exhibiting a behavior parallel to that of the corresponding monotonic biaxial test. This behavior is exhibited in the region of the descending portion of the upper envelope which shows that the curve will not follow a descending path upon further monotonic loading in this region. A similar behavior in the vertical direction is manifested by the fact that the σ_v-ε_v curve apparently reaches the monotonic curve if, at a given point, strain is applied monotonically. The monotonic branch of the σ_h-ε_v curve in test 5.4 acquires a slope equal to the initial loading slope but then slightly decreases in slope until failure. This might have been due to operator error in not keeping the horizontal strain at its required value thus inducing unintentional horizontal stress fluctuations.

An effect of the cyclic loading is that the horizontal stress at failure is lower than that which would have existed if the specimen were loaded monotonically from the beginning. This discrepancy with respect to the monotonic horizontal stress at failure increases at increasing confinement levels.

Stresses and Strains at Failure

Values of vertical and horizontal stresses and strains at the peak of the σ_v-ε_v curve for cyclic tests 5.2, 5.4 and 5.6 are shown in Table 4.9. Based on the data of this Table, peak stresses and strains are plotted on Figs. 4.10a and 4.10b respectively, for comparison with the data obtained in the previous tests.

As seen in Fig. 4.10a the stress points fall in the same region as the points corresponding to previous tests. The points corresponding to the strain states at failure in this Test Series are shown in Fig. 4.10(b) and they fall in the same region as those of previous tests too. This strengthens the concept of uniqueness of the stress-strain states at failure as discussed in Section 4.2.2.

4.4 Test Series 4 - Cycles Between Fixed Maximum and Minimum Stresses

Initially, an unconfined specimen, 6.6, was continuously cycled between zero vertical stress and a stress equal to 0.82 f'_c. The number of cycles to failure in this test was 35. Then three specimens, 6.3, 6.4, and 6.5, each under a different confinement level, were cycled 35 times between zero and a constant maximum vertical stress,

after which they were loaded monotonically to failure. It was originally intended to cycle each specimen to the same stress level. However, unintended specimen surface irregularities caused non-uniform stress and strain distributions, due to which the resulting curves had to be adapted to represent the actual stresses and strains acting in the central region of the specimen. The actual mid-specimen stress levels to which each of the specimens were cycled are shown in Table 4.11.

Uniaxial data for the batch tested in this Series is given in Table 4.10.

Concept	Batch 6
f'_c (psi)	4675
ε_o(με/in.)	3000
E (psi)	2.34×10^6
ν	0.22
ε_{hp}(με/in.)	1325

Table 4.10

Meaning of variables are the same as in Tables 4.1 and 4.4.

For the uniaxial cyclic test, 6.6, a σ_v-ε_v curve and a ε_v-ε_h curve were simultaneously recorded, while for each biaxial cyclic test a σ_v-ε_v curve and a σ_h-ε_v curve were obtained. Based on the curves, the data shown in the Table below (4.11) was obtained. The data includes the level of vertical stress to which the specimens were cycled, as

mentioned earlier, plus information similar to that obtained in test Series 2 and 3.

	Test			
Concept	6.6	6.3	6.4	6.5
$\sigma_{h\ in.}/f'_c$	-	0.24	0.48	0.72
$\varepsilon_{hc}(\mu\varepsilon/in.)$	-	325	890	1485
σ_{vcyc}/f'_c	0.82	0.73	0.96	1.21
σ_{vp}/f'_c	0.82	1.27	1.46	1.44
σ_{hp}/f'_c	-	0.52	0.70	0.77

Table 4.11

where σ_{vcyc} = maximum vertical stress to which the specimen was cycled

Meaning of each of the other variables is the same as in Table 4.6.

As seen in the Table, specimens confined at initial horizontal stresses of 0.24 f'_c, 0.48 f'_c and 0.72 f'_c, were cycled between zero and a vertical stress of 0.73 f'_c, 0.96 f'_c and 1.21 f'_c respectively. However, the data in the Table above should be considered approximate since it is based on curves which were modified in order to account for the effect discussed previously. All σ_v-ε_v curves are assumed to have the same initial slope E_{ef}, in accordance to results of previous Test Series (1, 2 and 3).

4.4.1 Uniaxial Cyclic Test

The stress strain behavior exhibited in this test was similar to that exhibited in previous tests of the same kind performed by Karsan and Jirsa (7). In the first few cycles the distance between upper peak of consecutive cycles decreases as the number of cyclies increases. The same behavior is exhibited at the lower peaks (at σ_v=0). This initial decrease in the rate of strain accumulation is typical of specimens su: :esively loaded to the same stress level. The rate of strain accumulation then becomes stable and towards the end of the test it slightly increases. A decrease in the slopes of the reloading and unloading curves can be appreciated towards the end of the test, and is associated with an increase in the degree of microcracking at higher strain levels. In this test the vertical strain at failure was less than the monotonic uniaxial strain at failure ε_o, while it actually should have been greater. The reason for this lies in the fact that the strain distribution due to surface irregularities was not uniform and higher strain levels existed near the edges of the specimen in a region not covered by the strain gages.

The ε_v-ε_h curve for this test follows the trend of other curves of the same type, with the plastic strain curve gradually decreasing in slope, indicating that the plastic horizontal strain increments grow at a faster rate than the vertical ones.

4.4.2 Biaxial Cyclic Tests

As mentioned before, specimens 6.3, 6.4 and 6.5, each under a different confinement level, were cycled between zero and given values of vertical stress (see Table 4.11) 35 times (no. of cycles to failure for uniaxial case) and then loaded monotonically to failure. From the resulting stress-strain curves it was immediately seen that the confined specimens were far from failing after 35 cycles, even those cycled at higher stress levels than in the uniaxial test 6.6, such as specimens 6.4 and 6.5, which were cycled up to vertical stress levels of 0.96 f'_c and 1.21 f'_c respectively. The beneficial effect of the confinement can be seen in that microcracking is inhibited and thus strain accumulation, both plastic and at the upper peaks of the curve, is considerably reduced with respect to the uniaxial case. A peculiar phenomenon in the confined tests is that after a certain number of cycles, no significant additional straining occurs and the stress-strain curve goes into a closed loop. Evidently in all cases, failure would have taken very long or probably would have never occured if cycling proceeded normally to the given stress levels. This would be understandable for tests 6.3 and 6.4 where the maximum vertical stress during cycling, σ_{vcyc}, was relatively low with respect to the biaxial strength σ_{vp}. In tests 6.3 and 6.4, σ_{vcyc} was equal to 0.57 σ_{vp} and 0.66 σ_{vp}, respectively. After all, it is known that for uniaxially loaded concrete, cycles to maximum stress levels equal to or lower than about 0.60 f'_c or 0.70 f'_c do not cause failure (7, 13). However, at a maximum stress level of 0.82 f'_c failure is certain to occur as seen in uniaxial test 6.6.

Making an analogy to the biaxial situation it is seen, however, that cycling up to 0.84 σ_{vp} probably never causes failure. The difference in behavior is related to microcracking inhibition in the biaxial test.

Total and plastic strains accumulated between the first and last cycles vary from one test to another, which is mostly due to the difference in maximum levels of vertical stress. The variation, however, is not considerable and average values of total and plastic strains accumulated between the first and last cycles are 450 με/in. and 360 με/in. In contrast, the corresponding strains increments in the uniaxial test are equal to 1200 με/in. and 830 με/in. Therefore, confinement decreases total and plastic strain accumulation to about 36% and 43% of the uniaxial magnitudes. This shows quantitatively the effectiveness of the confinement in reducing strain accumulation under cyclic loading.

Variations of horizontal stress during the tests were monitored in σ_h-ε_v curves. The curves corresponding to tests 6.4 ($\sigma_{h\ in.}$ = 0.48 f'_c) and 6.5 ($\sigma_{h\ in.}$ = 0.72 f'_c) present certain differences with respect to those of tests at similar confinement levels in Series 2 and 3. In the present tests, immediately following the first load-unload cycle, the upper peaks start descending and continue to do so throughout the remainder of the cyclic portion of the test. This is due to the fact that vertical stress always increases to the same level and hence no significant additional vertical straining occurs which may in turn induce higher horizontal stress increments. The envelope to

the upper peaks is approximately a straight line roughly parallel to the lower envelope joining the lower peaks. Therefore, the increments of horizontal stress upon reloading are approximately constant throughout the tests. The σ_h-ε_v behavior in test 6.3 ($\sigma_{h\ in.} = 0.24\ f'_c$) is different from that in tests 6.4 and 6.5 The upper envelope ascends during the first cycles after which it stabilizes at a given level while the lower envelope continuously descends. This means that while the vertical stress increments are always constant upon reloading, the horizontal stress increments continuously increase. Since horizontal stress increments are intimately related to vertical strain increments due to the Poisson effect, the exhibited behavior might be due to the fact that the vertical strain increments upon reloading continuously increase throughout the test. However this is hard to tell from the σ_v-ε_v curve since the cyclic branches are very close one to another.

The vertical and horizontal stresses at failure are shown in Table 4.11. The general trend of these stresses is similar to that observed in the other Test Series. The maximum strength was equal to 1.46 f'_c at a stress ratio of 0.48, and occured in test 6.4.

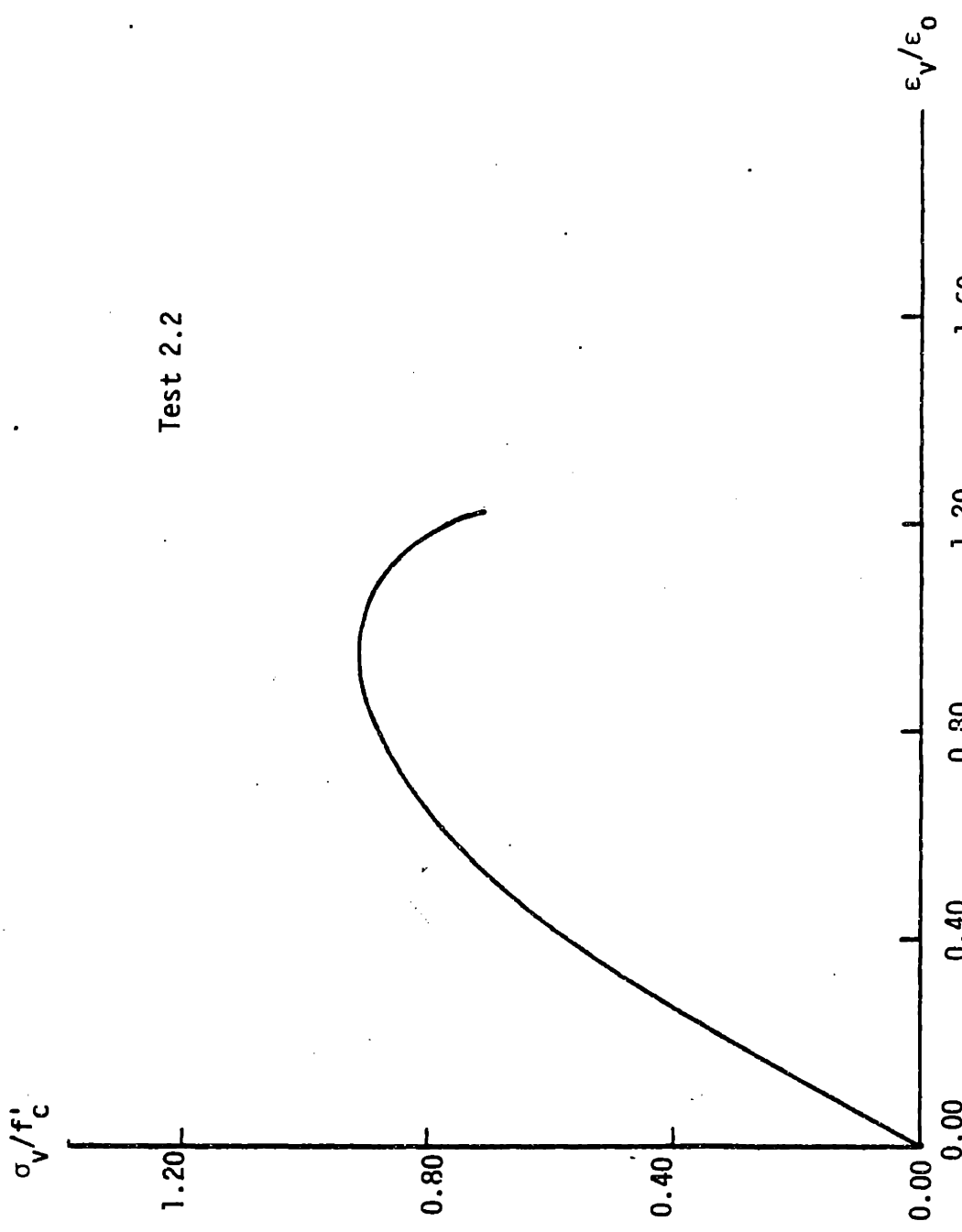

Fig. 4.1 - Uniaxial Monotonic Loading Test Series 1

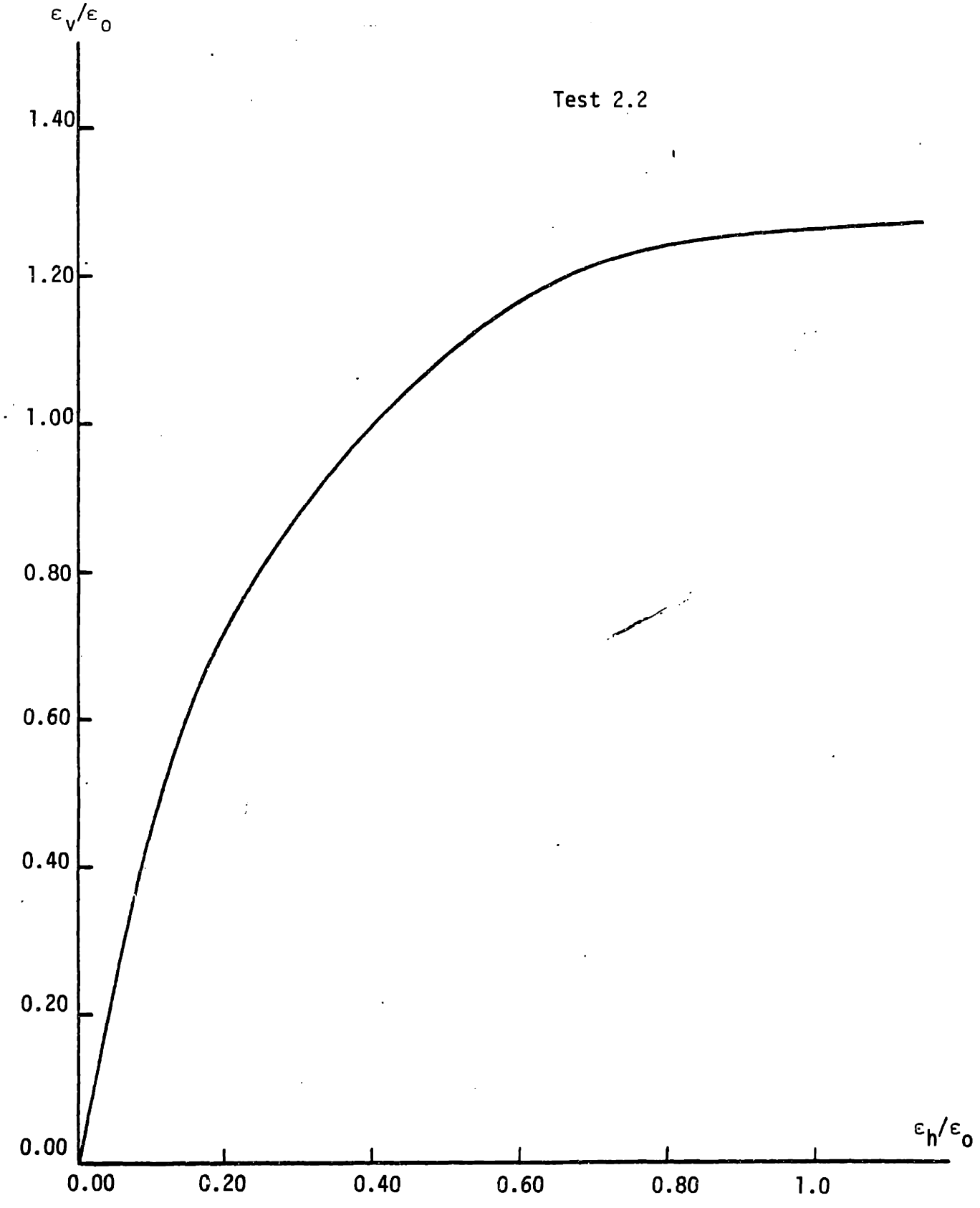

Fig. 4.2 - Relationship Between Vertical and Horizontal Strain in Uniaxial Monotonic Loading

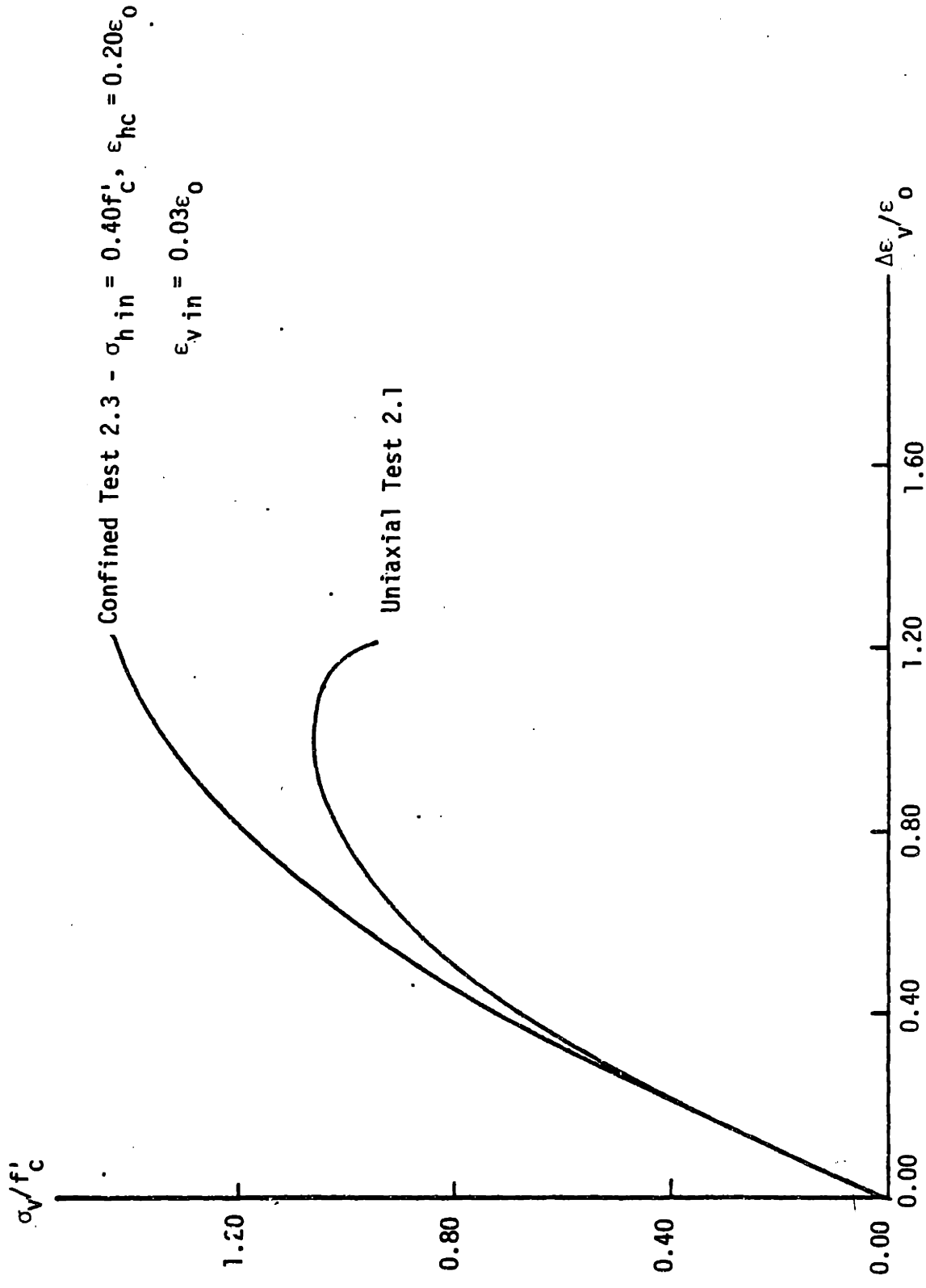

Fig. 4.3 - Uniaxial and Confined Monotonic Loading. Test Series 1

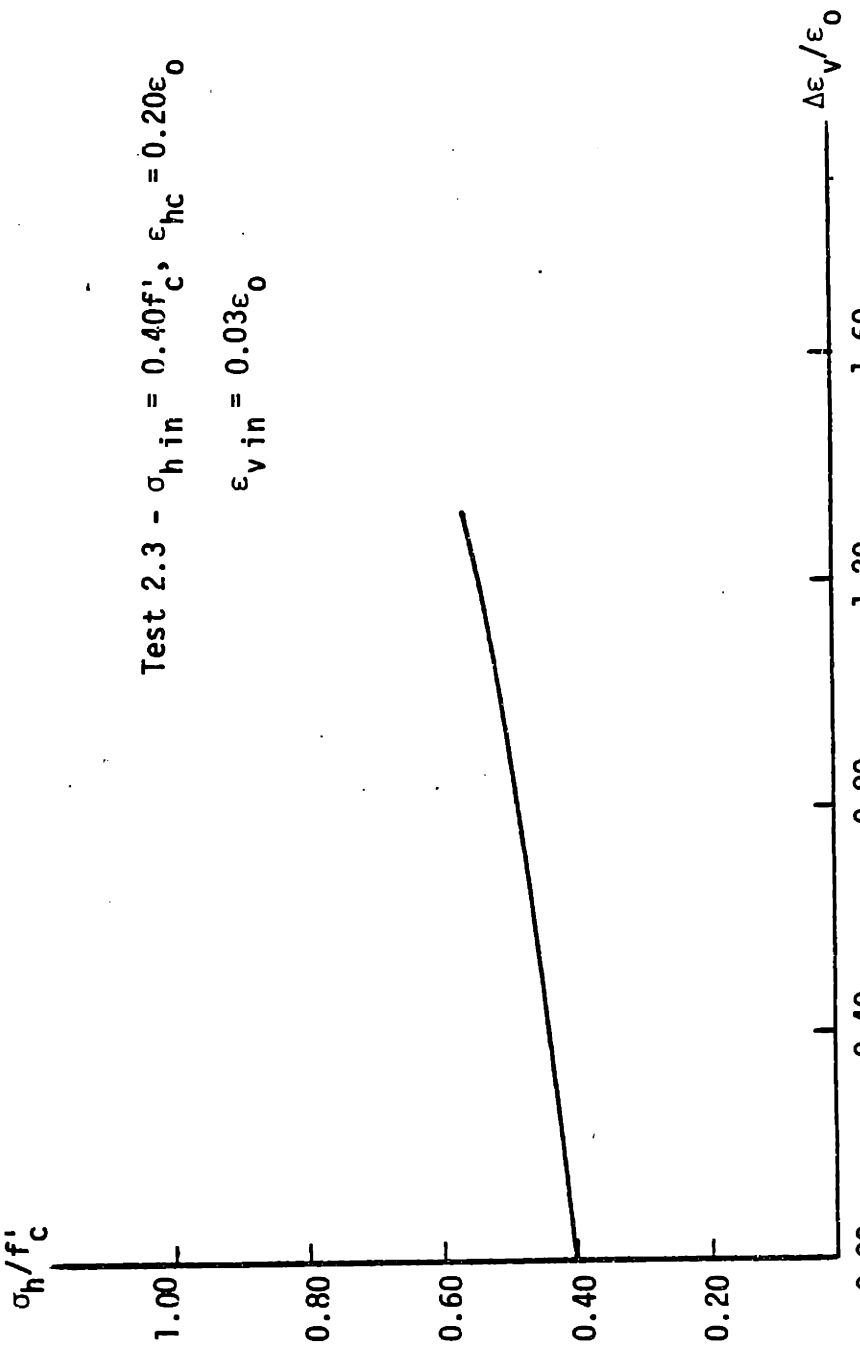

Fig. 4.4 - Horizontal Stress Variation Under Confined Monotonic Loading

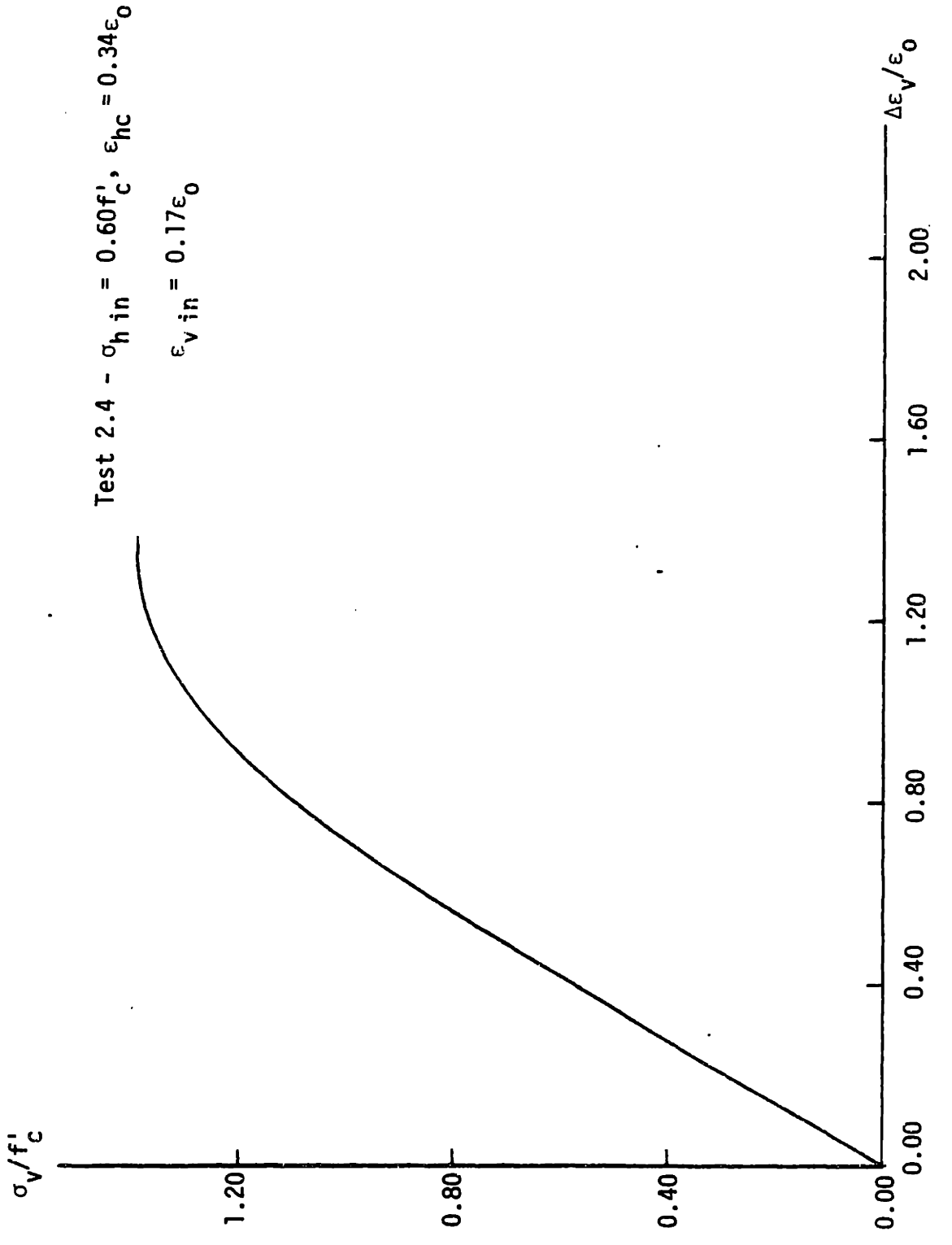

Fig. 4.5 - Confined Monotonic Loading. Test Series 1

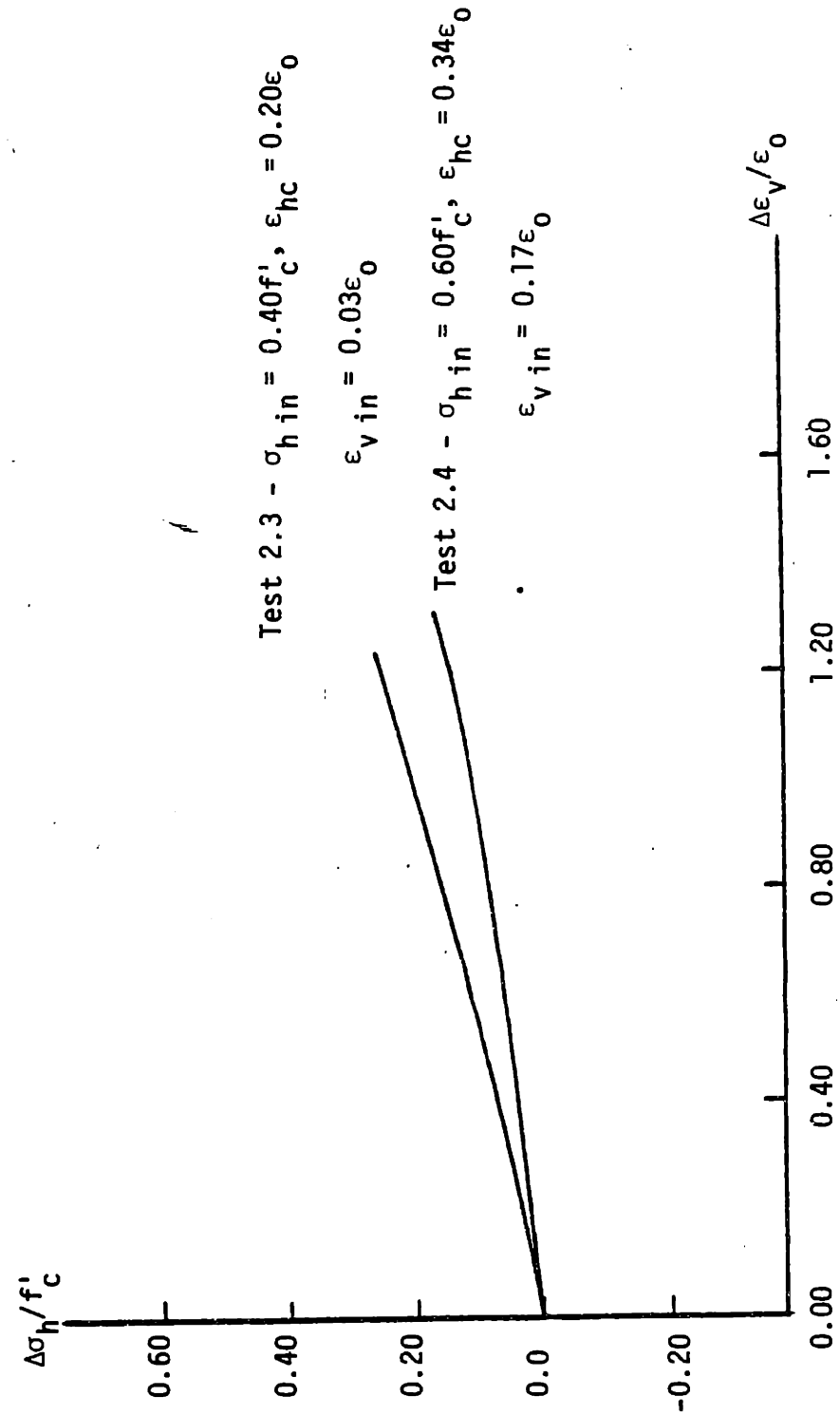

Fig. 4.6 - Horizontal Stress Variation Under Confined Monotonic Loading

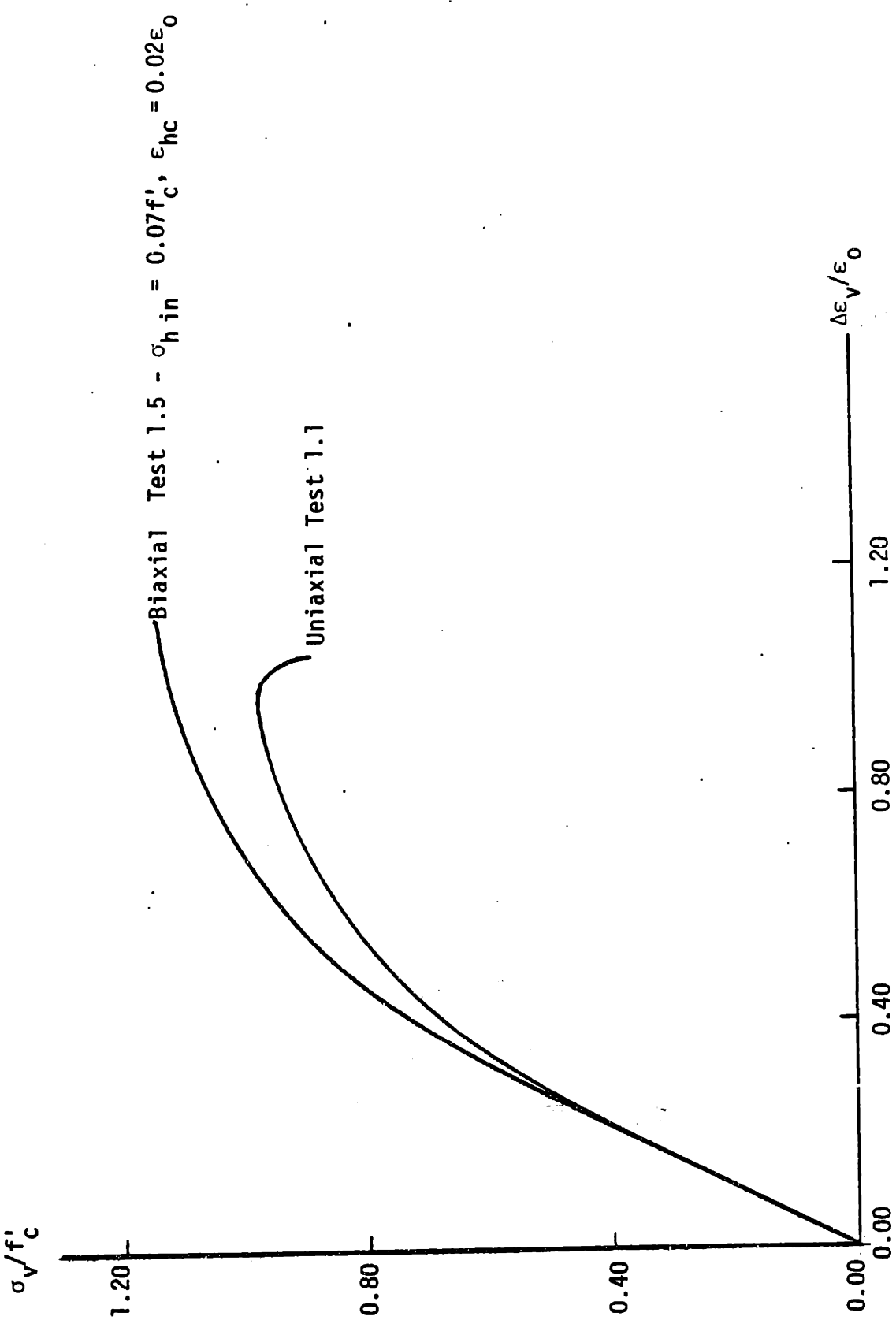

Fig. 4.7 - Uniaxial and Biaxial Monotonic Loading. Test Series 1

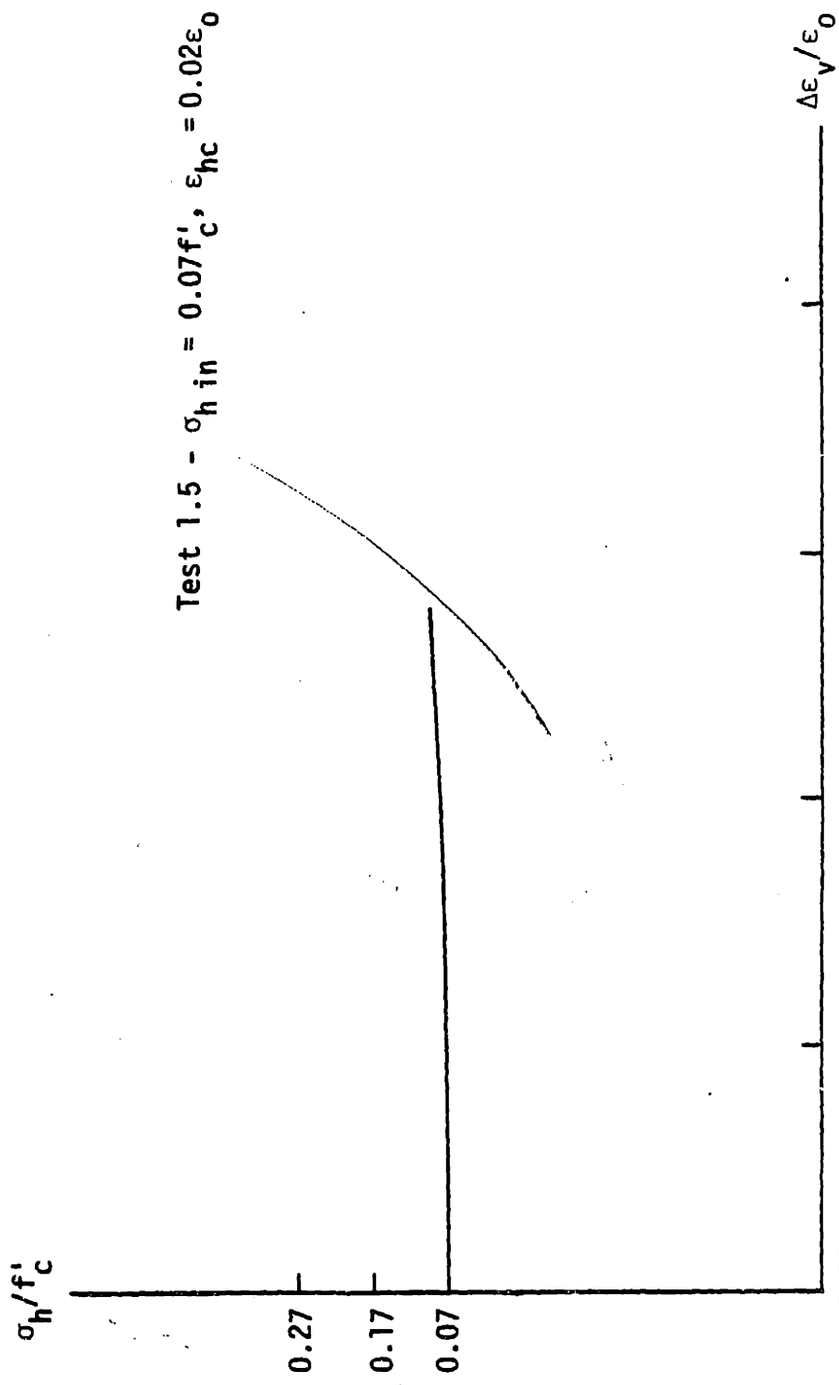

Fig. 4.8 - Horizontal Stress Variation Under Biaxial Monotonic Loading

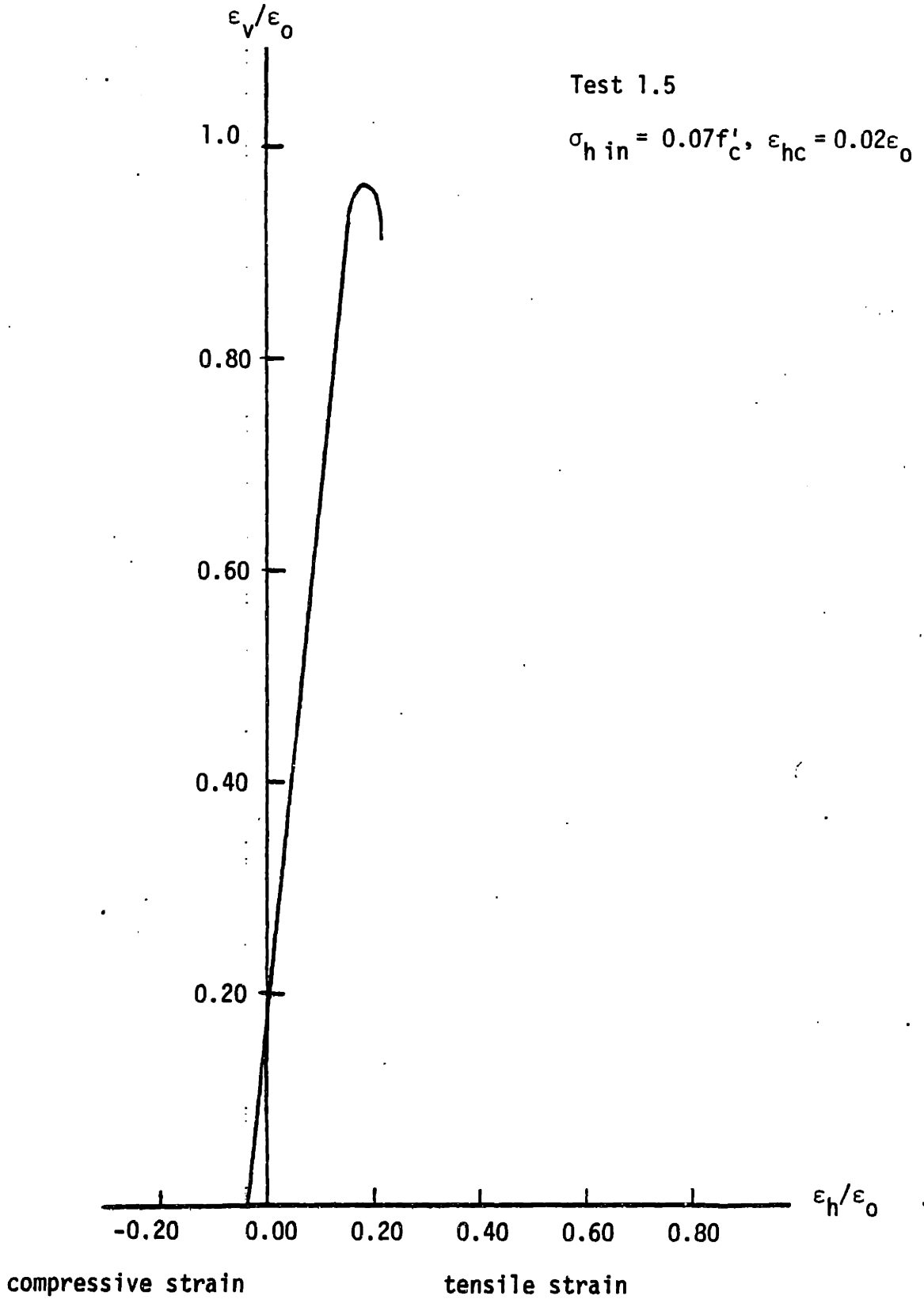

Fig. 4.9 - Relationship Between Vertical and Horizontal Strain in Biaxial Monotonic Loading

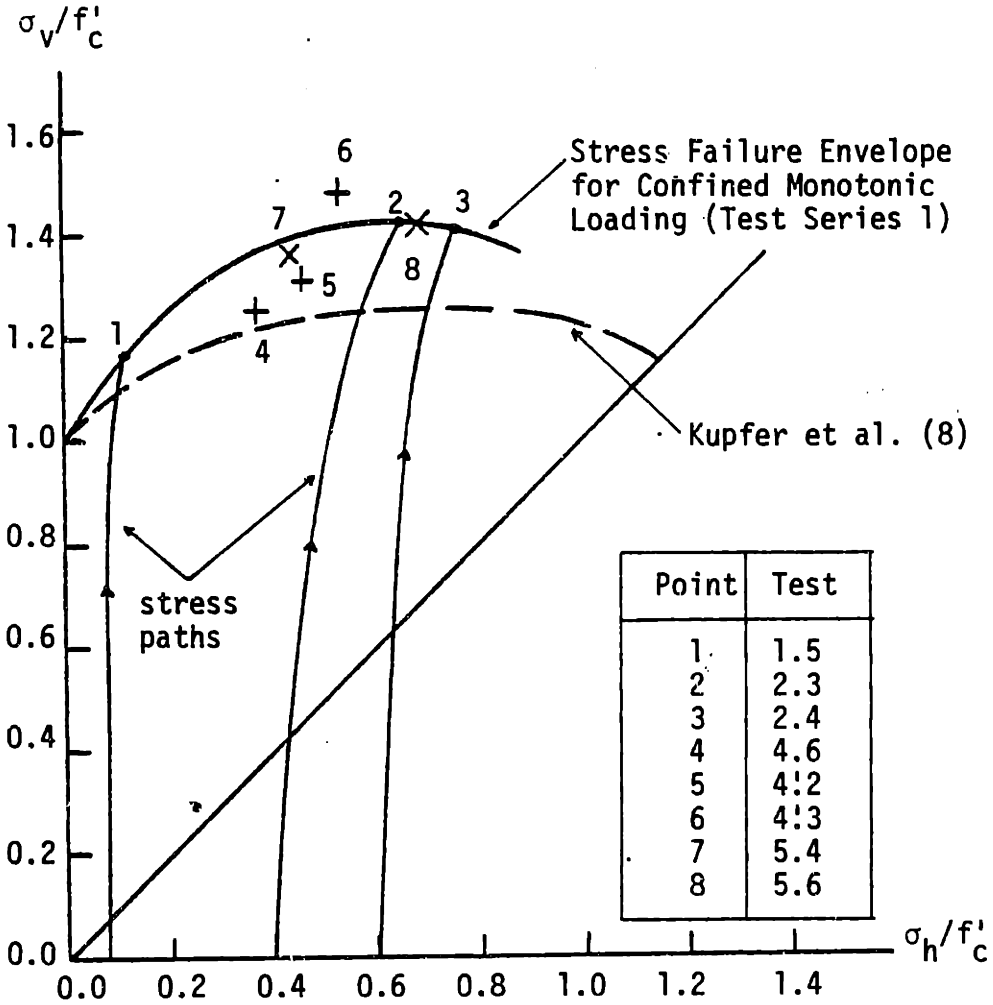

• Test Series 1. Monotonic Loading to Failure

+ Test Series 2. Cycles to the Envelope Curve

× Test Series 3. Cycles to Prescribed Values of Vertical Stress (and Subsequent Monotonic Loading to Failure)

Fig. 4.10(a) - Biaxial Strength of Concrete

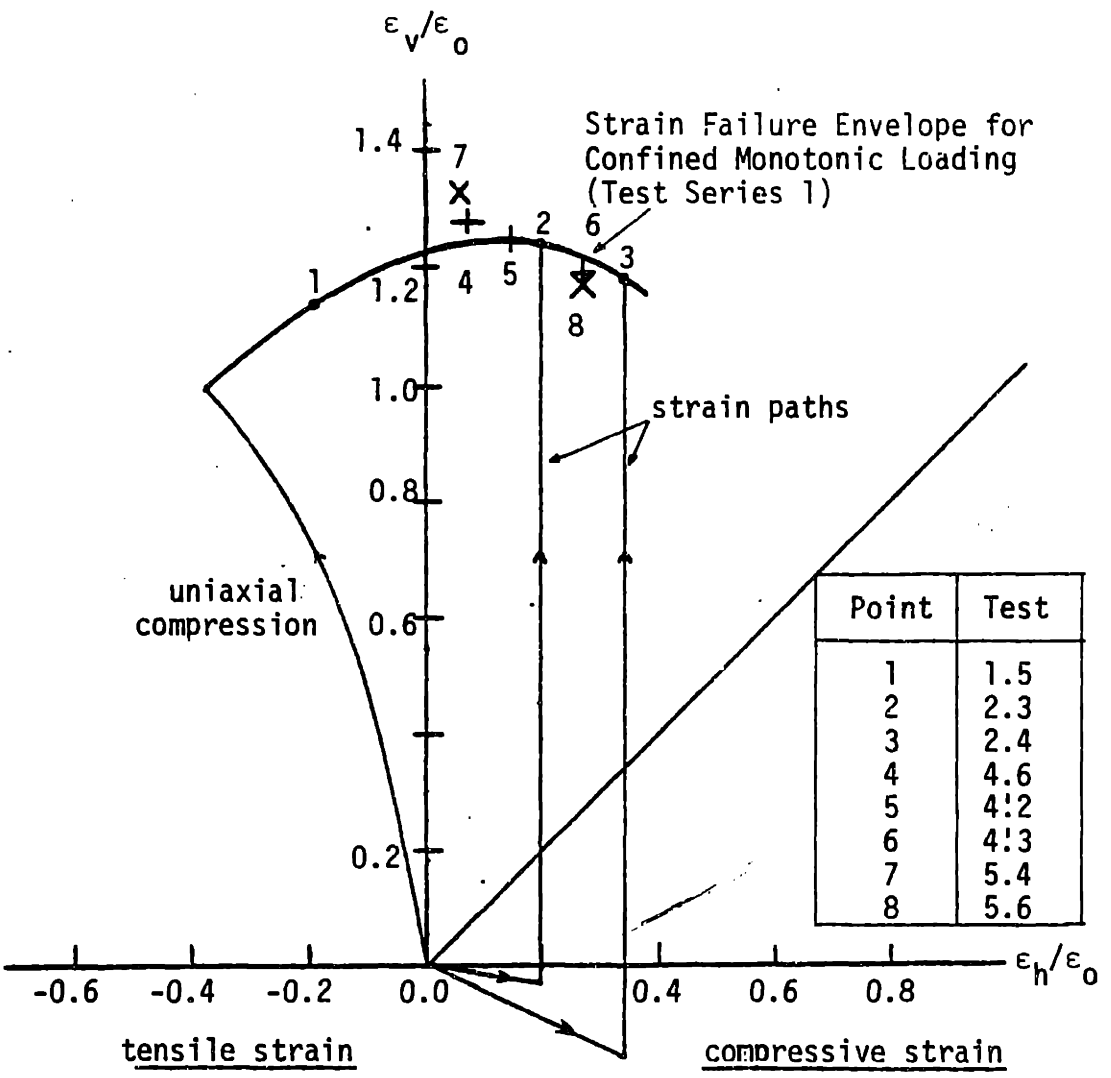

Fig. 4.10(b) - Strains at Failure Under Biaxial Loading

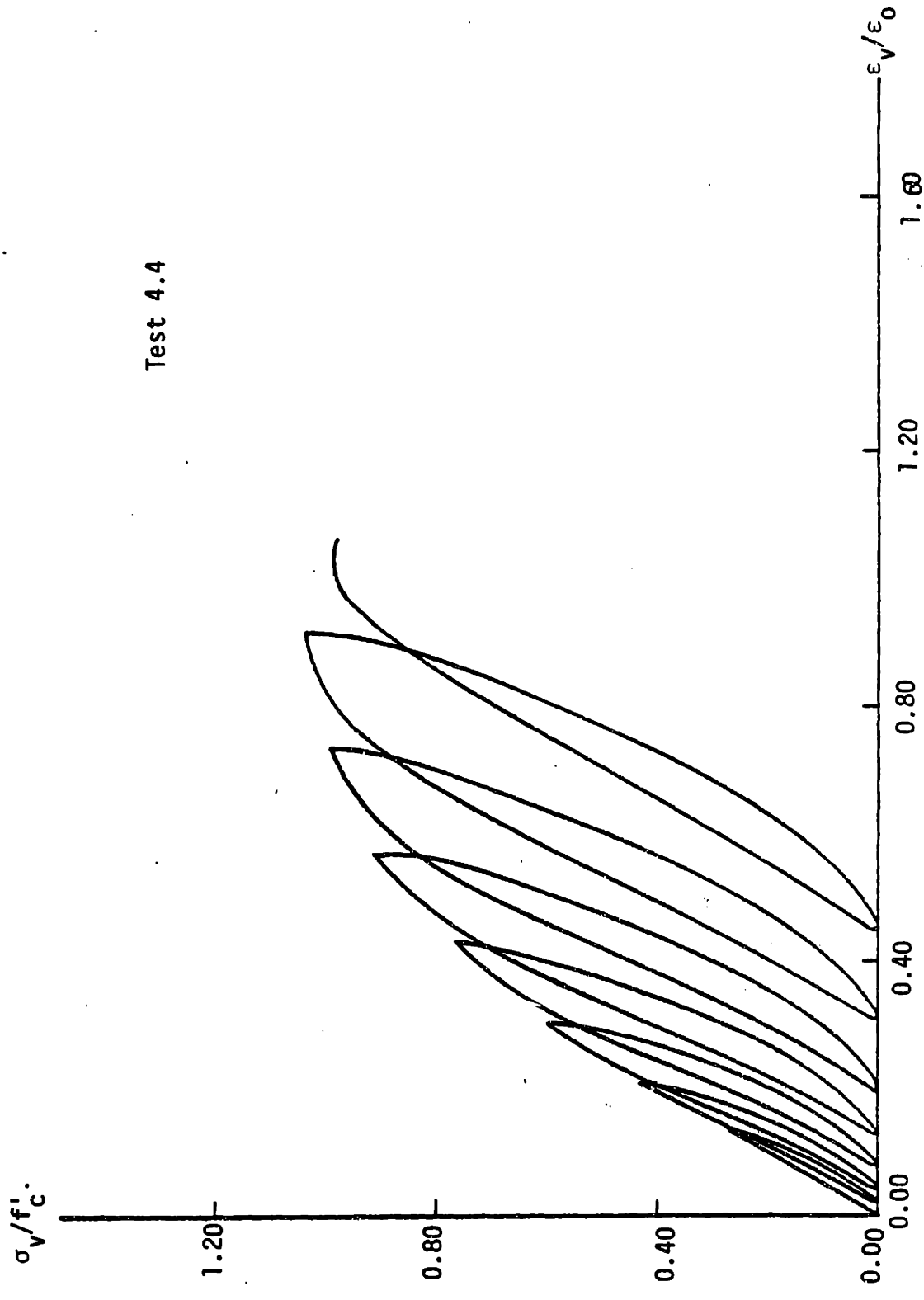

Fig. 4.12 - Uniaxial Cyclic Loading to the Envelope Curve.
Test Series 2

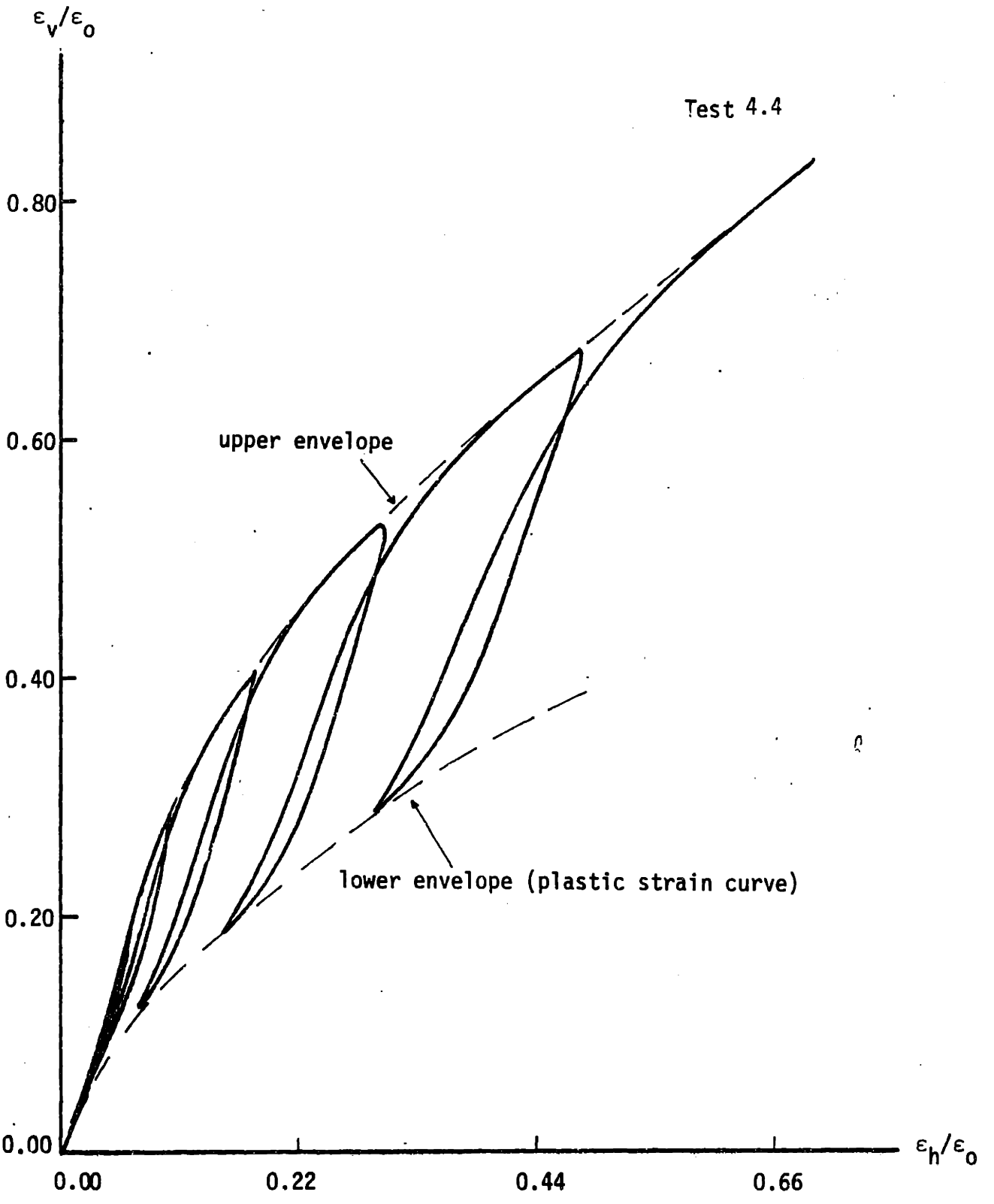

Fig. 4.13 - Relationship Between Vertical and Horizontal Strain Under Uniaxial Cyclic Loading

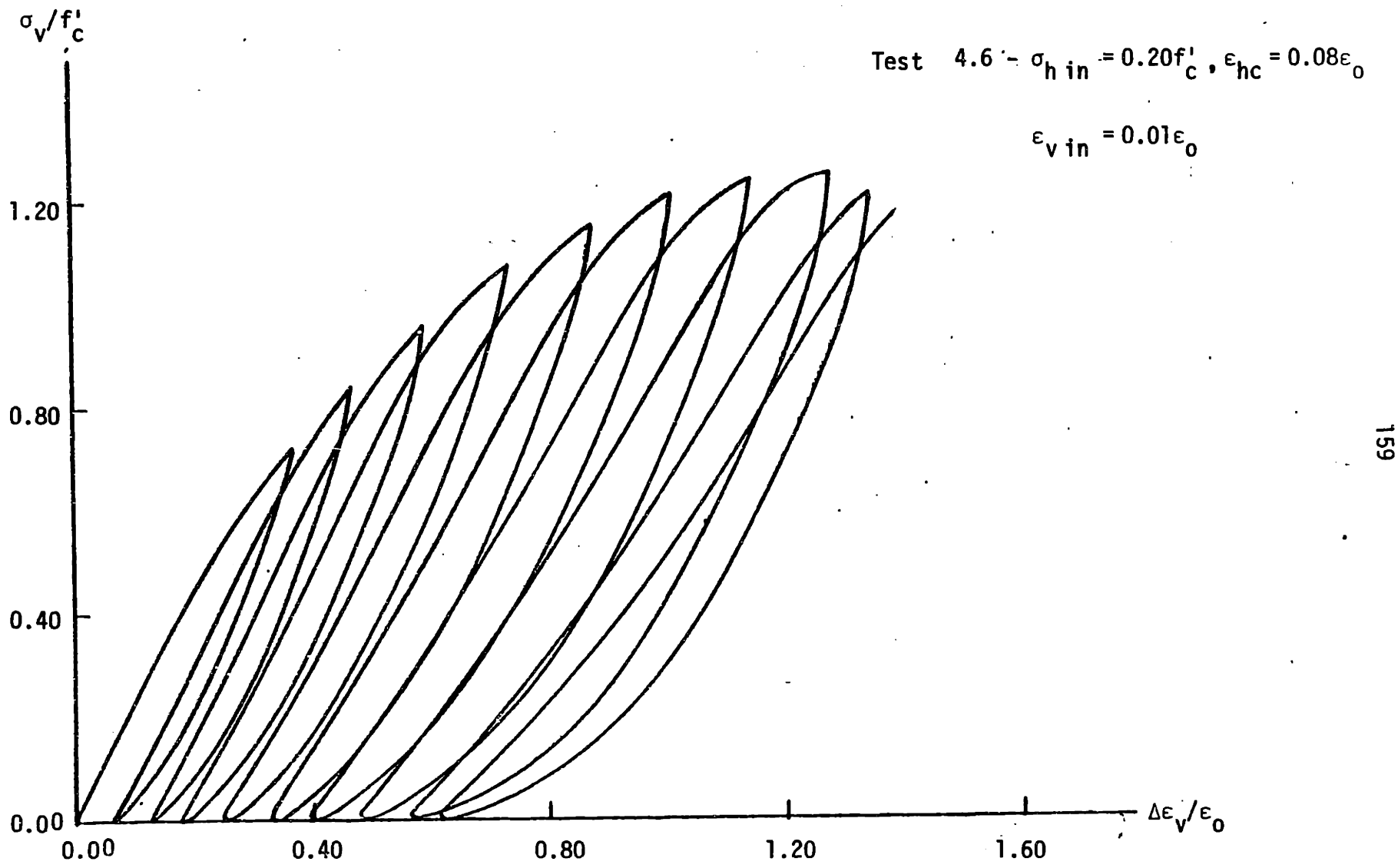

Fig. 4.14 - Confined Cyclic Loading to the Envelope Curve

Test Series 2

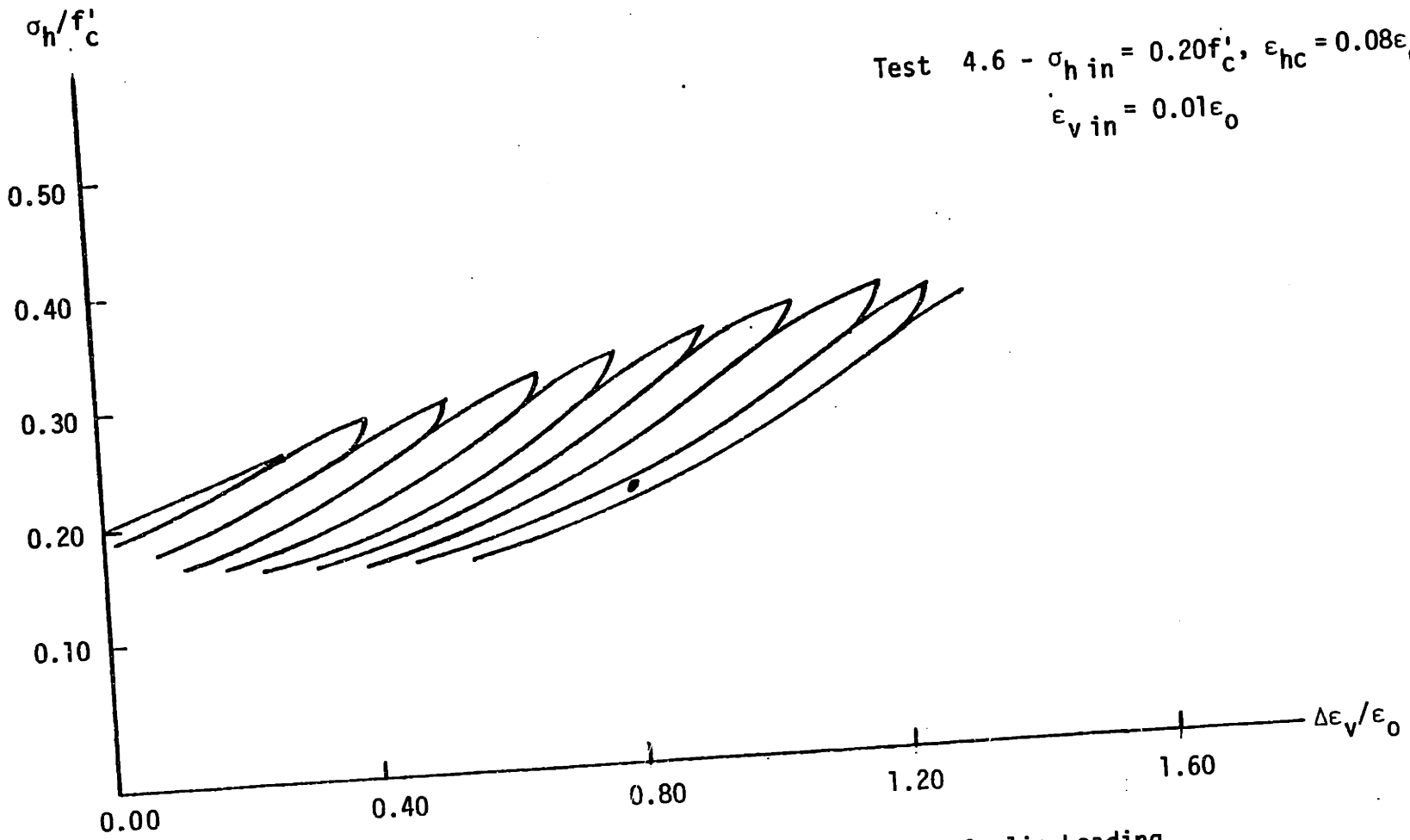

Fig. 4.15 - Horizontal Stress Variation Under Confined Cyclic Loading To The Envelope Curve

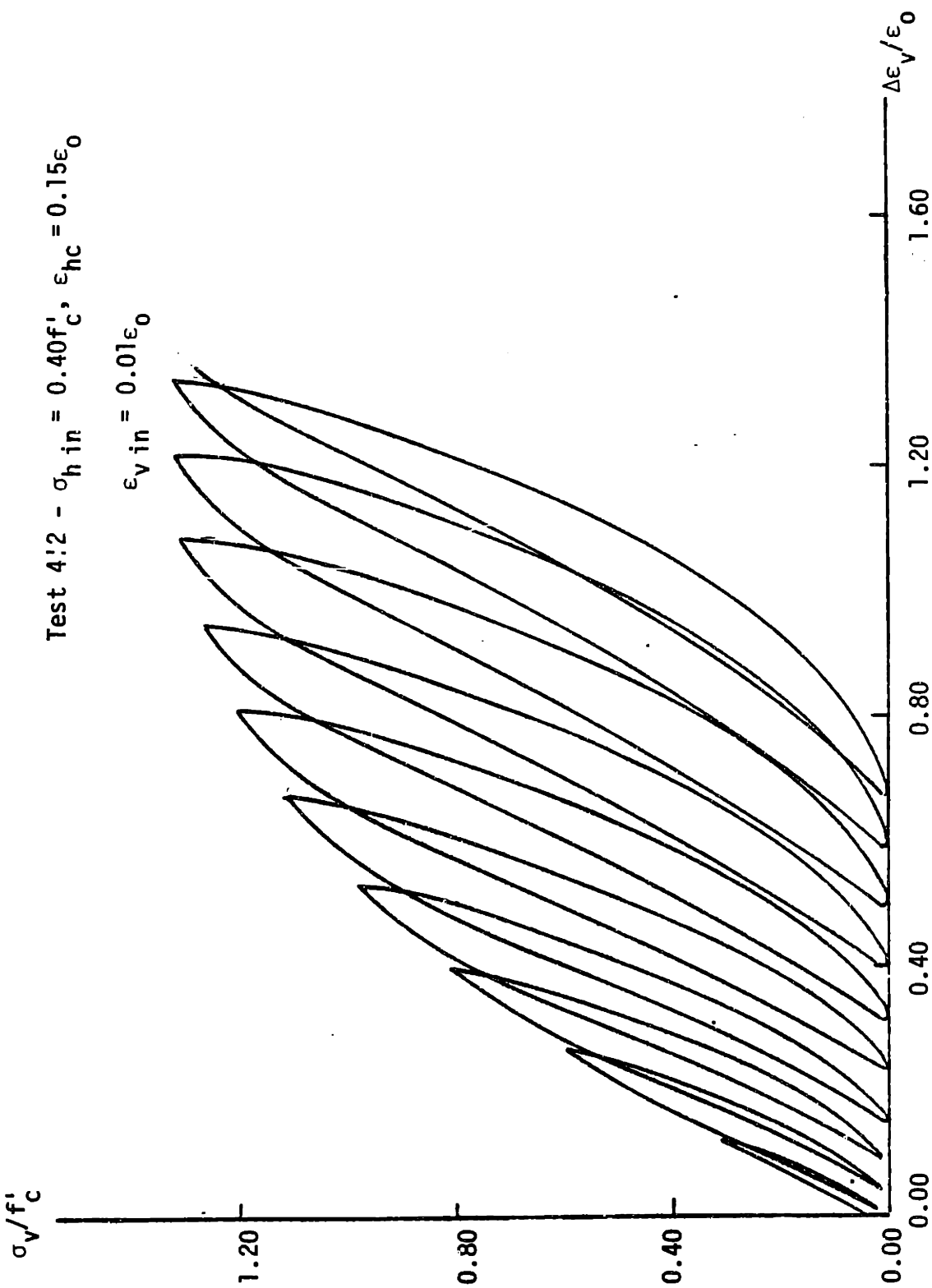

Fig. 4.16 - Confined Cyclic Loading to the Envelope Curve.

Test Series 2

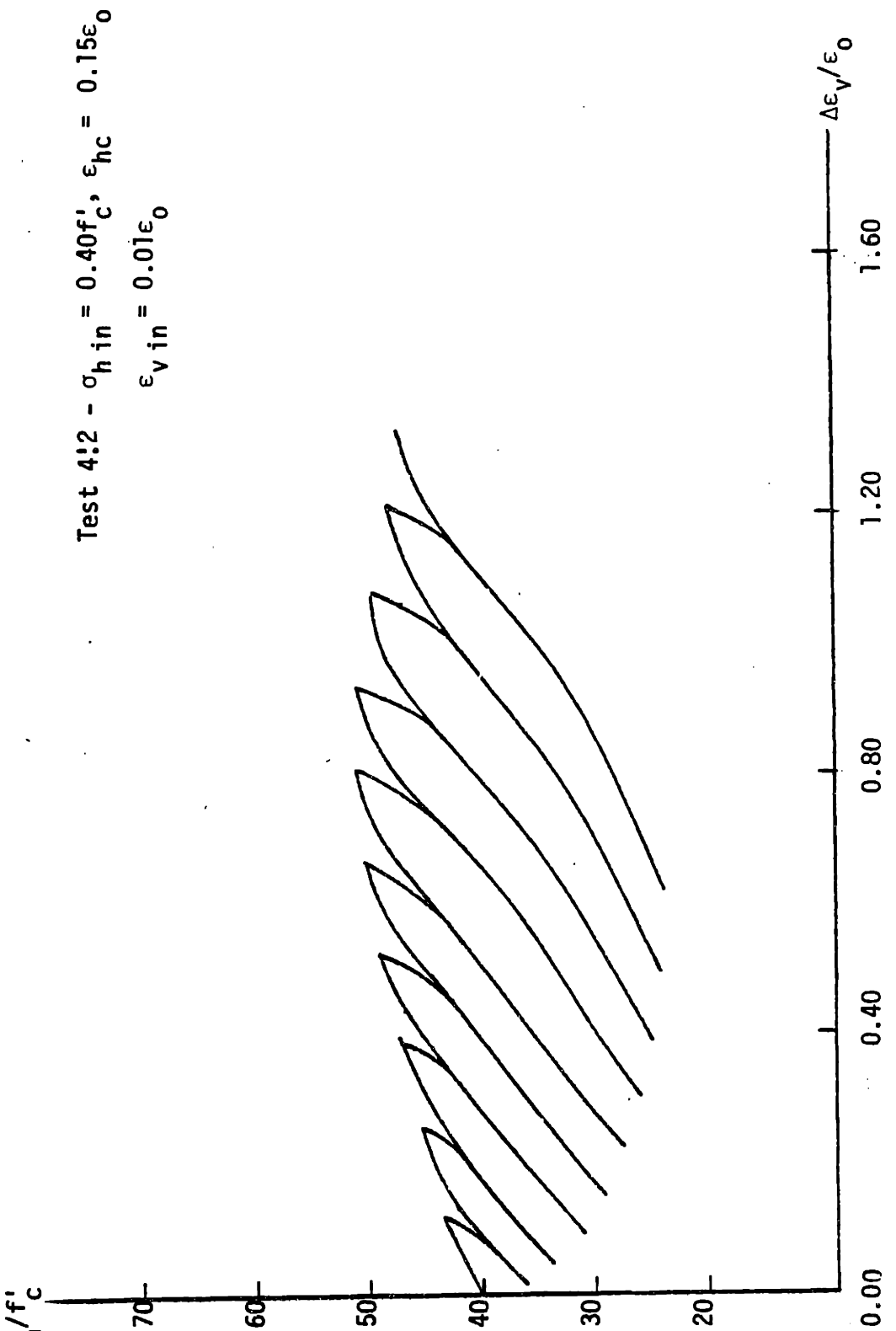

Fig. 4.17 - Horizontal Stress Variation Under Confined Cyclic Loading To The Envelope Curve

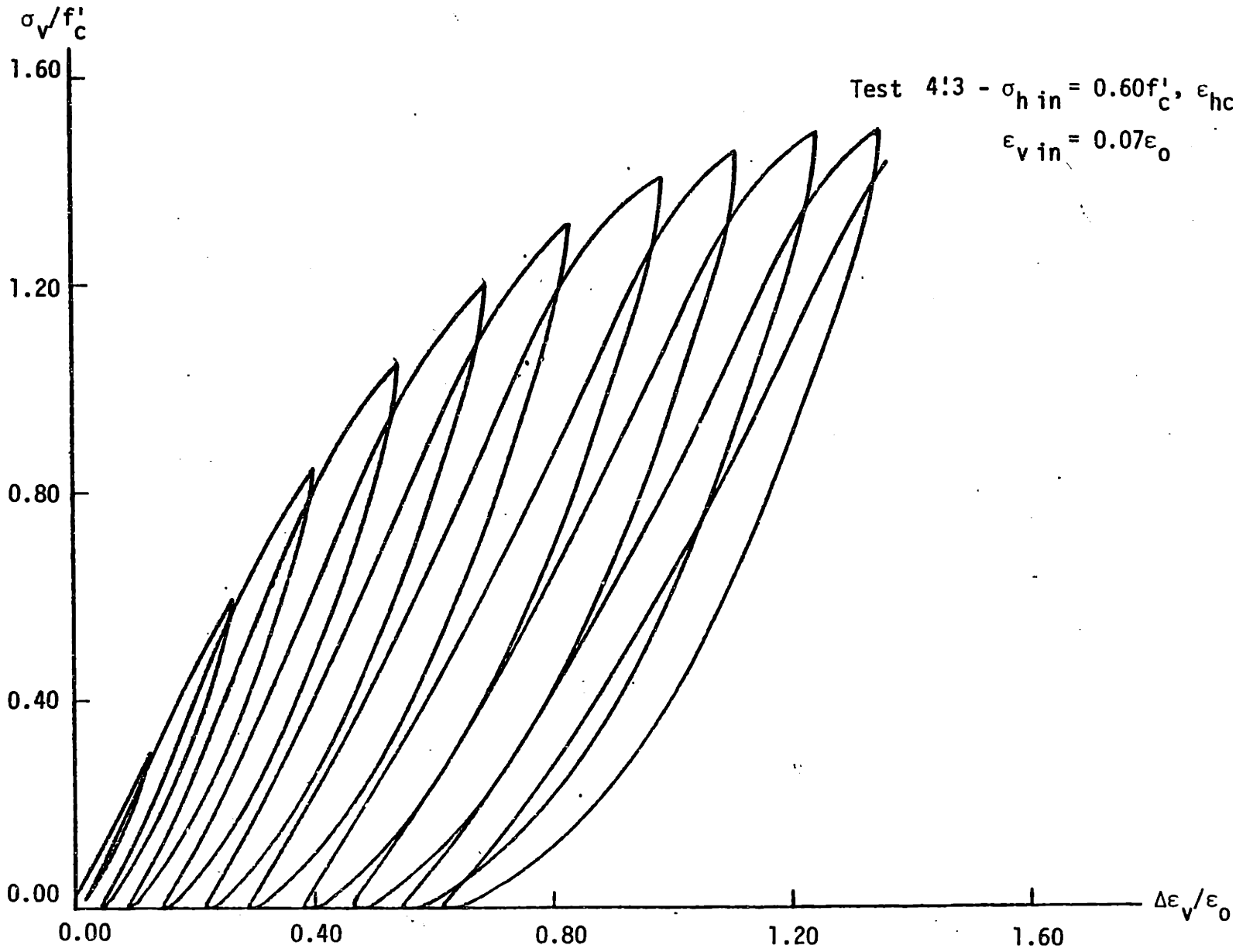

Fig. 4.18 - Confined Cyclic Loading To The Envelope Curve
Test Series 2

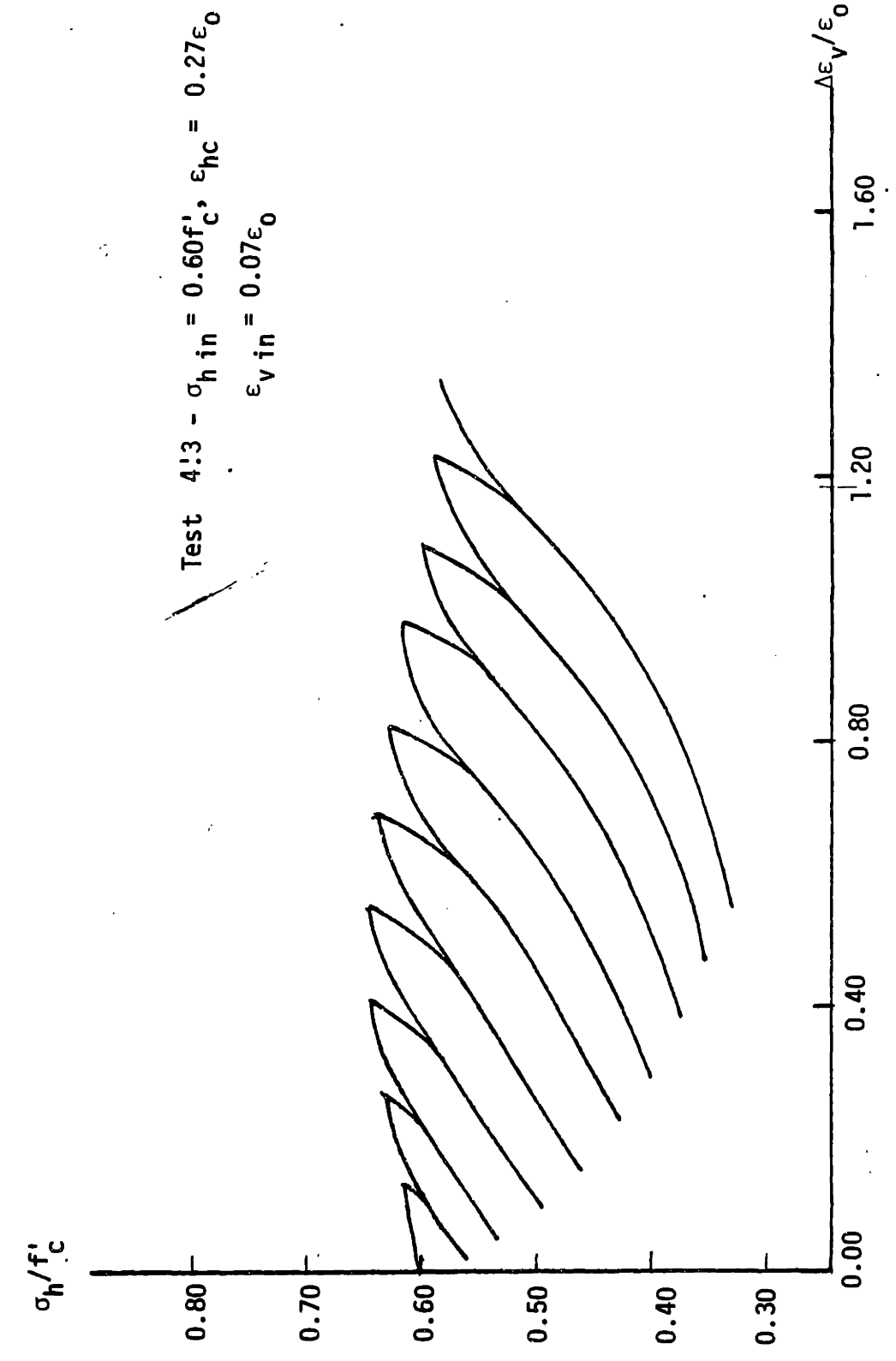

Fig. 4.19 - Horizontal Stress Variation Under Confined Cyclic Loading To The Envelope Curve

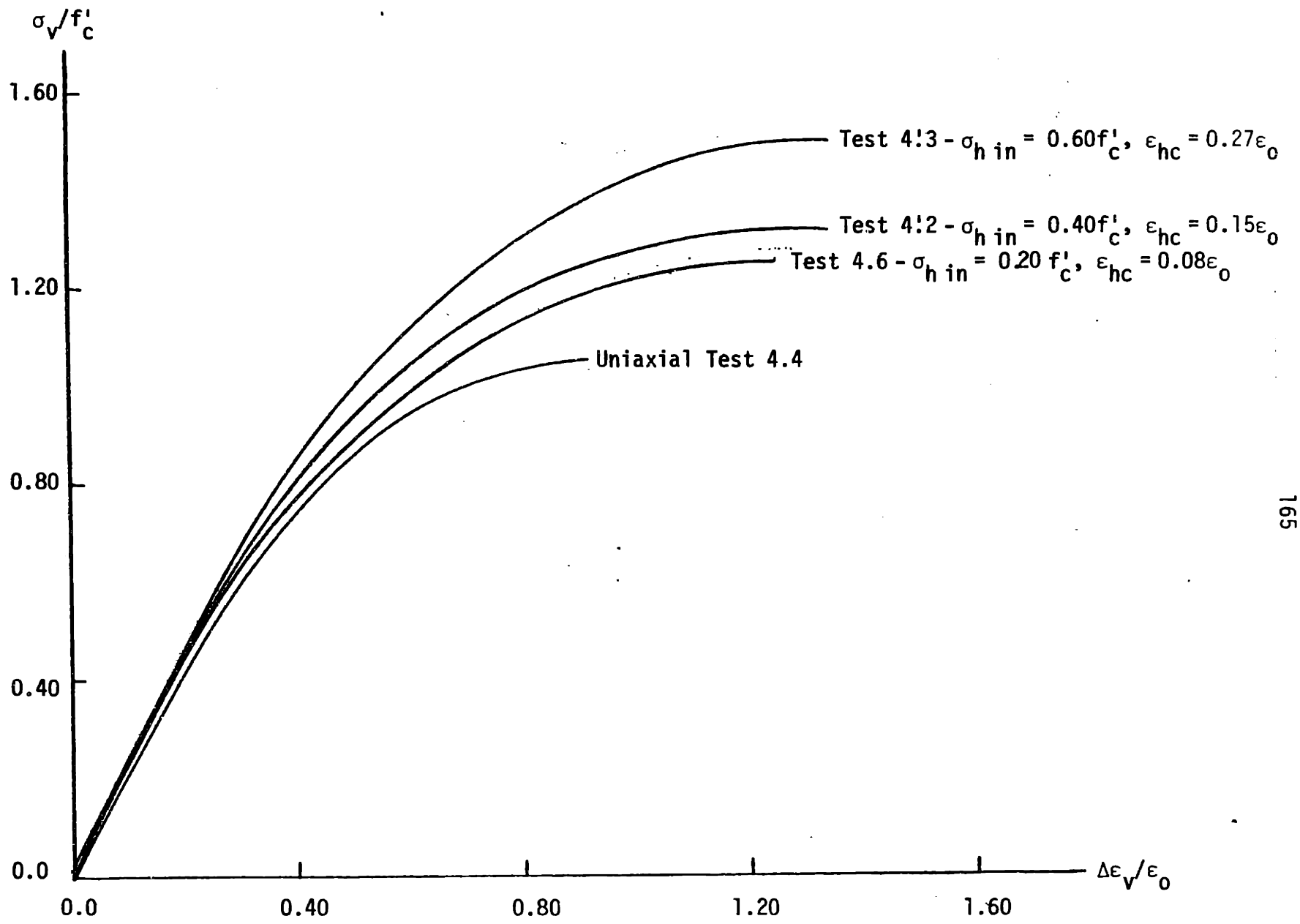

Fig. 4.20 - Envelopes of the Uniaxial and Confined Cyclic Curves

Test Series 2

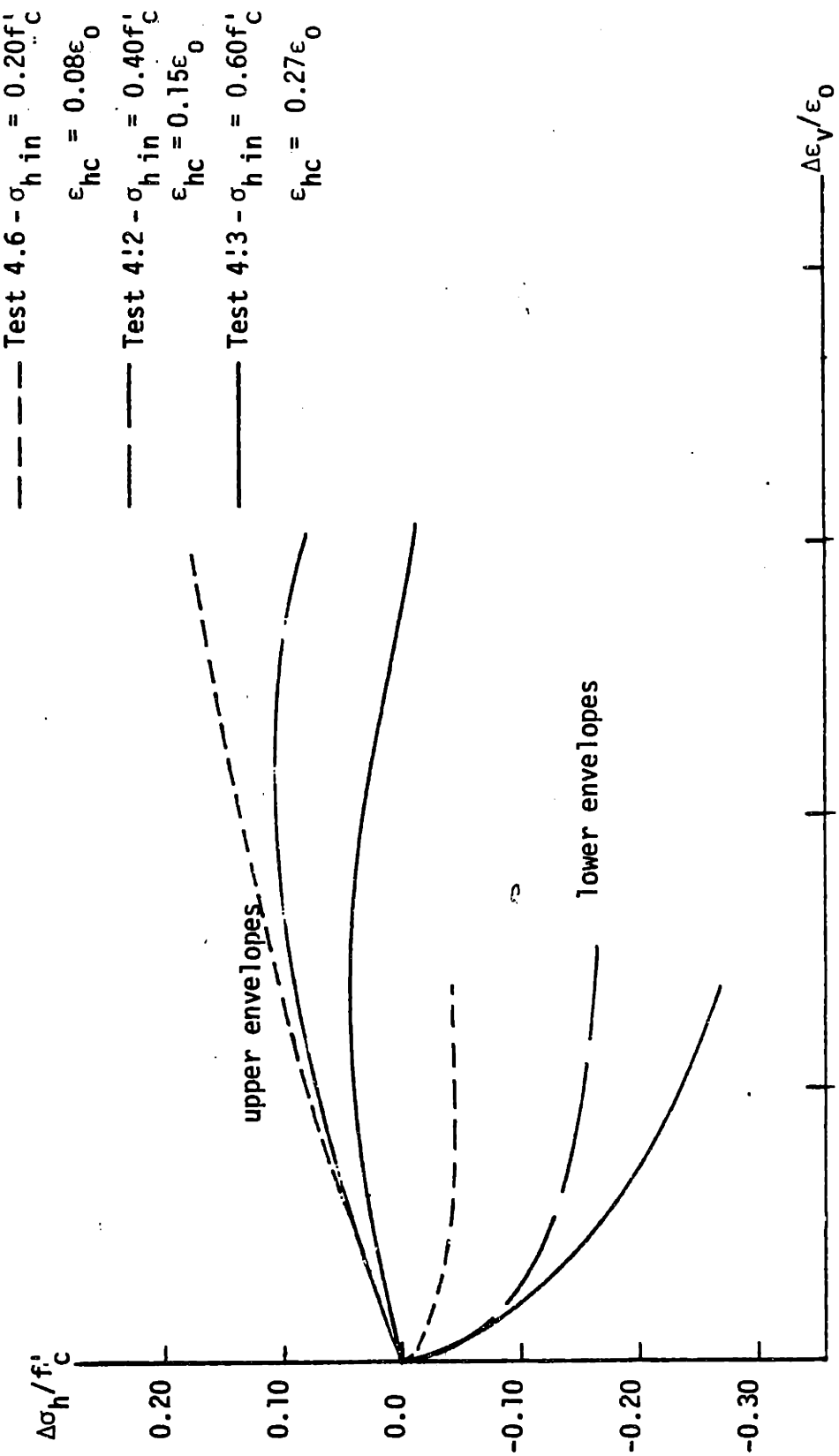

Fig. 4.21 - Upper and Lower Envelopes of σ_h-ε_v Curves Corresponding to Confined Cyclic Tests to the Envelope

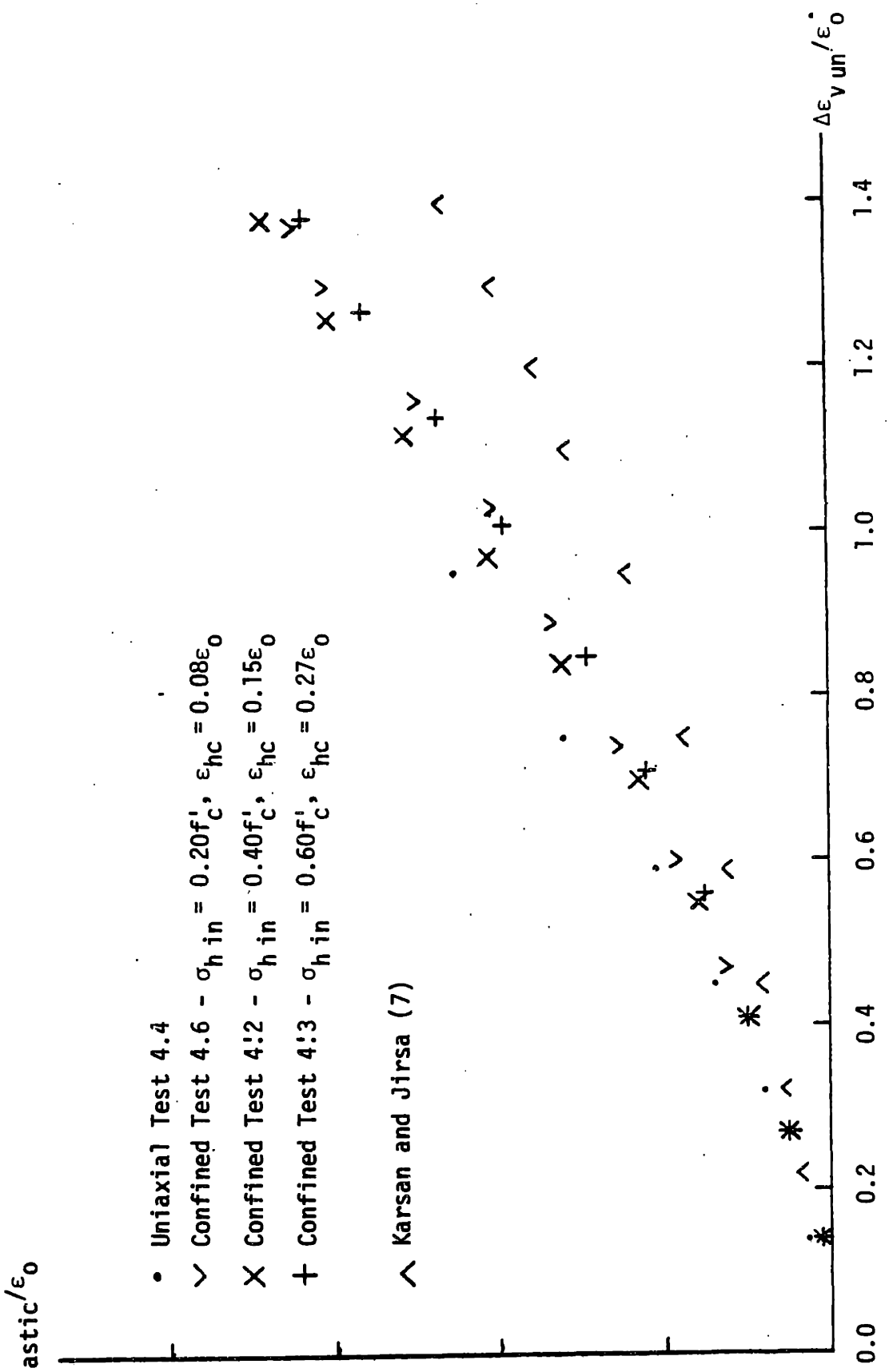

Fig. 4.22 - Relationship Between Plastic Strains and Envelope Strains at Unloading. Test Series 2

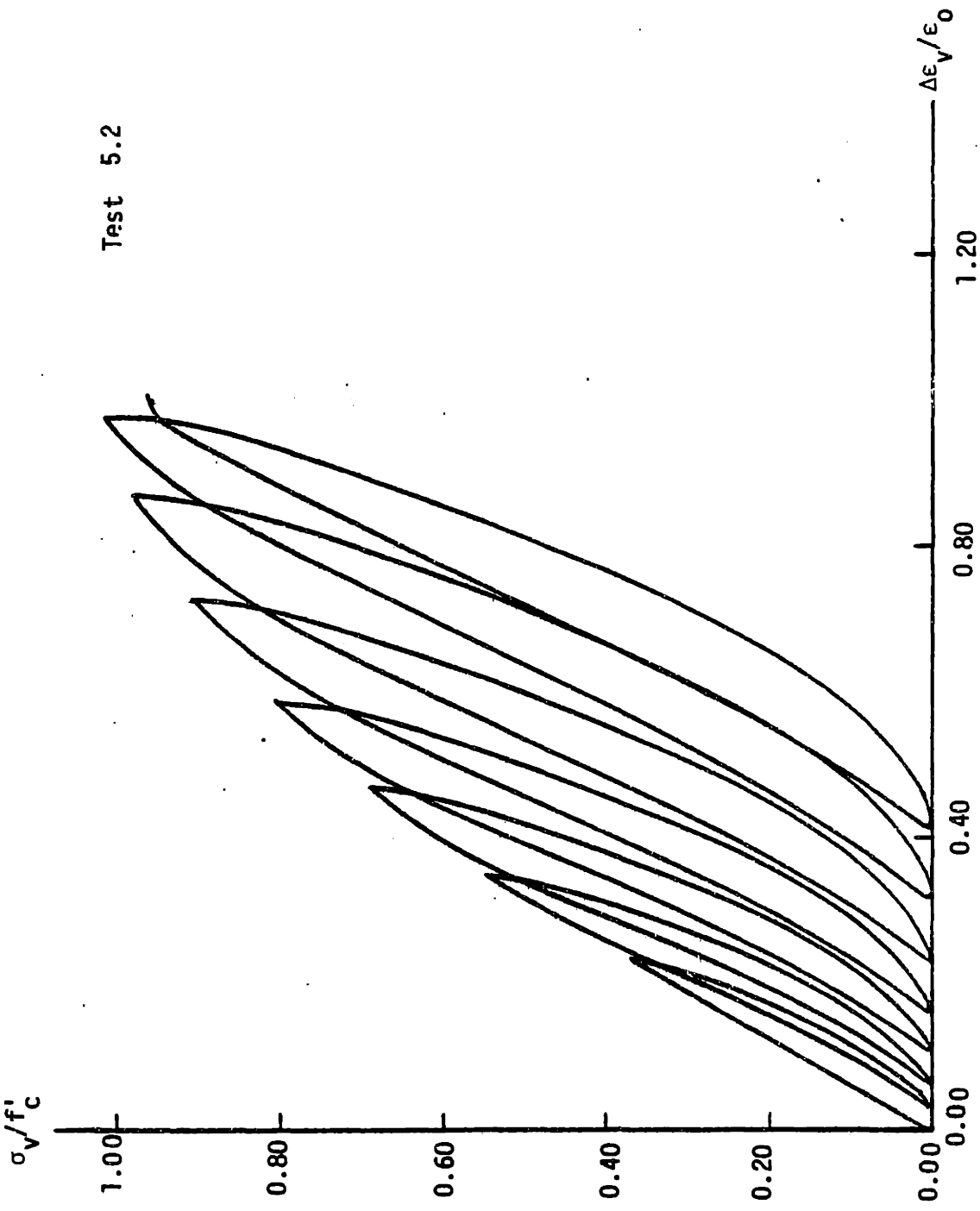

Fig. 4.23 - Uniaxial Cyclic Loading to the Envelope Curve
Test Series 3

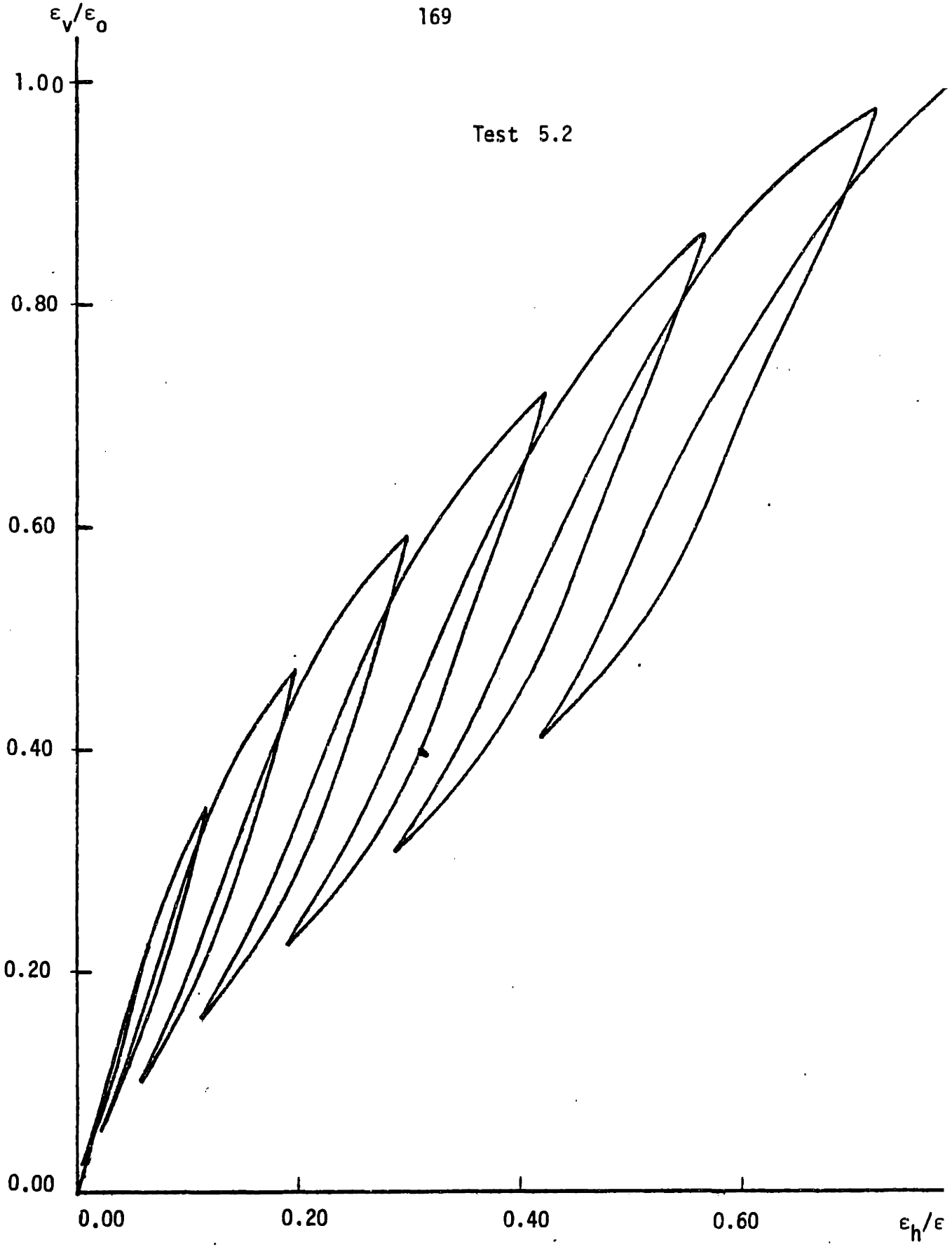

Fig. 4.24 - Relationship Between Vertical and Horizontal Strain Under Uniaxial Cyclic Loading

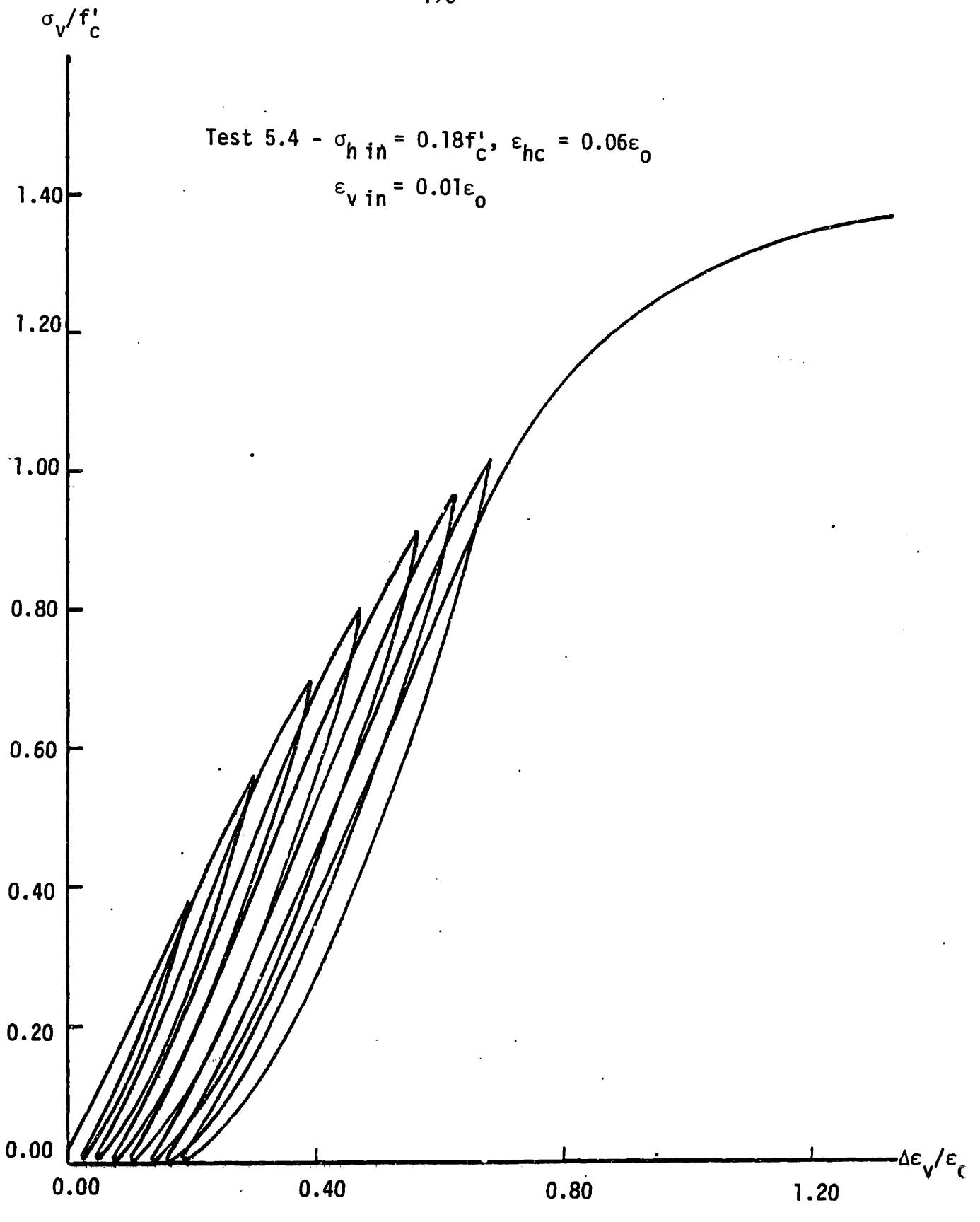

Fig. 4.25 - Confined Cyclic Loading to Same Vertical Stress Levels of Uniaxial Cyclic Test 5.2. Test Series 3

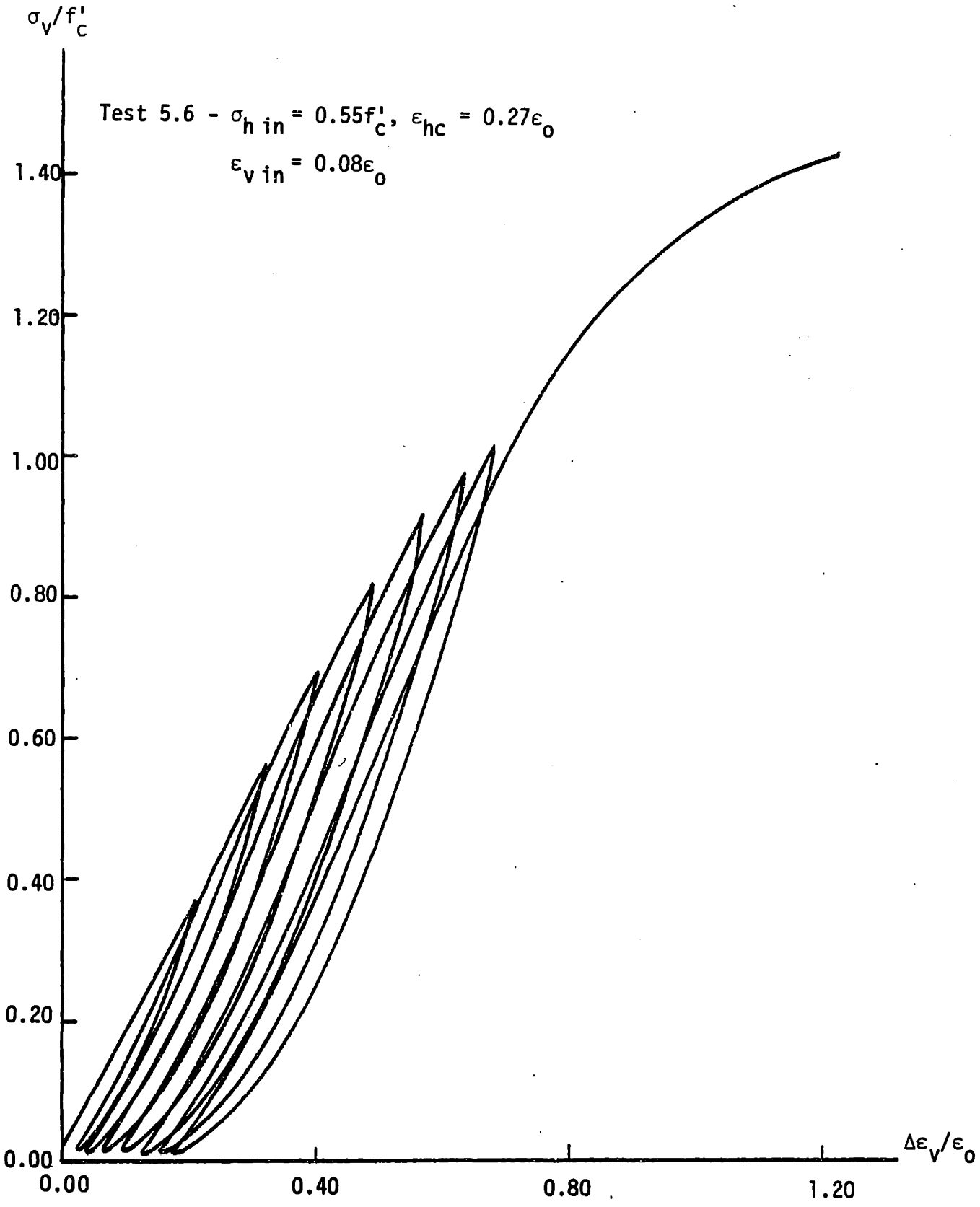

Fig. 4.26 - Confined Cyclic Loading to Same Vertical Stress Levels of Uniaxial Cyclic Test 5.2. Test Series 3

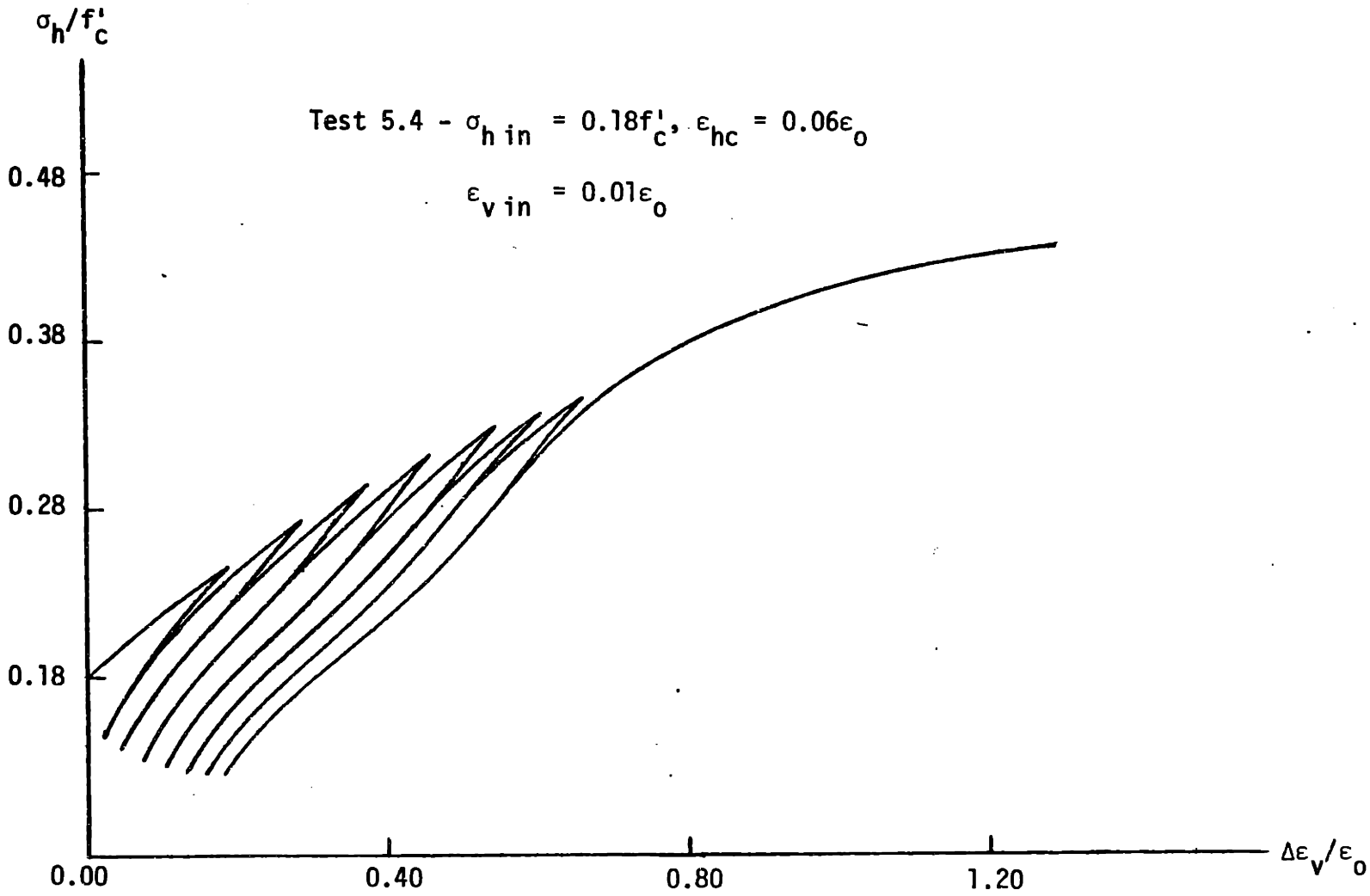

Fig. 4.27 - Horizontal Stress Variation Under Confined Cyclic Loading to Same Vertical Stress Levels of Uniaxial Cyclic Test 5.2

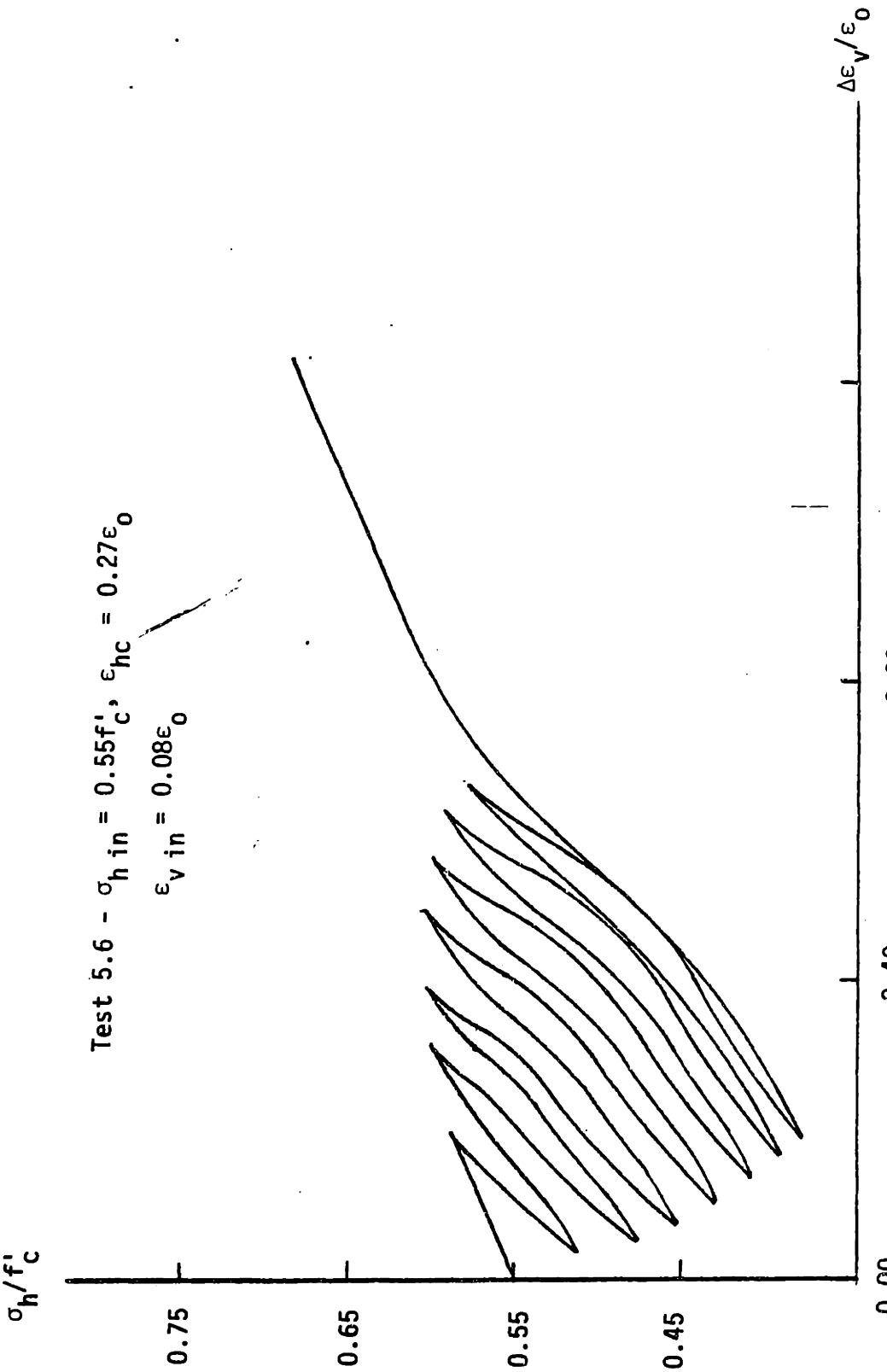

Fig. 4.28 - Horizontal Stress Variation Under Confined Cyclic Loading to Same Vertical Stress Levels of Uniaxial Cyclic Test 5.2

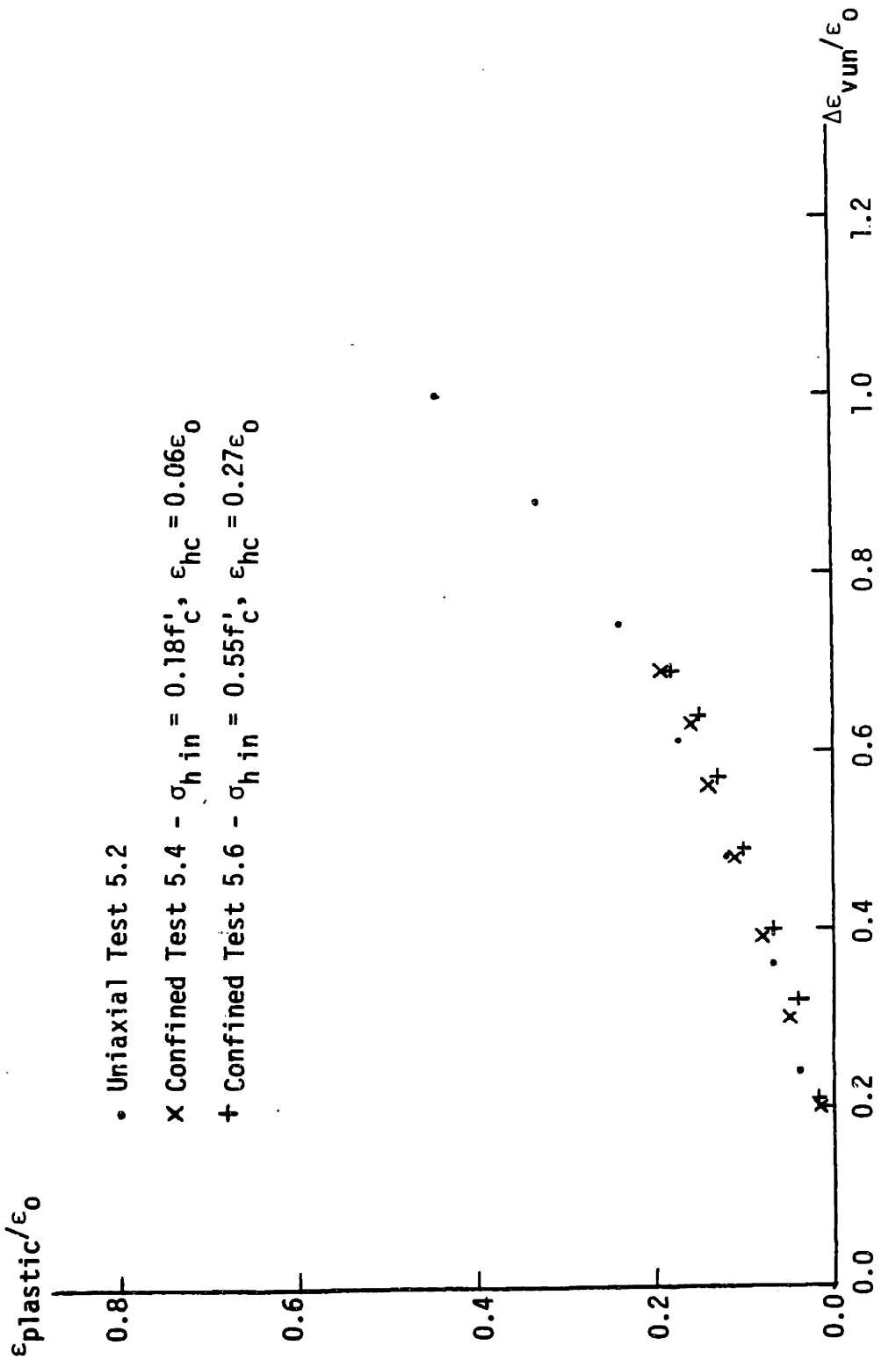

Fig. 4.29 - Relationship Between Plastic Strains and Strains at Unloading: Test Series 3

CHAPTER 5

SUMMARY, CONCLUSIONS AND RECOMMENDATIONS FOR FURTHER RESEARCH

5.1 Summary and Conclusions

The main objective of this investigation was to study the behavior of concrete under uniaxially confined cyclic and monotonic loading. For this purpose, square concrete plates measuring 5"x5"x1" were subjected to two loading phases: 1) initial confining phase where the specimen is loaded horizontally in its plane to a predetermined stress value and 2) application of in-plane cyclic or monotonic vertical stress during which the horizontal strain imposed in phase 1 is kept constant.

Vertical load was applied with an electro-hydraulic MTS machine operated manually under stroke control. An independent loading frame was constructed for applying load and confining the specimen in the horizontal direction. A manually operated screw jack fixed to the frame was used for applying the horizontal load. The frame lay on the MTS Load Frame platform. Brush bearing platens were used for transmitting the loads to the specimen. The brushes consist of thin steel plates flexible enough to deform laterally under applied pressure, thereby exerting no restraining lateral force on the concrete.

Vertical and horizontal strain measurements were taken with BLH foil strain gages. Two gages per direction, wired in series and attached to opposite sides of the specimen, were used. This procedure eliminated recording of bending strains by averaging the strains on both sides of the specimen. Vertical and horizontal loads were

measured by the MTS load cell and a load cell fixed to the horizontal loading frame, respectively.

A total of about 30 specimens were tested in four different Series, classified according to the type of loading history. The Test Series are: (1) monotonic loading to failure, (2) cycles to the envelope curve, (3) cycles to prescribed values of vertical stress and (4) cycles between fixed maximum and minimum stress levels.

Each test Series was performed on both unconfined specimens and specimens under different confinement levels in order to assess the behavior on a comparative basis. The confinement levels are characterized by the initial horizontal stress $\sigma_{h\ in}$ and the corresponding horizontal strain ε_{hc} which remains constant throughout the test. Complete stress strain histories were recorded in all tests. Vertical stress-vertical strain (σ_v-ε_v) and vertical strain-horizontal strain (ε_v-ε_h) curves were recorded for unconfined specimens, while vertical stress-vertical strain (σ_v-ε_v) and horizontal stress-vertical strain (σ_h-ε_v) curves were recorded for the confined specimens.

In Series 1 confined and unconfined specimens were subjected to monotonically increasing vertical strain until failure occurred. Vertical and horizontal stresses increased non-proportionally. The behavior was evaluated on the basis of the recorded stress-strain curves. Stresses and strains at failure were plotted separately on σ_v-σ_h and ε_v-ε_h plots and compared with the stresses and strains at failure observed by other investigators in previous biaxial tests where concrete is subjected to monotonic biaxial loading at constant stress ratios.

In Series 2 confined and unconfined specimens were loaded vertically to their envelope curves until failure. Similarities and differences in the recorded curves allowed to understand the deformational mechanism of concrete under cyclic loading and the effects of increasing confinement on the cyclic behavior. The effect of the confinement level on the variations of horizontal stress was analyzed. Stresses and strains at failure were compared to those obtained in the monotonic tests.

In Series 3 confined and unconfined specimens were all subjected to the same vertical stress history, which allowed to explicitely establish the effects of confinement on the behavior of concrete under cyclic loading. Total and plastic strain accumulations in the confined and unconfined tests are compared. The confined specimens were loaded monotonically to failure after being subjected to the same loading history. Stresses and strains at failure were plotted and compared to those of previous Series.

In Series 4 confined specimens were cycled between zero and constant maximum vertical stress levels a number of times equal to that required for failure of an unconfined specimen cycled between zero and a stress of 0.82 f'_c. After the required number of cycles was performed the confined specimens were loaded monotonically to failure. These tests provide useful information regarding the effects of confinement on stress-strain behavior of concrete subjected to repeated stress cycles of constant amplitude.

Based on the results of the present investigation, the following conclusions can be made:

1. Uniaxially confined concrete behaves orthotropically when loaded in a direction normal to the confinement. The tendency to expand in the direction of confinement is highly reduced with respect to that under uniaxial conditions (reduced Poisson ratio), due to which the increase in confining stress is lower than predicted by linear elastic isotropic theory. Under monotonic loading initial stress strain behavior in the direction of loading is not affected by the confinement; however, during inelastic deformation, confinement induces a behavior much stiffer than that under uniaxial compression. Stiffness and strength increase with the level of confinement.
2. Stress states and strain states at failure under biaxial monotonic compression seem to be influenced by the type of stress-strain path since the stress and strain failure envelopes obtained in the present tests, where stresses vary non-proportionally, do not coincide with those of previous tests (8,9,17), where stresses vary proportionally. Increases in strength of up to 43% of f'_c were observed.
3. Envelopes to the confined and unconfined cyclic stress strain curves corresponding to the direction of loading coincide initially. At higher values of strain the envelope curve rises higher at higher confinement levels.

4. In both uniaxial and biaxial cyclic tests to the envelope the initial slope of the first reloading curve is higher than that of the virgin loading branch, which indicates a hardening effect on the concrete produced by the first load-unload cycle. As cycling proceeds there is a continuous degradation of elastic moduli indicated by the progressive decrease of the slopes of the reloading curves. Reloading curves up to the common point may be defined on the basis of plastic strain at which they originate, regardless of the confinement level. The decrease in slope of the reloading curve after the common point is less pronounced at higher confinement levels.
5. Unloading curves corresponding to different tests (including the uniaxial test) and starting at the same values of vertical strain overlap when superimposed at their final point (σ_v=0).
6. Plastic strains due to unloadings from the envelope curve are not significantly affected by the level of confinement, and may be defined as a function of the envelope strain at unloading.
7. The degradation process of concrete under cyclic loading before peak stress appears to be mainly controlled by inelastic behavior of mortar, or more precisely, viscous flow of the cement paste, rather than microcracking.
8. The variations of confining stress under cyclic loading are highly influenced by the confinement level. Inelastic behavior in the direction of confinement is characterized by non-overlapping of the reload-unload branches of the confining stress-orthogonally

applied strain curve and the progressive decrease of minimum confining stress in successive reload-unload cycles. This behavior is related to the modulus in the direction of confinement, which is higher upon unloading than under loading if the confining strain is in the plastic region.

9. Stress-strain states at failure under biaxial loading appear to be unique, i.e., independent of the stress strain path, whether cyclic or monotonic. It therefore appears necessary to formulate the failure criterion for concrete under biaxial loading in terms of stress-strain states, rather stress states or strain states only.
10. Uniaxially confined concrete subjected to the same loading history as unconfined concrete accumulates considerably lower total and plastic strains.
11. Uniaxial confinement considerably extends the fatigue life of concrete. Confined concrete is far from failing when cycled continuously to constant maximum stress levels which produce failure in unconfined concrete. This occurs even for maximum stress levels which are higher than f'_c and constitute a high percentage of the corresponding confined strength.

5.2 Recommendations for Further Research

Since the tests performed in this investigation are the first of their kind it is considered necessary, as a first phase of further research, to verify the obtained results by carrying out similar tests in a second investigation. This implies basically the verification of

stress strain relationships at the different confinement levels, for given types of tests. On the other hand, the same types of tests should be carried out at new confinement levels in order to have a more solid basis for assessing the behavior.

For biaxial monotonic loading the following new levels of initial confining stress are suggested: 0.10 f'_c, 0.30 f'_c, 0.50 f'_c, 0.70 f'_c, 0.80 f'_c, 0.90 f'_c. At very high confinement levels the concrete will have undergone severe damage even before the vertical load is applied. Therefore, the practical application of results obtained under such levels is limited.

σ_v-ε_v curves and σ_h-ε_v curves can be obtained at each of the confinement levels. Behavioral trends observed in the present investigation may then be verified and more precisely defined. Recording of the stresses and strains at failure will allow for a more complete definition of the failure envelopes and provide a more solid basis for comparison with failure envelopes proposed by other authors (for tests at constant stress ratio). It is suggested that the strains in the direction normal to the free surface of the specimen be recorded in order to have a more complete description of the behavior and provide data useful in the development of a failure criterion. Such strains may be recorded by using embedded strain gages or dial gages.

Biaxial cyclic tests to the envelope should be performed at the same confinement levels used in the biaxial monotonic tests. Envelopes and corresponding monotonic curves should be compared in order to investigate the uniqueness properties of the envelope curve. This is

especially important since the uniqueness property couldn't be conclusively established on the basis of the tests carried out in the present investigation.

σ_v-ε_v curves and σ_h-ε_v curves can be obtained at each of the confinement levels. Such curves will reaffirm and more precisely define the behavior observed in the present tests. Loading and unloading curves in both diagrams (σ_v-ε_v and σ_h-ε_v) corresponding to different confinement levels must be compared in order to verify the uniqueness properties attributed to them in the present investigation. To facilitate the comparison it is advisable to unload at similar strain levels in the different tests since the strain at unloading is a major criterion for defining the curves. Stresses and strains at failure should be carefully recorded and compared with those obtained in the biaxial monotonic tests, in order to evaluate the effects of the stress strain path.

It is advisable to carry out cyclic tests where specimens under different confinement levels are subjected to the same vertical stress history. See Test Series 3 in the present investigation. Such tests permit an explicit evaluation of the effects of confinement on the stress strain behavior. The confinement levels should be those used in the present investigation plus the new levels proposed before.

More information is required on the behavior of concrete under biaxial fatigue. It is highly recommendable that the confinement levels used in the present tests be repeated since unintended specimen surface

irregularities caused some data distortion. New levels of initial confining stress should be introduced: 0.10 f'_c, 0.40 f'_c, 0.60 f'_c, 0.80 f'_c.

Previous investigations (7,13) have shown that in uniaxial cyclic tests failure eventually occurs when the load is cycled between some minimum stress level and a maximum stress level higher than about 0.70 f'_c. This was verified in the present tests where an unconfined specimen cycled between zero and a maximum vertical stress of 0.82 f'_c failed after 35 cycles. However, it was seen that if confined specimens were cycled between these same stress levels, failure would practically never occur due to the high reduction in strain accumulation induced by the confinement. Thus, a comparison of the number of cycles to failure for confined and unconfined specimens cycled between the same stress levels is impossible. Moreover, it was seen that even when a confined specimen was cycled between zero and a vertical stress level of about 85% of its confined monotonic strength failure did not occur and was far from occuring after 35 cycles. Therefore, failure under confined cyclic loading will occur only if the specimen is cycled to very high percentages of its confined monotonic strength σ_{vp}. Since the confined strength varies according to the level of confinement it appears impossible to fix a level of maximum vertical stress which will eventually cause failure of all confined specimens. An alternative would be to cycle each specimen between zero and a maximum vertical stress equal to a high percentage of its confined strength ($> 0.85\ \sigma_{vp}$) and compare the number of cycles to failure for each case. This, however, would not

yield very useful information regarding the effects of varying degrees of confinement on the behavior since the confined specimens would be subjected to different vertical stress levels in each test. Moreover, if many cycles are required to produce failure the manual procedure for performing the test becomes tiresome and impractical.

In view of the former, a different approach to this type of test is suggested, which is both practical and useful in studying the effect of the confinement for cycles between given stress levels. It consists in pre-selecting a maximum stress level (lower than the minimum confined strength) and cycling each confined specimen to that level the same number of times after which load is applied monotonically until failure. The total and plastic strain accumulation at the end of the cycles in each case would be a measure of the effect of different confinement levels on the behavior of concrete subjected to cycles between given stress levels. It would be interesting to observe if the final monotonic branch of the cyclic curve became tangent to the monotonic or envelope curve and failure occurred at the same stress and strain levels. This, however, should not be expected if strain accumulation prior to monotonic loading is excessive.

Due to test procedure, which involves manual manipulation of the jack, the rate of loading should be such that a cycle is completed in no less than 2.5 minutes. Therefore, a maximum number of about 50 cycles should be performed, where the minimum test duration will be about 2 hours. The maximum stress levels to which the confined specimens should be cycled must be equal to or less than about 90% of the minimum

confined monotonic strength σ_{vp}. It is also possible to select a maximum stress level low enough to produce failure in the uniaxial cyclic test ($> 0.70\ f'_c$). Then each confined specimen would be cycled to this maximum stress level a number of times equal to that required for failure in the uniaxial test.

Different minimum stress levels higher than zero can be tried while preserving the same maximum stress. Thus, the effect of varying the minimum stress in the cycles may be evaluated.

Uniaxial Cyclic Tests. Unconfined specimens should be subjected to different loading histories in order to assess the uniqueness properties attributed to the upper and lower ε_v-ε_h envelopes. The lower envelope has been defined as the plastic strain curve. After arbitrary cycling within the domain or region defined by both envelopes vertical strain should be monotonically increased or decreased and the path traced by the curve compared with the theoretical envelope.

Biaxial Tests. Different Types. The type of biaxial test carried out in the present investigation and discussed so far is the confined test, where vertical stress (strain) is applied while the horizontal strain is kept constant. However, there are many other possible types of biaxial tests depending on how the variables are controlled, for example, constant stress ratio tests where the principal stresses vary proportionally; tests where stress is applied in one direction while kept constant in the other direction (2-D analog of hydrostatic loading),

etc. A followup to the present investigation would consist in studying the behavior of concrete under such stress paths, applied both monotonically and cyclically.

Monotonic tests at constant stress ratio have been the most common type of biaxial tests performed up to date by different investigators. Therefore results obtained from such tests in the followup investigation would basically serve as verification of previously reported data.

Monotonic tests at constant horizontal stress, however, have not been previously performed and would provide new and useful information. This type of test would have an initial loading phase identical to that of the confined test, where the specimen is loaded horizontally up to a predetermined stress value. These values should be the same as those selected in the confined tests in order to establish comparisons. Then vertical stress is applied while horizontal stress is kept constant. In this case, the curves to be recorded are the σ_v-ε_v and ε_v-ε_h curves (maybe also σ_v-ε_h curves). These curves are of particular interest since their initial slopes represent the orthotropic properties E_v and ν_{hv} at the initial values of horizontal stress and strain. It should be recalled that assumptions regarding these properties were made in the present investigation in order to explain the observed stress-strain behavior of the confined specimens. E_v was assumed to be initially equal to E (uniaxial) and ν_{hv} was considered to be much lower than the initial Poisson ratio ν in uniaxial compression. The obtained curves would, therefore, verify these assumptions and also provide new information on the stress-strain behavior and deformations of concrete

under a different type of biaxial stress path. Stresses and strains at failure would be recorded and compared to those obtained in the confined and constant stress ratio tests.

Biaxial cyclic tests at constant stress ratio and constant horizontal stress may also be performed. Such tests could also be classified into the same series or categories as the confined tests, namely: cycles to the envelope curve, cycles to prescribed levels of vertical stress, cycles between fixed maximum and minimum stress levels. The curves to be obtained are σ_v-ε_v curves and ε_v-ε_h curves (and maybe σ_v-ε_h curves).

The biaxial cyclic tests to the envelope at constant stress ratios would be particularly useful since the stress-strain curve would verify the assumptions which constitute the basis of the model proposed by Darwin and Pecknold (5) for concrete under biaxial cyclic loading. This is an incrementally linear orthotropic model based on the uniaxial data of Karsan and Jirsa (7) since no biaxial data was available. Uniqueness of the envelopes to the σ_v-ε_v curves may be investigated by comparison with the corresponding biaxial monotonic curves. The unloading and reloading curves for each type of biaxial cyclic test should be carefully examined to determine whether they present uniqueness properties similar to those observed in the confined tests. The ε_v-ε_h curves corresponding to the constant horizontal stress tests will yield important information regarding the variation of the tangent Poisson ratio ν_{hv} (slope of the curve) at given levels of stress and strain during cyclic loading.

REFERENCES

1. Bazant, Z.P., and Bhat, P., "Endochronic Theory of Inelasticity and Failure of Concrete," Journal of the Engineering Mechanics Division, ASCE, Vol. 102, No. EM4, Proc. Paper 12360, April, 1976, pp. 701-722.

2. Bazant, Z.P., and Kim S., "Plastic Fracturing Theory for Concrete," Journal of the Engineering Mechanics Division, ASCE, Vol. 105, No. EM3, June, 1979, pp. 407-428.

3. Bazant, Z.P., and Shieh C.L., "Hysteretic Fracturing Endochronic Theory for Concrete," Journal of the Engineering Mechanics Division, ASCE, Vol. 106, No. EM5, October, 1980, pp. 929-950.

4. Buyukozturk, O., Nilson, A.H., and Slate, F.O., "Stress-Strain Response and Fracture of a Model of Concrete in Biaxial Loading," Journal of the American Concrete Institute, Proceedings, Vol. 68, No. 8, August, 1971, pp. 590-599.

5. Darwin, D., and Pecknold, D.A., "Nonlinear Biaxial Stress-Strain Law for Concrete," Journal of the Engineering Mechanics Division, ASCE, Vol. 103, No. EM2, April, 1977, pp. 229-241.

6. Darwin, D., and Pecknold, D., "Analysis of Cyclic Loading of Plane R/C Structures," Computers and Structures, Vol. 7, 1977, pp. 137-147.

7. Karsan, I.D., and Jirsa, J.O., "Behavior of Concrete Under Compressive Loadings," Journal of the Structural Division, ASCE, Vol. 95, No. ST12, December, 1969, pp. 2453-2563.

8. Kupfer, H., Hilsdorf, H.K., and Rüsch H., "Behavior of Concrete Under Biaxial Stresses," Journal of the American Concrete Institute, Vol. 66, No. 8, August, 1969, pp. 656-666.

9. Liu, T.C.Y., Nilson, A.H., and Slate, F.O., "Stress-Strain Response and Fracture of Concrete in Uniaxial and Biaxial Compression," Journal of the American Concrete Institute, Vol. 69, No. 5, May, 1972, pp. 291-295.

10. Maher, A., and Darwin, D., "Mortar Constituent of Concrete Under Cyclic Compression," SM Report No. 5, The University of Kansas Center for Research, Inc., Lawrence, Kansas, October, 1980.

11. Palaniswamy R., and Shah, S.P., "Fracture and Stress-Strain Relationship of Concrete Under Triaxial Compression," Journal of the Structural Division, ASCE, Vol. 100, No. ST5, Proc. Paper 10547, May, 1974, pp. 901-916.

12. Rosenthal, I., and Glucklich, J., "Strength of Plain Concrete Under Biaxial Stress," Journal of the American Concrete Institute, Proceedings Vol. 67, No. 11, November, 1970, pp. 903-914.

13. Shah, S.P., and Chandra, S., "Fracture of Concrete Subjected to Cyclic and Sustained Loading," Journal of the American Concrete Institute, Vol. 67, October, 1970, pp. 816-825.

14. Shah, S.P., and Chandra, S., "Critical Stress, Volume Change, and Microcracking of Concrete," Journal of the American Concrete Institute, Vol. 65, No. 9, September, 1968, pp. 770-781.

15. Sinha, B.P., Gerstle, K.H., and Tulin, L.G., "Stress-Strain Relations for Concrete Under Cyclic Loading," Journal of the American Concrete Institute, Vol. 61, No. 2, February, 1964, pp. 195-211.

16. Tasuji, E.B., Nilson, A.H., and Slate, F.O., "Biaxial Stress-Strain Relationships for Concrete," Magazine of Concrete Research, Vol. 31, No. 109, December, 1979, pp. 217-224.

17. Tasuji, M.E., Slate, F.O., and Nilson, A.H., "Stress-Strain Response and Fracture of Concrete in Biaxial Loading," Journal of the American Concrete Institute, Proceedings Vol. 75, No. 7, July, 1978, pp. 306-312.

18. Costello, S.D., "Behavior of Confined Concrete Under Cyclic Loading," Thesis presented to the Massachusetts Institute of Technology, February, 1980, in partial fulfillment of the requirements for the degree of Master of Science.

19. Lam, Y., "Behavior of Plain Concrete Under Cyclic Compressive Loading," Thesis presented to the Massachusetts Institute of Technology, February, 1980, in partial fulfillment of the requirements for the degree of Master of Science.